DESY 95-101
May 1995



# Classical and Quantum Chaotic Scattering in a Muffin Tin Potential

S. Brandis
*Fachbereich Physik, Universität Hamburg*



ISSN 0418-9833

DESY 95-101
May 1995

ISSN 0418-9833

# Classical and Quantum Chaotic Scattering in a Muffin Tin Potential

Dissertation
zur Erlangung des Doktorgrades
des Fachbereichs Physik
der Universität Hamburg

vorgelegt von
Sebastian Brandis
aus Berlin

Hamburg
1995

| | |
|---|---|
| Gutachter der Dissertation: | Prof. Dr. F. Steiner<br>Prof. Dr. H. Nicolai |
| Gutachter der Disputation: | Prof. Dr. F. Steiner<br>Prof. Dr. G. Mack |
| Datum der Disputation: | 26. Mai 1995 |
| Sprecher des Fachbereichs Physik und Vorsitzender des Promotionsausschusses: | Prof. Dr. B. Kramer |

## Abstract

In this paper, we study the classical mechanics, the quantum mechanics and the semiclassical approximation of the 2-dimensional scattering from a muffin tin potential. The classical dynamical system for Coulombic muffin tins is proven to be chaotic by explicit construction of the exponentially increasing number of periodic orbits. These are all shown to be completely unstable (hyperbolic). By methods of the thermodynamic formalism we can determine the Hausdorff dimension, escape rate and Kolmogorov-Sinai-entropy of the system . An extended KKR-method is developed to determine the quantum mechanical S-matrix. We compare a few integrable scattering examples with the results of the muffin tin scattering. Characteristic features of the spectrum of eigenphases turn out to be the level repulsion and long range rigidity as compared to a completely random spectrum. In the semiclassical analysis we can rederive the regularized Gutzwiller trace formula directly from the exact KKR-determinant to prove that no further terms contribute in the case of the muffin tin potential. The periodic orbit sum allows to draw some qualitative conclusions about the effects of classical chaos on the quantum mechanics. In the context of scaling systems the theory of almost periodic functions is discussed as a possible mathematical foundation for the semiclassical periodic orbit sums. Some results that can be obtained from this analysis are developed in the context of autocorrelation functions and distribution functions for chaotic scattering systems.



## Zusammenfassung

In dieser Arbeit untersuchen wir die klassische Dynamik, die Quantenmechanik und die semiklassische Näherung der 2-dimensionalen Streuung an einem muffin-tin-Potential. Mit Hilfe expliziter Konstruktion der exponentiell anwachsenden Anzahl von periodischen Bahnen wird gezeigt, daß das klassische dynamische System von muffin tins mit abgeschnittenen Coulomb Potentialen chaotisch ist. Diese erweisen sich alle als instabil (hyperbolisch). Mit den Methoden des Thermodynamischen Formalismus wird die Hausdorff Dimension, die Fluchtrate und die Kolmogorov-Sinai Entropie des Systems bestimmt. Eine erweiterte KKR-Methode wird entwickelt, um die quantenmechanische S-Matrix zu bestimmen. Wir vergleichen ein paar integrable Streusysteme mit den Ergebnissen der Streuung am muffin-tin-Potential. Als charakteristische Eigenschaften des Spektrums von Eigenphasen ergeben sich dabei im Gegensatz zu einem rein zufälligen Spektrum the Niveau-Abstoßung und die langreichweitige Steifheit des Spektrums. Bei der semiklassischen Analyse können wir die regularisierte Gutzwiller Spurformel direkt aus der exakten KKR-Determinante herleiten um zu zeigen, daß im Falle des muffin-tin-Potentials keine weiteren Beiträge auftauchen. Die Spurformel kann dann benutzt werden, qualitativ den Einfluß der klassischen Mechanik in der Quantenmechanik zu diskutieren. Für den Fall skalierender Systeme untersuchen wir die Theorie der Fastperiodischen Funktionen als mögliche mathematische Grundlage zur Behandlung semiklassischer Periodic Orbit Summen. Einige Ergebnisse dieser Klassifizierung werden im Zusammenhang mit Autokorrelationsfunktionen und Verteilungsfunktionen für chaotische Streusysteme entwickelt.

# Contents

# Chapter 1

# Introduction

*The nose of Cleopatra: Had it been shorter*
*the face of the whole world would be different.*
Blaise Pascal in PENSÉES

In science and especially natural science one is concerned with the determination of (natural) laws. These laws are laid down to describe causal relations between measurable observables in reproducible experiments. Thus one connects numbers by logical conclusions. The natural language for the formulation of these laws is mathematics.

The idea is then to predict the result of a natural event on the basis of the relevant laws and the initial or boundary conditions. The success of this deterministic description procedure over the last 300 years is overwhelming and determining our every day life. Nevertheless the majority of phenomena still to be understood seems to be governed by probabilistic rather than deterministic laws. Many events in the observed nature seem to behave completely irregular and random. The striking feature of the study of chaos is that this seemingly random and probabilistic behaviour can often be reproduced by very simple and completely deterministic dynamical systems.

Thus the general theory of dynamical systems, of which a subset describes natural laws, covers a large variety of types of behaviour between the two extremes of being completely predictable, called *integrable*, and unpredictable, known as *chaotic*. We shall explain both terms in more detail after we have given more precision to the notion of a dynamical system.

In this thesis we are only interested in Hamiltonian dynamical systems on finite dimensional spaces. This means that we have an 2N-dimensional vector space (called the *phase space*) with vectors $(\vec{q}, \vec{p}) = (q^1, ..., q^N, p^1, ..., p^N)$ equipped with a Hamiltonian function

$H(\vec{q},\vec{p})$ that is time independent and governs the dynamics by the differential equations

$$\begin{aligned} \dot{q}^i &= \frac{\partial H(\vec{q},\vec{p})}{\partial p^i} \\ \dot{p}^i &= -\frac{\partial H(\vec{q},\vec{p})}{\partial q^i}, \end{aligned} \tag{1.1}$$

where the dot denotes the derivative with respect to time as usual. The subspace determined by the first $N$ components will be called *coordinate space*. In such a system the Hamiltonian, which is equal to the energy of the system, is constant along a solution. This determines a $(2N-1)$-dimensional hypersurface on which the motion actually takes place. The time evolution of an initial state is also called the flow of the system. In some cases the phase space is restricted by some additional boundary condition. For the moment being we will assume a bounded coordinate space and extend it to unbounded systems only later when we come to include scattering problems. A dynamical system and its various properties introduced below can be much more general, but this setting is general enough for our purposes.

Integrable systems have $N-1$ further constants of motion. These can be taken as coordinates for the coordinate space. The equations (1.1) then become trivial and the motion described in these coordinates is linear in time. These constants restrict the motion down to an $N$-dimensional subspace that has the topology of an $N$-dimensional torus. The phase space has a clean structure and the long-time behaviour of the system can be predicted. Integrability however should not be confused with simplicity, since it can be arbitrarily difficult to find the constants of motion.

Unfortunately the term chaotic does not have such a clear, generally accepted definition yet. It is similar to the difference between order and mess: Order is usually easy to detect, but a mess can be messy in many different ways. Chaos covers generally all phenomena of irregular behaviour in dynamical systems, which are usually due to some nonlinearity either in the differential equation or the boundary condition. Long before chaos became such a focus of interest mathematicians have developed a variety of precise classes of dynamical systems in the context of ergodic theory, of which we shall give some basic concepts now (see, e.g., [1, 2]).

## 1.1 Chaos in Bounded Systems

### 1.1.1 Classical Chaos

It was Poincaré [3] who first observed in 1892 that the trajectories of the 3-body problem can become arbitrarily complicated and may spread over a large region of phase space. On the other hand, Boltzmann [4] needed to assume, when he treated the Boltzmann-Gibbs-Gas model in 1887, that the trajectories spread over the whole $2N-1$ dimensional energy surface with equal density. This *ergodic* hypothesis marked the foundation of statistical

mechanics, although until today ergodicity can be proven for very few systems only. One example is the famous 2-D torus billiard with a circular obstacle, named after Y. Sinai, who provided the proof in 1963 [5].

To be more precise, a dynamical system is called ergodic, when the average over phase space of a given observable equals the average over time in the limit where time approaches infinity. In the mathematical framework of ergodic theory (see, e.g., [6]) systems have been found to obey even stronger requirements, which classify these as *mixing* or even as $K$-systems. In the case of mixing the meaning is still quite intuitive: The measure of the intersection of a subset B of the coordinate space with another, time evoluted subset A approaches the product of the measure of the two subsets separately as time approaches infinity. This local condition is already rather close to a probability law: The probability of two independent events to occur simultaneously is the same as the product of the probabilities of each event.

Ergodic, mixing and K-systems, which in this order describe increasing degrees of chaos, are purely measure-theoretic classifications. A Hamiltonian system like the one above is additionally equipped with a metric. This allows a different form of classification by means of the distance between single points in phase space and its evolution in time. This provides the idea of *stability* of trajectories by studying their infinitesimal environment. The most unstable systems known are so called *Anosov*-systems. In these systems the tangent space to a point in phase space splits under the Hamiltonian flow into three subspaces. One is exponentially contracting, one is exponentially expanding and the third one along the direction of motion stays constant under the evolution of time. It is in general hard to prove that a system carries these properties. Anosov-systems are mixing (and therefore ergodic) and in most cases even K-systems.

In spite of the extreme differences between integrable and chaotic systems, there is something like a thread through all dynamical systems. This is the set of fixed points (of the discretization of the dynamical system) or periodic orbits of the (full) system. In studying the transition from the integrable to the chaotic case by perturbation of an integrable system, the KAM-theorem (see, e.g.,[7]) has shown that the tori, on which the periodic solutions live, break up into many more but smaller tori in phase space. In the completely chaotic case only an infinite number of isolated periodic orbits remains. As we will see, the periodic solutions play an important role as well in the classical as in the quantum case. An important tool to analyze the structure of phase space is the Poincaré Map. It is a two-dimensional cut in phase space in some direction of the $2N-2$-dimensional subspace orthogonal to the direction of motion. Especially for $N=2$, where motion takes place on a three-dimensional hypersurface of phase space, the Poincaré Map displays the whole structure. In higher dimension one usually needs more than one cut. This is one of the reasons, why mostly two-dimensional problems have been studied up to now.

### 1.1.2 Quantum Chaos

As the degree of irregularity in deterministic classical chaos manifests itself in the degree of randomness and the sensitive dependence on initial conditions, an analogous criterion should be looked for in the definition of quantum chaotic systems.

In principle the situation is similar. We are dealing with a differential equation, the Schrödinger equation,

$$i\hbar\frac{\partial}{\partial t}\psi = H\psi \tag{1.2}$$

and some boundary condition. In this case however the differential equation is *linear* in time (as long as the Hamiltonian is time-independent) and there is no irregularity to be expected in the long-time behaviour. Thus one is left with the stationary equation

$$(H - E)\phi = 0 \tag{1.3}$$

and interested in finding some characteristic behaviour in the distribution of energy eigenvalues and eigenfunctions. Therefore the object of quantum chaos is the study of stationary quantum mechanics of classical chaotic systems, where one tries to find tools for a quantum mechanical classification.

Some sort of stochastic behaviour was found in the spectra when they were compared to those calculated from the theory of random matrices (RMT) [8]. It was found that short-range energy correlations agree in most cases very well with the results of an ensemble of random matrices [9]. Usually one considers ensembles of hermitian matrices that are only invariant under orthogonal or unitary transformations according to whether the system shows time inversion symmetry or not. These ensembles are named after their symmetry classes Gaussian Orthogonal Ensembles (GOE) or Gaussian Unitary Ensembles (GUE) [10, 11, 12]. Long-range correlations however are not reproduced and in some cases, as for example in the case of arithmetic chaos [13, 14, 15], even short-range correlations fail to agree, although the underlying classical dynamics is a K-system.

Recently a new quantity has been conjectured to give a unique identification of a quantum chaotic system [16, 17]. Consider the staircase function $N(E)$ that counts the number of energy levels below some given value $E$. Then one may split this function into its mean and an oscillatory remainder, $N(E) = \bar{N}(E) + N_{osc}(E)$. The conjecture states essentially that the normalized distribution of values of $N_{osc}(E)$ is a Gaussian and thus universal for all quantum chaotic systems.

Another approach to understand quantum chaotic systems is the semiclassical one. It is especially suitable as we intend to study the impact of classical chaos on the quantum level and it may elucidate this relation particularly well. Furthermore, in contrast to RMT, it includes the complete dynamics of each particular system and can therefore provide a dynamical explanation for the stochastic behaviour. A disadvantage one has to cope with is that in the method of stationary phase approximation, mainly used to obtain semiclassical expansions, very little is known about the estimation of the remainder terms.

Very recently higher order corrections were calculated in [18, 19]. Nevertheless, the theory developed over the last 15 years has celebrated remarkable success in explaining various phenomena even in long-range correlations of energy spectra (for reviews see [21, 22]).

The starting point for the semiclassical analysis is the path integral formulation of the propagator. From this exact quantum mechanical expression one can deduce by the stationary phase approximation a form that contains an infinite sum over classical trajectories. As $\hbar$ is the only non-classical quantity in this expression, it is sometimes even called the (quasi-)classical propagator. A Laplace-transformation in time renders the approximation to the Green's function. The Green's function $G(q'', q', E)$ contains all quantum mechanical information as it obeys the equation

$$(H - E)G(q'', q', E) = \delta(q'' - q'). \tag{1.4}$$

The semiclassical approximation satisfies the equation up to second order in $\hbar$, for which reason it is thought of as an approximation for $\hbar$ being small compared to all other quantities involved, i.e., a semiclassical approximation [23]. There has been and still is a debate about the convergence of these semiclassical sums over classical trajectories. Looking at eq. (1.4) one is reminded that the Green's function is a mathematical distribution rather than a function as it misleadingly called. Therefore, only to resemble the quantum mechanical singlarities well, *in general* no absolute convergence can be expected. This implies that numerical treatment requires some regularization procedure [60, 20]. Nevertheless, we will come across some cases, where absolute convergence is present.

By focusing on the energy statistics first, one may take the trace of the Green's function and thus obtain an expression for the density of states as a sum over $\delta-$functions. Gutzwiller found [25] that on the classical side, if the trajectories are isolated as it is generally the case in chaotic systems, only trajectories periodic in phase space remain. This trace formula has been subject to intensive research, known under the name of *Periodic Orbit Theory* (POT). It has been tested in many systems like the Hydrogen atom in a magnetic field, the anisotropic Kepler problem, Euclidean billiards of many shapes or billiards on a surface of constant negative curvature [21, 26]. In the latter case, Gutzwillers trace formula coincides with the *exact* Selberg trace formula. Trace formulae have also been generalized to integrable systems as for the torus or the circular billiard [27].

The mathematical form of the semiclassical sums is that of a generalized Dirichlet series. Thus many interesting mathematical connections are used and established such as the theory of zeta functions (of dynamical systems) and number theory in general. More recently the old subject of almost periodic functions has come into play again, which we shall discuss in more detail below.

## 1.2 Unbounded Systems

We shall not repeat all the above points again but simply mark the differences to bounded systems and how chaos can be defined here. By unbounded systems we mean a typical

scattering situation with an infinite coordinate space, well defined (free) initial and final states and a finite interaction region.

### 1.2.1 Classical Scattering Chaos

On first glimpse, no chaos can be expected in a scattering system: The long-time behaviour is completely regular outside the interaction region. Two neighbouring trajectories separate only linearly as time approaches infinity. Nevertheless, in many systems some observables display a sensitive dependence on initial conditions as there is, e.g., the deflection angle (or the time-delay) as a function of the initial impact parameter. Moreover there is a fractal set of initial conditions, where these quantities become singular. 'Fractal' here means that a pattern of singularities can be found on all scales. This has sometimes been taken as a definition for chaotic scattering [28, 29, 30]. To capture the full scattering properties and find an analogous tool to the Poincaré Map, Jung developed the idea of a Poincaré Scattering Map (PSM). It is the iteration of the scattering, where the output parameters are taken as input parameters for the succeeding scattering. Here one finds again fixed points and can identify stable and unstable areas in phase space, but a strict mathematical classification is difficult.

Another way of looking at a scattering system is to find periodic structures within the flow itself. Indeed the above mentioned fractal structure is the consequence of infinitely long trapped orbits. As in the bounded case, there is usually an infinite number of periodic orbits in the interaction region that influence the whole flow, although their measure in phase space is typically zero. These are sometimes easier to find by associating uniquely a symbolic string to each periodic orbit. This way one can count the orbits systematically. Thus, in analogy to the bounded case, one can define ergodicity of a scattering system by restricting the flow to the set of bounded (not only periodic) orbits [31]. Thus one "regularizes" the flow by subtracting the infinite part and concentrates on the finite region. The link between the two types of periodicity in the PSM and the truly periodic orbits is still not found.

### 1.2.2 Quantum Scattering Chaos

We have defined quantum chaos as the quantum mechanics of classical chaos. The randomness in the case of scattering cannot be found in the spectrum, since it is continuous. The discrete structure in this case, usually thought of as the analog to the energy spectrum in bounded systems, are the resonances, i.e., the poles of the S-matrix. The density of resonances or a resonance counting function are now defined on the complex energy plane, because resonances have a finite lifetime. But there is only very little known on these distribution functions in general, even in the integrable case. This poses a problem on universal statements on statistics of resonances as one needs a well defined procedure for the unfolding. In fact only recently mathematicians start to develop some estimates

[33, 34, 35]. Instead of the resonances one might therefore concentrate on the spectrum of a different operator, the S-matrix, i.e., its eigenphases. For real energies, the eigenphases are real and one can discuss statistics as above. One finds that the sum of eigenphases plays the role of the spectral staircase function of the bounded system as it has been shown recently for billiards [38].

RMT again provides some predictions for correlation functions of resonances and eigenphases. The distribution on normalized resonance widths should follow a so called Porter-Thomas distribution [39]. This has not been studied very well in chaotic systems as usually the number of resonances determined is too small to do reasonable statistics. As for the eigenvalues of the S-matrix, which is unitary, it should follow the results of Circular Ensembles. Some agreement has been found in [37], although the long-range correlation is less certain.

According to the preceding chapter, semiclassically there seem to be two perspectives. To include the full scattering information, one should take a semiclassical approach to the S-matrix as it has been formulated by Miller [40] by expressing the S-matrix in the form of classical scattering orbits. This is the corresponding object to the PSM on the classical side. Some studies of matrix elements have been done by taking traces of powers of the S-matrix [41]. Usually it is quite hard to get full account of the periodic orbits of the PSM and their physical meaning is not clear.

A closer link to the bounded case is given by taking the trace of the Green's function. The density of states obtained is, because of the continuous spectrum, infinite. Again we have to apply a regularization, this time by subtracting the free Green's function. By taking the trace over configuration space, one looses information like, e.g., the angular dependence of the scattering. But one ends up with a well defined trace formula, that contains periodic orbits of the flow itself and allows to calculate resonances and the sum of the eigenphases (see, e.g., [44, 45, 46, 47]). As this sum is the analogue to the spectral staircase in bounded systems, it may exhibit similarly universal fluctuations. Again one can discuss the properties of the dynamical zeta-function and usually finds that convergence is better in this case.

## 1.3 The muffin tin model

A main motivation of this work is to study chaos in a generic physical system. Most applications up to know have been concentrating on billiards of various types and a few exceptional potentials. The problem is thus to find a potential that can be proven to be chaotic in its classical behaviour and can be solved as a quantum mechanical system. This is what we are going to perform on a muffin tin potential. Muffin tin potentials have been used as models in many branches where quantum mechanics was applied, such as solid state physics, nuclear physics or chemistry. It is the name for an array of non-overlapping potentials, reminding in certain arrangements of the baking form for muffins.

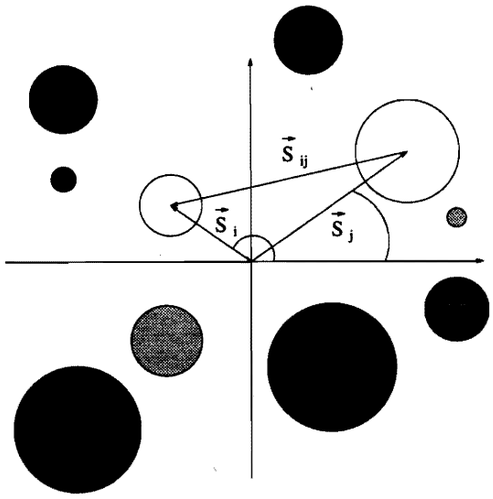


Figure 1.1: A typical muffin tin potential. The areas of non-vanishing interaction are encircled. Different shading indicates different types and strengths of interaction.

Only recently though from the viewpoint of quantum chaos, some special arrangements and potentials have been studied classically and semiclassically as well [42, 41, 43, 30]. Influenced by the work of [31] we have chosen the following setting. The simplest Coulombic muffin tin potential $V$ in a two-dimensional configuration space, which is chaotic, is that of 3 distinct Coulomb singularities [32]

$$V(\vec{q}) = -\sum_{i=1}^{3} \begin{cases} \left( \dfrac{Z_i}{|\vec{q}-\vec{s}_i|} - \dfrac{Z_i}{R_i} \right) & \text{, for} \quad |\vec{q}-\vec{s}_i| \leq R_i \\ 0 & \text{, else} \end{cases} . \tag{1.5}$$

The $R_i$ are the local radii, where the Coulomb interaction is switched off. We have added a constant to each Coulomb center to achieve a continuous connection to the outside free part. It does not change the equations of motion but it guarantees that the momentum of the particle changes continuously. The centers $\vec{s}_i$ are fixed but arbitrary and the strengths $Z_i$ are all chosen to be positive. We will compare a symmetric and an asymmetric configuration to eliminate all discrete symmetries that might conceal the fingerprints of chaos. Another possibility to achieve this is to desymmetrize the system and concentrate on the fundamental domain. This has been studied in detail in [48, 49].

The thesis is organized as follows. Chapter 2 is devoted to the classical dynamics. We draw the connection of a Hamiltonian flow to a geodesic flow in differential geometry. We observe the fractal structure of the deflection function and study therefore the distribution and properties of periodic orbits. These are determined by a symbolic dynamics. By analyzing their stability we see that all periodic orbits are hyperbolic and carry no conjugate points. Other quantities like escape rate and fractal dimension of the repellor

are determined by the method of the topological pressure.

In chapter 3 we solve the quantum mechanical problem by deriving a generalized KKR method and an eigenvalue equation for the eigenphases. We discuss the statistical properties of the eigenphases and compare them to RMT predictions. Finally we shed some light on the distribution function of the oscillating part of the sum of eigenphases.

The link between both classical and quantum mechanics is analyzed in chapter 4, where the semiclassics is discussed. We derive a semiclassical periodic orbit sum for the sum of the eigenphases and study how far this can be used in practical calculations for the case of potential scattering. At the end of the chapter, in a more general context, we discuss the strong link of semiclassical periodic orbits sums to the theory of almost periodic functions and to what extend it can be fruitful. Finally we summarize the main results and end with a few remarks on possible further developments.

# Chapter 2

# Classical Dynamics

## 2.1 Scattering Orbits

The Hamiltonian of a system governs the classical motion. For the scattering of a particle with mass $m = 1$ and momentum $\vec{p}$ on a fixed potential $V(\vec{q})$ it is given by

$$H(\vec{q},\vec{p}) = \frac{\vec{p}^2}{2} + V(\vec{q}) = E \tag{2.1}$$

The potential is taken from eq. (1.5), where the coordinate space is two-dimensional. The classical trajectories starting at $\vec{q}'$ and arriving at $\vec{q}''$ are now the solutions of the eqs. (1.1) above with given initial conditions. More fundamentally, according to the principle of Maupertius and Euler, these solutions extremize the classical action

$$S(\vec{q}'',\vec{q}';E) = \int_{\vec{q}'}^{\vec{q}''} \vec{p}\, d\vec{q}. \tag{2.2}$$

That is to say, under a variation of the paths on the energy surface the variation of the action vanishes only for the classical trajectories, i.e.,

$$\delta S = 0. \tag{2.3}$$

We will exploit this mechanical principle further down.

In the Coulombic muffin-tin potential the solutions are combinations of free motion and Kepler trajectories that are glued together on the boundaries. The pieces of free motion are trivial and, as the momentum is independent of the position, the action reduces to

$$S_f(\vec{q}'',\vec{q}';E) = \sqrt{2E}|\vec{q}'' - \vec{q}'|, \tag{2.4}$$

where the index labels the free motion. The time a particle needs to travel a given distance is here

$$t_f(\vec{q}'',\vec{q}';E) = \frac{|\vec{q}'' - \vec{q}'|}{\sqrt{2E}} \tag{2.5}$$

and is generally given by

$$t(\vec{q}'', \vec{q}'; E) = \frac{\partial S(\vec{q}'', \vec{q}'; E)}{\partial E} \tag{2.6}$$

The Kepler solutions for a given Coulomb center can be found in local polar coordinates $(r, \phi)$ by separating variables in the usual way. As the local angular variable is cyclic, the local angular momentum

$$l = r^2 \dot{\phi} = \text{const.} \tag{2.7}$$

is conserved. Transforming eq. (2.1) and replacing the angular velocity the radial velocity can be expressed as

$$\dot{r} = \pm \sqrt{2(E' + \frac{Z}{r}) - \frac{l^2}{r^2}}, \tag{2.8}$$

where plus or minus belong to outgoing or incoming branches respectively. We have dropped the indices here and shifted the energy according to the shift made in eq. (1.5), i.e., $E' = E - \frac{Z}{R}$. Deriving the analogous equation for $\dot{\phi}$ we can substitute variables and obtain the solution in the well known parametric form

$$r(\phi) = \frac{P}{1 + \varepsilon \cos(\phi - \phi_0)}. \tag{2.9}$$

Here we have adopted the usual choice of parameters

$$P := \frac{l^2}{Z} \quad \text{and} \quad \varepsilon^2 := 1 + \frac{2E'l^2}{Z^2}. \tag{2.10}$$

In our case of elementary mechanics we know that $\vec{p} = m\dot{\vec{q}}$ and thus $\vec{p}$ is always parallel to $d\vec{q}$. For the action we can therefore write

$$\begin{aligned} S(\vec{q}'', \vec{q}'; E) &= \int_{\vec{q}'}^{\vec{q}''} |\vec{p}| \, |d\vec{q}| \\ &= \int_{\vec{q}'}^{\vec{q}''} \sqrt{2(E - V)} \, |d\vec{q}| \\ &= \int_{t'}^{t''} 2(E - V) \, dt. \end{aligned} \tag{2.11}$$

The last form now allows a straight forward way of calculating the action in this case by expressing $dt$ through a separation of variables in eq. (2.8). The action is the same on the outgoing and the incoming branch of the Kepler trajectory such that we calculate twice from the radius $R$ to the turning point $r_0$. In the energy region $E' > 0$ the solutions

are pieces of hyperbolas in configuration space and we obtain for one branch (the index $C$ abbreviating Coulomb)

$$S_C(R, r_0; E') = \sqrt{2E'} \left[ \sqrt{R^2 + \frac{Z}{E'}R - \frac{l^2}{2E'}} + \frac{Z}{2E'} \ln \left( \frac{2\sqrt{R^2 + \frac{Z}{E'}R - \frac{l^2}{2E'}} + 2R + \frac{Z}{E'}}{2r_0 + \frac{Z}{E'}} \right) \right]. \tag{2.12}$$

The integrated time for the same distance amounts to

$$t_C(R, r_0; E') = \frac{1}{\sqrt{2E'}} \left[ \sqrt{R^2 + \frac{Z}{E'}R - \frac{l^2}{2E'}} - \frac{Z}{2E'} \ln \left( \frac{2\sqrt{R^2 + \frac{Z}{E'}R - \frac{l^2}{2E'}} + 2R + \frac{Z}{E'}}{2r_0 + \frac{Z}{E'}} \right) \right]. \tag{2.13}$$

We observe that time and action remain finite, when the local angular momentum vanishes, i.e., when the particle collides with a Coulomb singularity. The flow is not defined on the singular collision points, because the potential is not well defined. Imagine a few trajectories that surround the singularity nearby. The closer it gets to the Coulomb center, the closer the outgoing trajectory comes to the point were it started. Thus we regularize the flow most naturally by adding a backscattering orbit, whenever a collision takes place. Another point that seems to be singular on first sight are the values for $E' \to 0$. But a careful examination exhibits a finite limit for time and action, as it should be resembling the parabolic solution of the Kepler equation. From now on we will concentrate on the case $E' > 0$.

An important property of this muffin tin potential is the absence of scaling. If a potential is homogeneous, i.e., for any real number $\lambda$, where $V(\lambda\vec{q}) = \lambda^\alpha V(\vec{q})$ holds for some value $\alpha$, simple scaling laws transform trajectories of different energies $E_1$ and $E_2$ into each other: In eq. (2.1) one can see that replacing coordinates $\vec{q}_2 = \lambda\vec{q}_1$ and momenta $\vec{p}_2 = \lambda^{\alpha/2}\vec{p}_1$, scaling the energy by $E_2 = \lambda^\alpha E_1$ renders again a solution. As the action also scales with $S_2 = \lambda^{1+\alpha/2}S_1$, one can fix the energy once and then obtain all other solutions by simple multiplication [53].

In our system there are inner scales fixed by the distances $|\vec{s}_i - \vec{s}_j|$ between muffin tins and their radii $R_i$. Thus no exact scaling can be expected, but an approximate scaling for certain quantities is achieved for high energies.

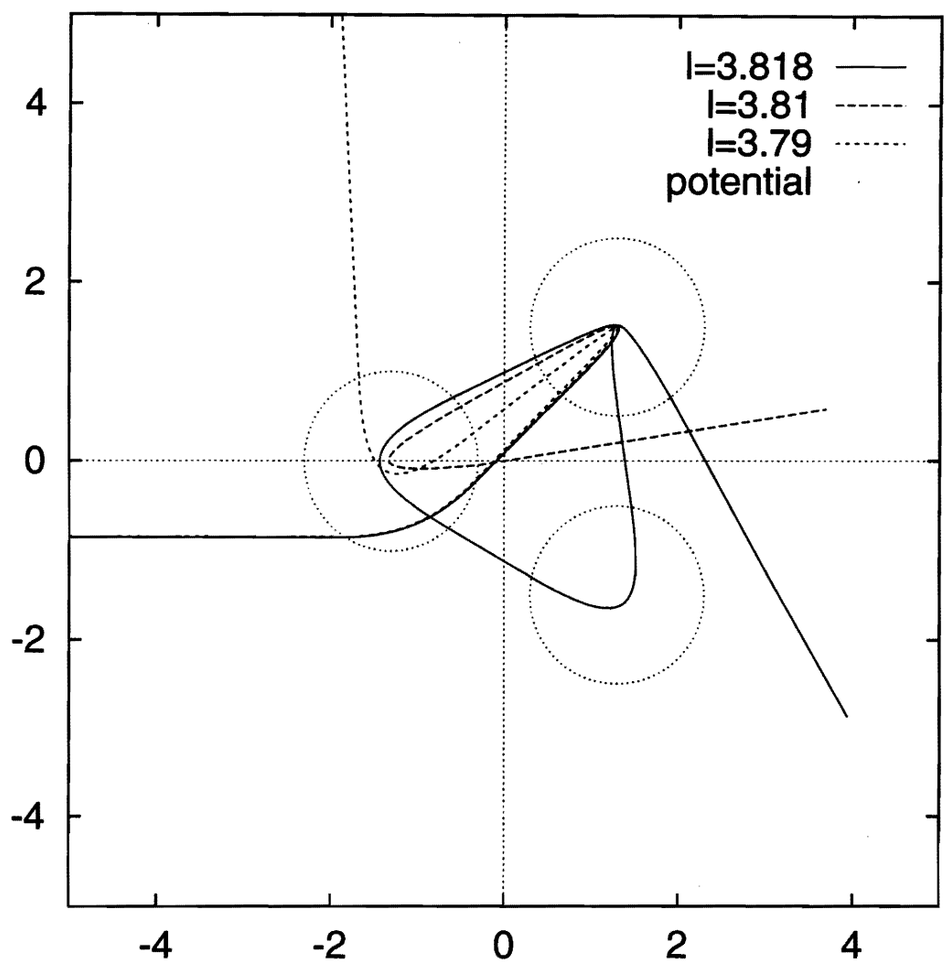


Figure 2.1: 3 typical scattering orbits coming in from the left parallel to the x-axis, which are almost indistinguishable before the scattering (note the different angular momenta) and scattered all over the place afterwards

To see the chaotic behaviour of the scattering in an intuitive way, we have drawn a few scattering orbits in Fig. 2.1. To illustrate the meaning of sensitive dependence on the initial conditions, we have chosen 3 values of the initial impact parameter that are almost indistinguishable on this scale. After only 2-3 scatterings from muffin tins, the final scattering angle and angular momenta are completely different. This is sometimes referred to as the production of information [50]: Practically equal initial states evolve into different states under the flow. Recalling the definition of chaotic scattering mentioned in the introduction, we have a look at the fractal structure of the deflection function of the potential. Fig. 2.2 displays the final scattering angle $\theta''$ as a function of the initial angular momentum $l'$ in a certain range. Additionally there are two blow-ups below, indicating that the structure remains the same on all scales, note the units on the x-axis. We will see that this is the consequence of the existence of an infinite number of periodic orbits and their hyperbolic nature.

### 2.1.1 Differential Geometric Description

Now we come back to the fundamental principle in eq. (2.3) and draw the well established but sometimes neglected connection to a differential geometric description due to Hamilton and Jacobi. Instead of saying the dynamics is governed by the Hamiltonian one might as well say that the motion is actually free, but lives on a non-trivial metric. Thus eq. (2.2) can be interpreted as the length of a path on a space with the line-element $ds$ defined by

$$\begin{aligned} ds &= \sqrt{2E}\sqrt{g^E_{\mu\nu}\, dq^\mu dq^\nu} \\ &:= \sqrt{2E}\sqrt{\left(1-\tfrac{V}{E}\right)\delta_{\mu\nu}\, dq^\mu dq^\nu}. \end{aligned} \tag{2.14}$$

The superscript $E$ on the metric indicates the explicit energy dependence of $g^E_{\mu\nu}(q)$. By the extremum principle of eq. (2.3) this trajectory becomes a geodesic and the Hamiltonian equations are equivalent to the geodesic equation [51]. The advantage of this point of view is to exploit the general tools established for any given metric $g_{\mu\nu}$. In particular we are interested in local stability of the geodesics. It is characterized by the deviation of the orbit in its infinitesimal vicinity. Thus we want to study the motion in coordinates locally orthogonal to the direction of motion. To find these is generally quite clumsy, especially in the presence of singularities, where the coordinates might become singular as well. But on a surface equipped with a (locally) Riemannian metric, the existence of so called geodesic coordinates is guaranteed (see, e.g., [52]). Moreover, studying the second variation of the classical action above yields for the orthogonal component $y$ of a vector field along the geodesic the Jacobi equation

$$y''(s) + K^E(\vec{q}(s))\, y(s) = 0, \tag{2.15}$$

where $K^E$ is the Gaussian curvature of the surface. The prime denotes the derivative with respect to the arc length s. Without explicitly writing down the coordinates, one

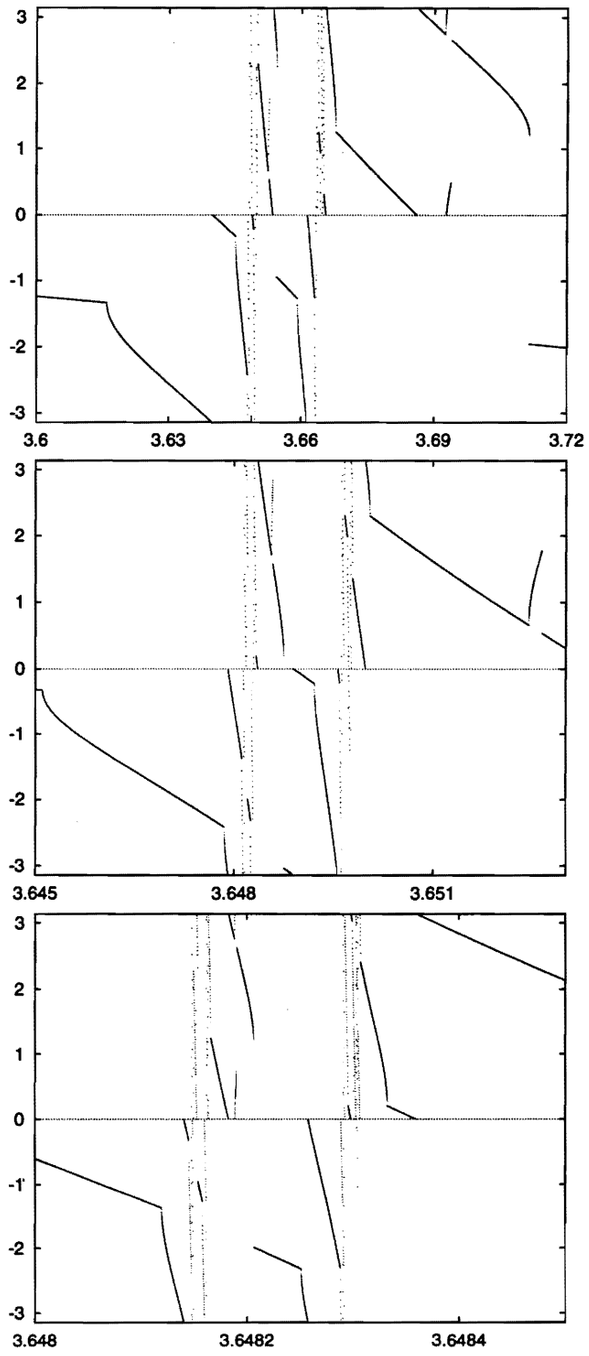


Figure 2.2: $\theta''(l')$ with two enlargements below

can calculate its evolution by solving the Jacobi equation. The Gaussian curvature is calculated via the Riemann tensor

$$K = \frac{R_{1212}}{\det(g_{\mu\nu})} \tag{2.16}$$

which is given by

$$R^{\mu}_{\nu\alpha\beta} = \frac{\partial \Gamma^{\mu}_{\nu\beta}}{\partial x^{\alpha}} - \frac{\partial \Gamma^{\mu}_{\nu\alpha}}{\partial x^{\beta}} + \Gamma^{\mu}_{\rho\alpha}\Gamma^{\rho}_{\nu\beta} - \Gamma^{\mu}_{\rho\beta}\Gamma^{\rho}_{\nu\alpha} \tag{2.17}$$

and the connection

$$\Gamma_{\mu\alpha\beta} = \frac{1}{2}\left(\frac{\partial g_{\mu\alpha}}{\partial x^{\beta}} + \frac{\partial g_{\mu\beta}}{\partial x^{\alpha}} - \frac{\partial g_{\alpha\beta}}{\partial x^{\mu}}\right). \tag{2.18}$$

The curvature on the free part vanishes as the metric is constant. In the domain of Coulomb interaction the metric in the coordinates $(r, \phi)$ reads

$$g^{E}_{\mu\nu} = \begin{pmatrix} 1 + \frac{Z}{E'r} & 0 \\ 0 & r^2 + \frac{Z}{E'}r \end{pmatrix} \tag{2.19}$$

and a straightforward calculation provides the curvature as

$$K^{E}(\vec{q}) = -\frac{Z}{2E'\left(|\vec{q} - \vec{s}_i| + \frac{Z}{E'}\right)^3}. \tag{2.20}$$

There are a few important points to mention. The curvature stays finite as we approach a singularity. This is a further justification of the regularization of the flow by adding a backscattering orbit: Next to the finite travel time it has a well defined stability. Furthermore we observe that the curvature becomes weaker for high energies. Hence for high energies the trajectories approach straight lines as we will confirm in the numerics later on. Most important for the stability is the strict negativity of the curvature for positive energies and positive coupling $Z$. The curvature in the whole coordinate space is therefore equal to or smaller than zero, an important feature for a chaotic situation. Some of the best studied chaotic dynamical systems are billiards on a surface of constant negative curvature. The negativity guarantees that two nearby trajectories locally spread exponentially in time (see, e.g., [7, 2]).

As we are interested in the stability of the orbit in phase space rather than in coordinate space, we shall rewrite the second order Jacobi equation (2.15) into two first order equations for the $y$ and $y'$ component separately. Writing these two vectors into a matrix $\tilde{\mathbf{M}}$ we have to solve the equation

$$\tilde{\mathbf{M}}'(s) = \begin{pmatrix} 0 & 1 \\ -K^E & 0 \end{pmatrix} \tilde{\mathbf{M}}(s) \quad \text{with} \quad \tilde{\mathbf{M}}(0) = \begin{pmatrix} 1 & 0 \\ 0 & 1 \end{pmatrix}. \tag{2.21}$$

Note that a for a differential equation of this form, the determinant of the solution stays constant. In our case this reflects the Liouville theorem of volume preservation in phase space.

Changing this differential equation from arc length to time by reparametrization with eq. (2.2), we can apply it to the position and velocity components $dq_\perp$ and $\dot{dq}_\perp$ orthogonal to the direction of motion, such that

$$\begin{pmatrix} \dot{dq}''_\perp \\ dq''_\perp \end{pmatrix} = \mathbf{M}(t) \begin{pmatrix} \dot{dq}'_\perp \\ dq'_\perp \end{pmatrix}. \tag{2.22}$$

For the free part, this matrix can be calculated directly and yields simply

$$\mathbf{M}_f = \begin{pmatrix} 1 & t_f \\ 0 & 1 \end{pmatrix}, \tag{2.23}$$

where $t_f$ is the time a particle needs to get from one muffin tin to the next (cf. eq. (2.5)). In the Coulomb region, an analytical solution is difficult to find and a numerical integration is much faster. The Runge-Kutta method is good enough and can be checked easily by controlling the determinant. The stability matrix of an orbit that passes several centers is then calculated by the multiplication of the various parts. We will use this later on to calculate stability exponents of periodic orbits.

## 2.2 Periodic Orbits

The complicated scattering behaviour is due to multiscattering . Moreover Fig. 2.1 gives the intuitive idea that this form of the deflection function or long dwell times comes from almost bounded orbits. In fact they come very close to truly bounded orbits, of which a subset is periodic. This set of periodic orbits is densely distributed in the set of bounded orbits and thus forms a sort of "skeleton" of the classical flow. We look for a systematic way to find these periodic orbits. The trajectories are very sensitive to initial conditions, such that using a numerical simulation of the flow and waiting for the initial conditions to be reached again is very ineffective.

This problem can be solved by using symbolic dynamics. The idea is to represent the periodic orbits uniquely in terms of codewords made out of symbols. The codeword usually marks a certain region of phase space. Restricting the search to this subset of phase space then allows to find the periodic orbit by some minimum principle.

### 2.2.1 Symbolic Dynamics

A natural code seems to be to label the orbit by the numbering of the Coulomb-centers it passes during its traversal. Thus for our potential with 3 muffin tins the codeword would

consist of the symbols $\{1,2,3\}$. Indeed we will show that the periodic orbits are in a one-to-one correspondence with infinitely long periodic chains of numbers, where no repetition of symbols are allowed and cyclic permutations of the period are identified. This is true under the two following conditions: 1.) The code is valid for energies $E > \max(\frac{Z_i}{R_i})$ only, due to the fact that it requires the Kepler trajectories to be hyperbolas. 2.) The centers $\vec{s}_i$ have to be arranged on the corners of a (convex) triangle, such the corridors, on which trajectories can move between two muffin tins, do not intersect (see Fig. 2.1). There are indications that this code can readily be generalized to more than 3 centers as long as they are placed on the corners of a convex polygon.

The main ingredient to the geometric proof is that the Kepler pieces of the orbits are hyperbolas. Thus after a turn around a center the outgoing branch cannot intersect the incoming one because of the finite angle between the two, i.e., self-intersection is inhibited (see upper right corner of Fig. 2.3).

Therefore we first note that a repetition of numbers cannot occur, because an orbit has to touch another muffin tin before it can turn around the first one a second time. It is clear that the chain has to be periodic when the orbit is periodic. We are left with the problem of uniqueness:

"=>" Given a periodic orbit, is there only one code? For an orbit to be periodic, it has to turn around the centers again and again. Hence, given a periodic orbit, it has a well defined path through the muffin tins and thus a single code (modulo its cyclic permutations).

"<=" Given a code one needs to show that there is only one periodic orbit. This is the more difficult bit. The essential ambiguity is the orientation in which the orbit turns around a given center. We shall exclude for a moment the orbits colliding with a singularity. Since the points $\vec{s}_i$ are then excluded, two orbits cannot be transformed continuously into each other, i.e., they are not homotopic, when they turn around the same center in a different orientation once (or more often) during their traversal of the orbit. As the code is fixed, we know, which centers the periodic orbit passes during the traversal. Any other orbit with this code is either (a) homotopic to the first one or (b) topologically different, which means that it runs around one of the muffin tins in a different orientation. We can already exclude (a): Since we know that the Gaussian curvature is non-positive, only one geodesic per homotopy class is possible (see e.g.[52]). To exclude (b) we split up the code into smaller parts and find three different types of pieces a periodic code can consist of (cf. enumeration in Fig. 2.3):

(1): $...abc....$,

where $a, b, c \epsilon \{1,2,3\}$ and $a \neq c$, $a \neq b$ , $b \neq c$. Whether the orbit turns around $b$ clockwise or anti-clockwise (see Fig. 2.3), is fixed by the explicit numbers, because the Kepler orbit being a hyperbola does not allow self-crossing after one turn. Hence given a sequence like the above one in a code the orbit has a well defined orientation.

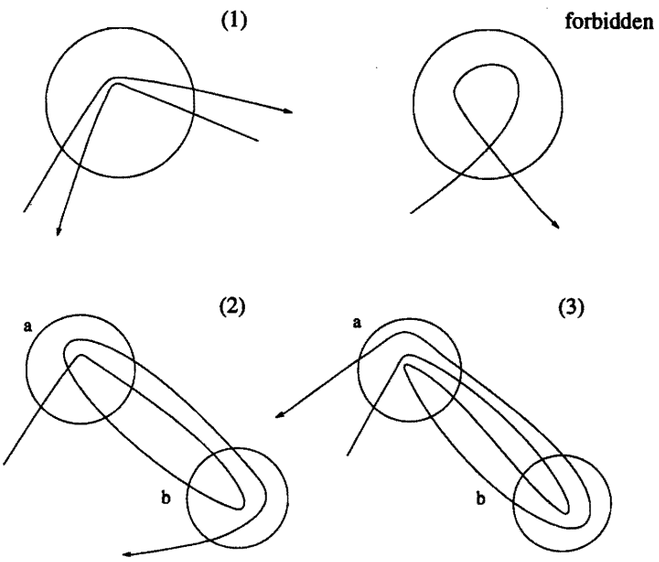


Figure 2.3: Schematic description of the various arguments in the proof

(2):...*cabab...ababc*...

in the familiar notation. On this pendulum like motion between $a$ and $b$ the scattering angle spreads or decreases constantly because of the hyperbolas at each center. Thus it will not change the orientation in between, when it comes out the same way it went in. This is the case in (2), since the last three letters are just a cyclic permutation of the first three.

(3):...*cabab...abac*....

In this case the orientation has to change, as it comes out of the pendular motion the opposite way it went in. But as a result of the avoided self-crossing the turn around will happen exactly in the middle of the term. The pattern looks like a squeezed ancient Greek meander.

Finally, the orbits colliding with a center have to have a mirror symmetry in their code because of their backscattering nature. In fact, every code with this symmetry is a colliding one, which is then unique.

With this code the periodic orbits are shown to be countable. Remember that the set of points for which the scattering quantities are singular was fractal and hence uncountable. The periodic orbits are therefore only a true subset of all bounded orbits. A systematic way of counting the orbits is to count them by the codelength of their period. To find the number of primitive periodic orbits $Z(N)$ to a given codelength $N$, we follow the following reasoning: The total number of (not necessarily periodic) codewords $C(N)$ of length $N$

that can be constructed; one has $C(N) = 3(2^{N-1})$. Periods can be those, where the last number differs from the first. Now the only ones that drop out are the ones where the last but one, i.e., position $N-1$ differs from the first, because only those can have an agreement of the last with the first. But these are just the number of periodic ones of length $N-1$. Hence for the number of periodic codewords $C_p(N)$ we have the following recursion relation

$$C_p(N-1) + C_p(N) = C(N) \tag{2.24}$$

and we find by induction that

$$C_p(N) = 2^N + (-1)^N 2 \tag{2.25}$$

satisfies this relation. Therefore the number of *primitive* periodic orbits $Z(N)$, i.e., where all multiples of shorter lengths and permutations have been taken out, is

$$Z(N) = \frac{1}{N}(2^N + (-1)^N 2 - \sum_{m|N} m\, Z(m)). \tag{2.26}$$

A formula for a similar situation can be found in [54]. One can see that the number of periodic orbits grows exponentially as a function of the length of the codeword (there are no forbidden orbits as they appear sometimes in the symbolic dynamics of billiard systems). This exponential growth is a typical feature for chaotic systems. The growth rate, here $\ln 2$, is called the topological entropy (with respect to the length of the codeword). This name origins from the analogy to thermodynamics as it is a measure for the number of topologically different periodic "states" of the system.

### 2.2.2 Geometric Construction of Periodic Orbits

Given a one-to-one code with an appealing geometrical interpretation, we can construct each periodic orbit by an algorithm. The p.o. consists of pieces of free motion and Kepler trajectories. Passing the muffin tin with number $i$ in the codeword, the orbit sweeps over an angle given by a Kepler hyperbola. The scattering angle therefore is given by conversion of the eq. (2.9) (thus the index $Kep$) plus an additional piece coming from the impact parameter $l_i/p$, when it hits the boundary (in eq. (2.9) $\phi$ is the angle of the position of the particle, whereas $\theta$ here is the angle of the momentum)

$$\begin{aligned}(\theta_{i+1} - \theta_i)_{Kep} = \; & \mathrm{sgn}(l_i)\left(2\arccos\left(\left(\frac{P_i}{R_i} - 1\right)\frac{1}{\varepsilon_i}\right) - \pi\right) \\ & + 2\arcsin(\frac{l_i}{pR_i}).\end{aligned} \tag{2.27}$$

It is a function of the incoming relative angular momentum $l_i$. Here $\theta_i$ is the direction of the momentum before the $i-$th center and $P_i$ and $\varepsilon_i$ are the known parameters of the

trajectory defined in (2.10). $p$ is the absolute value of the momentum of the free motion. On the other hand the relative angular momenta $l_i$ (relative to the appropriate muffin tin) transform into each other by geometrical arguments

$$l_{i+1} = l_i + |\vec{s}_i - \vec{s}_{i+1}|\, p\, \sin(\alpha_{i,i+1} - \theta_{i+1}), \tag{2.28}$$

$\alpha_{i,i+1}$ being the angle of the vector $\vec{s}_i - \vec{s}_{i+1}$ with respect to the $x$-axis in a cartesian coordinate system. Inverting this equation we arrive at an additional, purely geometrical condition for two consecutive scattering angles as a function of the angular momentum

$$\begin{aligned}(\theta_{i+1} - \theta_i)_{geo} = \; & \alpha_{i,i+1} - \alpha_{i-1,i} - \left(\arcsin\left(\frac{l_{i+1} - l_i}{|\vec{s}_i - \vec{s}_{i+1}|\, p}\right)\right. \\ & \left. - \arcsin\left(\tfrac{l_i - l_{i-1}}{|\vec{s}_{i-1} - \vec{s}_i|\, p}\right)\right) .\end{aligned} \tag{2.29}$$

For periodic orbits (and for each index $i$) the functions in (2.27) and (2.29) have to be equal. Thus the problem of determining p.o.'s is reduced to finding the zeros of the difference of (2.27) and (2.29) in N-dimensional angular space as a function on the N-dimensional angular momentum space, when the length of the code is N.

In general the problem of finding a root in an N-dimensional system of transcendental equations can be rather difficult numerically, depending on the explicit function. In this case however, we find that it works very well. One only has to keep track of the variables $l_i$ staying in their domain and give a good first guess for the root. The latter can easily be constructed by the code. This guarantees fast convergence. But even for starting values far away from the solution, we always find a single solution, as it should be from the above proof for the uniqueness of the code, since this already reveals the orientation at each turn. As an intuitive argument one can imagine the good convergence coming from the monotonicity of the arc-functions. We have tested this up to codelength 17, which corresponds to 16510 primitive orbits, i.e., orbits that are traversed only once. There are 107 more, when one includes multiple traversals. $N = 17$ is not the final limit of this method, but it is a practical one, as the CPU time increases exponentially with the codelength. Fig. 2.4 shows a typical orbit, this one belonging to the codeword (1231213). This is one of the first non-trivial ones. One can see that it crosses itself in muffin tin no. 1, but only after it has hit several other muffin tins. The codeword contains a symmetry under the interchange of 2 and 3, but it has no mirror symmetry and it therefore does not collide with any singularity. In Fig. 2.4 a) and b) the muffin tins are located on an equilateral triangle and only the energy is changed form $E = 8$ to $E = 50$ respectively. As the solutions do not scale with the energy. Fig. 2.4 displays the dependence of a periodic orbits on the energy. The classical action is approximately a linear function of the momentum $p$ as the energy dependence of the free part prevails that of the Coulomb interaction.

The topologically different orbits become geometrically very similar as the energy rises. This gives rise to a number of non-generic features in quantities we shall look at in the following.

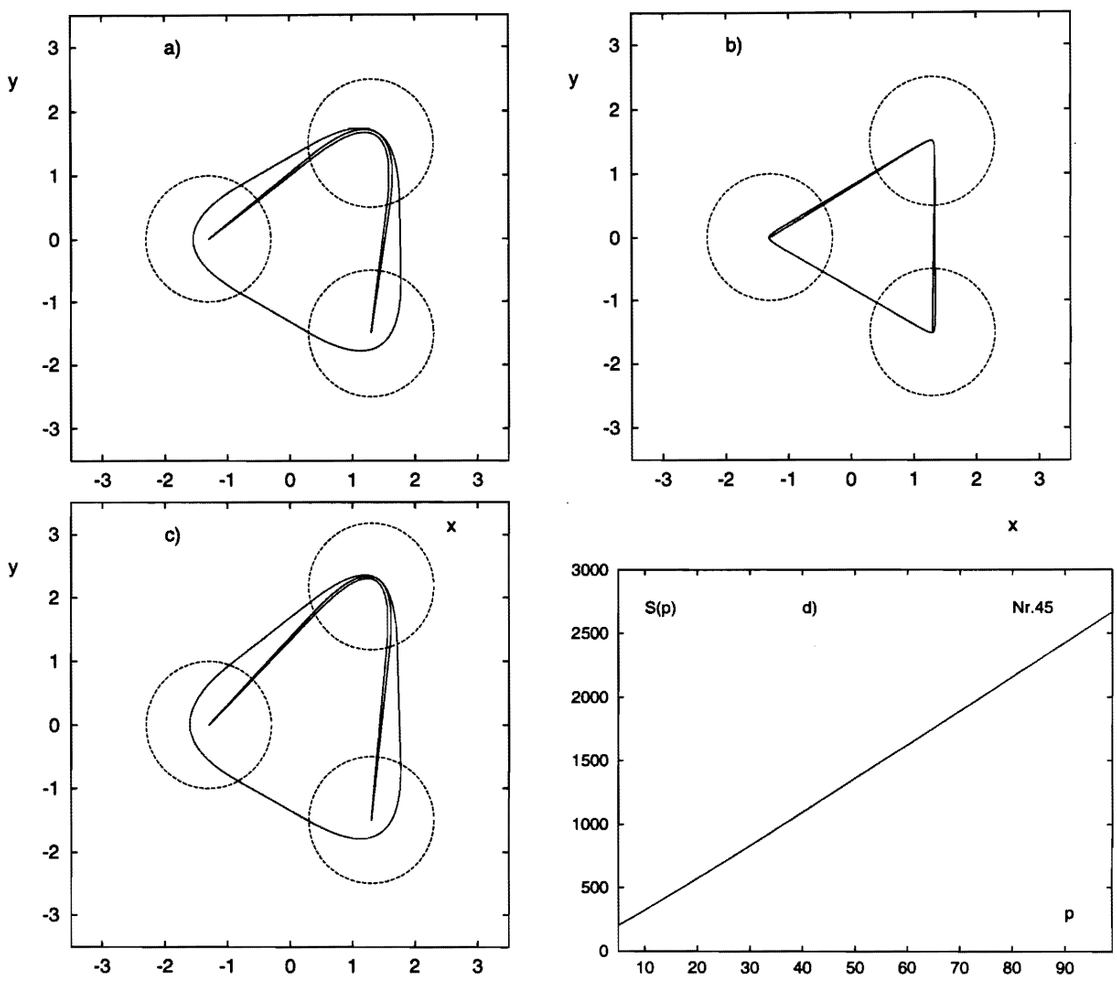


Figure 2.4: The periodic orbit corresponding to the codeword (1231213) for an equilateral configuration of muffin tins with (a) $E = 8$ and (b) $E = 50$. (c) shows the same orbit in a slightly asymetric setting ($E = 50$). In (d) one can see how the action of this orbit changes with the momentum $p$, where $p^2 = 2E$.

The effect of the high symmetry of the equilateral triangle on the classical dynamics has intensively been studied by the works on three discs [44]. Instead of reducing our system to the fundamental domain to extinguish the non-generic symmetries, we vary the positions of the muffin tins. In Fig. 2.4 c) the angles of the triangle are slightly changed to be 50, 60, 70 degrees, again representing the orbit to the same codeword.

The number of periodic orbits $N(T)$ with periods below a certain period $T$ proliferates exponentially in chaotic systems. With $\tau$ denoting the topological entropy with respect to time $N(T)$ reads asymptotically

$$N(T) \approx \frac{\exp(\tau T)}{\tau T} \text{ as } T \to \infty. \tag{2.30}$$

In our case this is strongly linked to the exponential increase of the number of codewords. At high energies the period becomes essentially a multiple of the free parts of the orbit as shown in Fig. 2.5 b). The metric becomes nearly flat for very high energies. The pronounced staircase behaviour of $N(T)$ washes out only as one gets to longer p.o.'s, which is a difficult region to reach numerically, or to lower energies as in Fig. 2.5 a). To eliminate the non-generic staircase we destroy the high symmetry by changing the equilateral triangle as above. The effect on $N(T)$ can be seen in Fig. 2.5 c).

To determine the topological entropy, we fit an exponential to the staircase function. As we only know the asymptotic behaviour, there is a freedom in choosing the fitting function, as long as the asymptotic behaviour remains the same. Experience with a lot of systems has shown, that the exponential integral $\mathrm{Ei}(x)$ usually leads to a much better fit (with $x = \tau T$). It is defined as the principle value of $\int_{-\infty}^{x} \frac{\exp t}{t}\, dt$. Fig. 2.5 a)-c) confirms, how well this function resembles the mean behaviour, keeping in mind that we concentrate on the asymptotic behaviour.

In the case of billiards one can define an energy independent entropy in units of the geometric length of the periodic orbits. Here there is no such simple *exact* relationship and we have to calculate it for each energy separately (see Table 2.1). Nevertheless in the high energy region, as the geometry of the orbits hardly changes any further, the classical action scales with $\sqrt{2E}$ approximately.

Another interesting plot is the probability distribution $p_N(T)$ of periods for a given codelength $N$. Thus we collect all orbits to a given codelength $N$ and determine the probability for different periods to appear. This has already been studied in the hyperbola billiard and the 3 disc system [54, 47]. If one finds this distribution to approach a smooth Gaussian for large codelength (and an overlap for different codelengths), there cannot be a minimal time $\Delta T$, of which all periodic orbits are just multiples, since this would yield a staircase function. The Gaussian behaviour would prove a system (as long as it is an Anosov system) to be weakly mixing and to have the mentioned exponential asymptotic behaviour of $N(T)$ [57, 31]. Our numerical tests indicate this behaviour (Fig. 2.5), although numerics in this context has to be viewed with much care. For one, the statistics is rather poor to overcome the strong geometric influence of the muffin tin setting

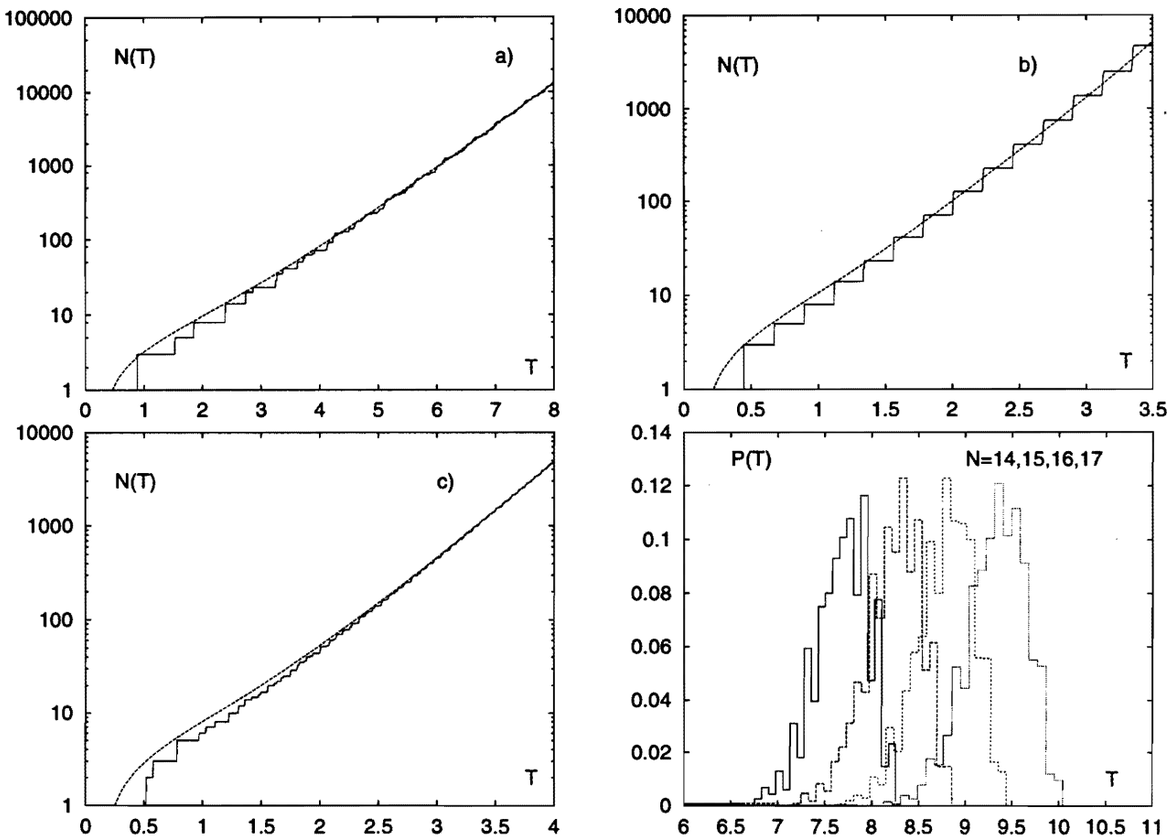


Figure 2.5: $N(T)$ for the symmetric configuration at energies (a) $E = 10.125$ and (b)$E = 50$. The asymmetric case is shown in (c) ($E = 50$). The dashed lines show the fit to the function $\mathrm{Ei}(\tau T)$ for which the values of $\tau$ are given in Tab.2.1. (d) displays the distribution of lengths for codelength $14, 15, 16, 17$ in the asymmetric system at energy $E = 10.125$ (full, dashed, dotted and dashed-dotted respectively).

and we do by far not reach a Gaussian. Furthermore, the numerical spreading might as well be a consequence of larger multiples of a few basic lengths as has been pointed out by Knauf [58].

The nearest neighbour spacing (NNS) of energy levels in chaotic systems has been the subject of many discussions in the literature (see e.g.[21]) By the semiclassical trace formula there is an interesting duality between the energy spectrum on the quantum mechanical side and the length spectrum of periodic orbits on the classical side. Thus it seems to be natural to ask, whether the NNS statistics of the length spectrum reveals any characteristic features [54]. As one includes more and more orbits, it seems to approach a Poissonian rather than, e.g., a distribution due to an underlying GOE. This would agree with an observation made for other chaotic systems as well [54, 59].

## 2.3 Stability and Conjugate Points

Given a periodic orbit or any other trajectory one can calculate its stability, i.e., the linear approximation of the motion in its vicinity by the Jacobi equation introduced above (eq. 2.15). The stability matrix for a periodic orbit is often called monodromy matrix. In our case it is a product of those matrices that correspond to the pieces the orbit traverses:

$$\mathbf{M}(T) = \prod_{i=1}^{N} \mathbf{M}_C^i \mathbf{M}_{free}^i. \tag{2.31}$$

Here $T$ is the period of the orbit. The eigenvalues of the monodromy matrix now determine the spreading of orbits. The entries of the monodromy matrix are all positive, because the solution of the differential equation (2.21) with the given initial condition has to be positive. Since the determinant of the monodromy matrix is equal to 1, their eigenvalues are inverse to each other. As they are both positive, we can write them as exponentials $e^{\pm u}$ and remain with the stability exponent as the only parameter, which is defined by

$$u(T) := \ln\left(\frac{1}{2}|\mathbf{Tr}\mathbf{M}(T)| + \sqrt{(\mathbf{Tr}\mathbf{M}(T))^2 - 4}\right) \tag{2.32}$$

and

$$\lambda(T) := \frac{u(T)}{T} \tag{2.33}$$

determines the celebrated Lyapunov exponent. These are strictly positive, because entries of the matix solution of (2.21) are always positive. Therefore the motion orthogonal to the periodic orbit splits into an expanding and a contracting manifold in phase space, which characterizes the periodic orbit to be a hyperbolic fixed point of the flow (cf. introduction).

The different features of energy dependence in the length spectrum manifest itself in a similar manner in the Lyapunov or stability exponents. Fig. 2.6 a) shows that to a good

| $p=\sqrt{2E}$ | config. | $\tau$ | $\bar{\lambda}$ |
|---|---|---|---|
| 4.5 | sym. | 1.48 | 2.19 |
| | asym. | 1.27 | 2.02 |
| 10 | sym. | 3.09 | 4.74 |
| | asym. | 2.69 | 4.28 |
| 30 | sym. | 8.72 | 12.47 |
| | asym. | 7.65 | 11.28 |

Table 2.1: Values for $\tau$ and $\bar{\lambda}$ at various energies. $\tau$ is determined by fitting the Ei-function to the staircase and $\bar{\lambda}$ is the arithmetical mean of all the calculated Lyapunov exponents (assumed to resemble the limit $N \to \infty$)

approximation the stability exponent becomes energy independent for large energies. It depends almost linearly on the period, where the spread around the mean widens as the energy decreases or the symmetry is destroyed (Fig. 2.6 b)). Fig. 2.6 c) displays the distribution of Lyapunov exponents around their mean in the "most generic case" of the ones we have looked at, which is the asymmetric configuration at low energies. The two dips around the mean in the distribution can be understood as a remainder of the nearby symmetric triangle. The arithmetical mean of the Lyapunov exponents $\bar{\lambda}_N$ is always larger than the topological entropy as can be seen in Table 2.1, a typical feature for scattering systems. This plays an important role for the question of convergence of the semiclassical trace formula [60]. The index $N$ states that we have taken the mean over all Lyapunov exponents up to codelength $N$ and $\bar{\lambda} := \lim_{N\to\infty} \bar{\lambda}_N$. The arithmetical mean settles at low $N$ already, such that we assume from now on (see Tab. 2.1)$\bar{\lambda} \approx \bar{\lambda}_{17}$.

A small remark should be added concerning the stability of scattering orbits. The stability matrix is then a product of three parts: The incoming part $\mathbf{M}_{in}$, a matrix with finite entries for the finite time it dwells within the interaction region $\mathbf{M}_{int}$, and an outgoing part $\mathbf{M}_{out}$. The first and the last matrix are of the form of (2.23) and are the only ones that diverge for the scattering orbits coming or going to infinity. The trace of the whole stability matrix is maximally linear in time, such that for the Lyapunov exponent for finite time $T_{scatt}$ of the scattering orbit we have

$$\lambda(T_{scatt}) = O\left(\frac{\ln(T_{scatt})}{T_{scatt}}\right). \tag{2.34}$$

Therefore the Lyapunov exponent vanishes for $T_{scatt} \to \infty$.

Not quite as vital for the classical discussion, but essential in the context of semiclassics are the so-called conjugate points. The number of conjugate points along a periodic orbit determines (if there are no reflections on hard walls) the Maslov index in the Gutzwiller trace formula [49].

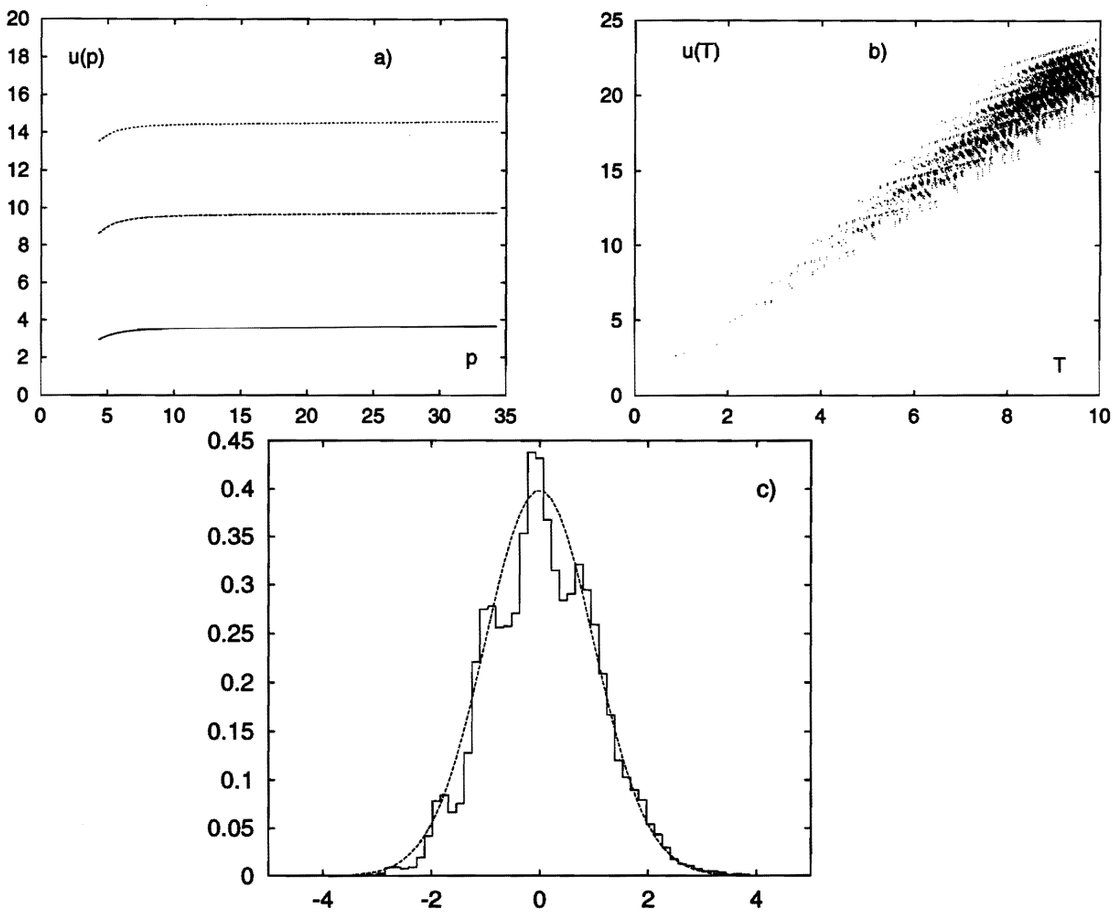


Figure 2.6: Stability exponents of 3 different orbits are plotted in (a) as a function of the momentum. In (b) the stability exponents are plotted against the period length (for $E = 10.125$ in the asymmetric case). (c) shows the distribution of Lyapunov exponents around their mean for the same setting.

Conjugate points can be understood in many ways. We are going to sketch a proof for the fact that in this system there are no conjugate points along periodic orbits. For this purpose we present a picture of conjugate points that is closely linked to the reasoning of the proof. Imagine a trajectory in configuration space and a family of trajectories starting at the same point with different directions of the initial momenta. This fan of trajectories then spans a volume element in phase space. Whenever the dimension of this volume element shrinks on the trip through the trajectory, a point conjugate to the starting point has been hit. This is called a conjugate point. In some direction of phase space it has then crossed a trajectory that has started at the same point, but in a different direction. Now we return to the more technical definition and demonstrate the absence of conjugate points in our muffin tin model.

Let $c(s,v)$ be a geodesic parameterized by arc length $s$ and let $v$ be a variation, such that for all values of $v$ $c(s,v)$ is a geodesic. Running $v$ spans a whole family of geodesics. A Jacobi field $Y$ is a vector field along $c(s,v)$ generated by

$$Y(s) := \frac{\partial}{\partial v} c(s,v)|_{v=0}. \tag{2.35}$$

Taking geodesic coordinates and the dual basis in tangent space, one gets for the transversal component of the Jacobi field , let us call it $y(s)$, the Jacobi equation eq. (2.15). The existence of conjugate points is equivalent to the existence of a non-trivial Jacobi-field that vanishes at the beginning and the conjugate point. So we have to show that such a field cannot exist:

As long as $c(s,v)$ is differentiable with respect to $s$, $y(s)$ is differentiable as well. Since the curvature $K^E$ is never positive, the solution of the Jacobi equation is either only convex or only concave (depending on the initial condition $\dot{y}(0)$). But then it is impossible to find a non-vanishing, differentiable solution of the Jacobi equation with $y(0) = y(s_1) = 0\,, s_1 > 0$. So there are no conjugate points.

This is a slight extension of the proof found in [52] for non-smooth $c(s,v)$. Note that $\dot{c}(s,v)$ has to be continuous.

## 2.4 Topological Pressure

The central role of periodic orbits in dynamical systems – bounded as well as unbounded – becomes most obvious in the context of the thermodynamic formalism [55]. From this elaborate and abstract theory we shall only concentrate on a small part, namely the concept of topological pressure $P(\beta)$. This enables us in principle to calculate various quantities that characterize a given chaotic system from the single function $P(\beta)$, such as topological entropy, mean Lyapunov exponents, escape rate, fractal dimensions, etc.

Starting with the *classical* time evolution operator (as compared to the more familiar quantum operator), one can define a Fredholm determinant that satisfies a secular

equation for the determination of its eigenvalues [61]. The spectrum consisting of the fundamental modes of the system governs its dynamical evaluation in time. Whereas for integrable systems the spectrum is found to be discrete, it is continuous for chaotic systems [7]. More detailed information about chaotic systems though is contained in the structure of resonances in complex mode space [61]. They have started to be studied recently but shall not be our subject here.

The above determinant can be expanded in terms of classical trajectories. It turns out that this leads to a product of so-called zeta-functions. The latter is a special case of the Ruelle zeta-function $\zeta_\beta(s)$ [55]. In this particular case the factors in the infinite product over primitive periodic orbits are weighted by the stability. To be more precise, it is defined as

$$\zeta_\beta(s) = \prod_\gamma \left[1 - \exp\left(-(s + \beta\lambda_\gamma)T_\gamma\right)\right]^{-1}, \tag{2.36}$$

where $\gamma$ labels the primitive periodic orbits, $\lambda_\gamma$ denotes their Lyapunov exponent and $T_\gamma$ is the corresponding time of the periodic orbit. The analyticity properties are well established. The zeta function $\zeta_\beta(s)$ is known to be holomorphic in the half-plane $\mathrm{Re}s > P(\beta)$ and has a pole at $\mathrm{Re}s = P(\beta)$. Thus it determines the abscissa of absolute convergence of $\zeta_\beta(s)$, which means more accurately

$$P(\beta) := \inf\left\{\sigma \in I\!R \Big| \sum_\gamma \exp\left(-(\sigma + \beta\lambda_\gamma)T_\gamma\right) < \infty\right\}. \tag{2.37}$$

The resonances lie all below this boundary. As the Euler product (2.36) does not converge there, one needs different techniques for the analytical continuation to determine these poles.

Since we are only interested in $P(\beta)$, we simply have to find the highest root of $\zeta_\beta(s)^{-1}$, which we do by evaluation of eq. (2.36). The result is plotted in Fig. 2.7. As $\lambda$ and $T$ are energy dependent, we show the result for various energies. The plots have been computed with the length spectrum of the asymmetric configuration. Numerically we have only a finite number of factors in (2.36), such that we can only approximate the root. We studied the quality of the behaviour of the approximation as we include more and more orbits and finally extrapolate the root by fitting with a rational function. We have tested this procedure on the Riemann zeta function, where the result is known (the topological pressure is exactly $P(\beta) = 1 - \beta$) and achieve an accuracy of at least 2 decimals. An alternative method is to expand eq. (2.36) into a Dirichlet series. This procedure is not as fast but allows much better accuracy (and gives consistent results) [61].

In Table 2.2 we have listed all quantities one can read off from the topological pressure. In the following we shall explain them in more detail.

For $\beta = 0$ the Lyapunov-exponents in eq. (2.36) do not contribute and we are left with the periods of the periodic orbits. The infinimum of real numbers $\sigma$ that prevent the sum in eq. (2.37) from divergence has to be just the growth rate of the number of prime

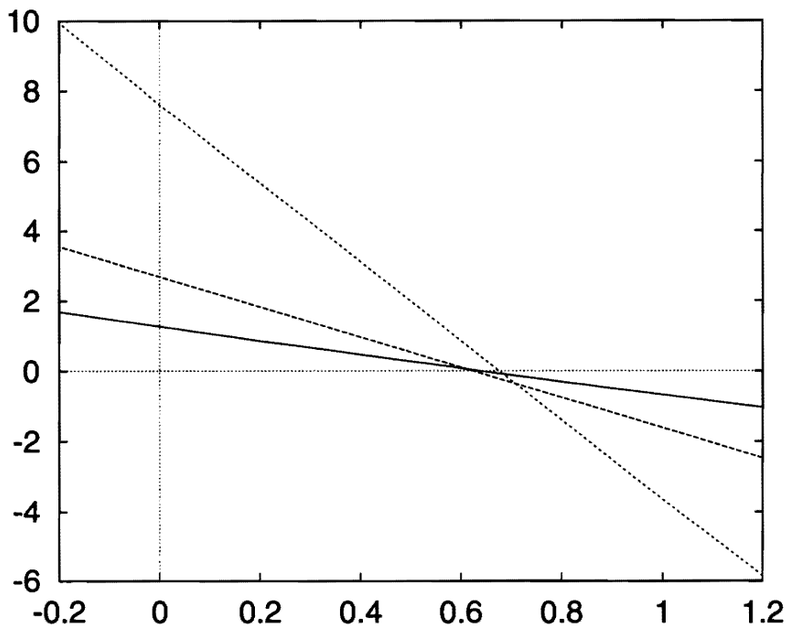


Figure 2.7: The topological pressure at energies $E = 10.125$ (full), $E = 50$ (dashed) and $E = 450$ (dotted).

| $p =$ | 4.5 | 10 | 30 |
|---|---|---|---|
| $\tau$ | 1.27 | 2.69 | 7.60 |
| $\overline{\lambda}$ | 2.02 | 4.30 | 11.32 |
| $\Gamma$ | 0.64 | 1.62 | 3.65 |
| $\hat{\lambda}$ | 1.81 | 4.29 | 11.18 |
| $h_{KS}$ | 1.14 | 2.68 | 7.53 |
| $D_H$ | 2.27 | 2.26 | 2.35 |
| $D_I$ | 2.25 | 2.25 | 2.35 |

Table 2.2: Dynamical quantities read off from the topological pressure in Fig.1.7, corresponding to the asymmetric case

periodic orbits. Thus we have $P(0) = \tau$, the topological entropy. Using this result, one can prove for $P(\beta)$ the more explicit form

$$P(\beta) = \tau - \beta < \lambda >_\beta, \tag{2.38}$$

where the average $< ... >_\beta$ is defined by

$$< \lambda >_\beta := -\frac{1}{\beta} \lim_{T\to\infty} \frac{1}{T} \ln \left\{ \frac{\sum\limits_{T\le T_\gamma \le T+\delta} \exp\left(-\beta\lambda_\gamma T_\gamma\right)}{N(T+\delta) - N(T)} \right\} \tag{2.39}$$

and the limit is independent of $\delta$ [62]. $N(T)$ is just the staircase function of eq. (2.30).

From this representation one can see after some calculation that $P'(0) = -\bar{\lambda}$. Thus we have determined $\tau$ and $\bar{\lambda}$ by two independent methods and find very good agreement by comparing the values in Table 2.1 and 2.2.

A chaotic system produces information as explained above. Illustrated on scattering orbits, this is equally valid for bounded orbits. It is a consequence of the exponential divergence of two neighbouring trajectories. A measure for this gain of information is the Kolmogorov-Sinai entropy $h_{KS}$ (for an exact definition see [50]). For a *bounded* system, it is linked to an average over Lyapunov-exponents by $h_{KS} = \hat{\lambda}$, where $\hat{\lambda} := -P'(1)$ (this average is more complicated than the arithmetical mean as one can see from the definition in eq. (2.38)). For an *unbounded* system, one has to take into account the number of orbits leaving the interaction region. They are "lost" for the growth of information within the bounded orbits. In chaotic systems the proportion of particles $n(T)$ that remain in the interaction region after the time $T$ decays exponentially, i.e.,

$$n(T) \sim \exp\left(-\Gamma T\right) \tag{2.40}$$

and $\Gamma$ is called the escape rate [50]. It is given here by $\Gamma := -P(1)$. In this case the Kolmogorov-Sinai entropy is determined by

$$h_{KS} = \hat{\lambda} - \Gamma. \tag{2.41}$$

$P(\beta)$ is monotonic and convex in general [55]. This leads to inequalities of the form $\hat{\lambda} \le \bar{\lambda}$ and $h_{KS} \le \tau$. In our case the topological pressure is nearly linear, a feature that has been observed for the three and four disc system as well, such that $\hat{\lambda} \approx \bar{\lambda}$ and $h_{KS} \approx \tau$.

Another interesting and often discussed quantity is the fractal Hausdorff dimension $D_H$. It measures in a certain sense the fraction of phase space occupied by the strange repellor, being the set of all bounded orbits. We find it here via the root of the pressure, $P(d_H) = 0$, where $D_H = 2\,d_H + 1$. In bounded chaotic systems with two degrees of freedom, where the escape rate $\Gamma = 0$, such that $d_H = 1$, the repellor fills the whole phase

space ($D_H = 3$). In our case the repellor is restricted to a fraction of the interaction region (see Table 2.2). A similar measure is the information dimension $D_I = 2\,d_I + 1$, which is given by $d_I = \frac{h_{KS}}{\lambda}$. From the above inequalities we have $D_I \leq D_H$ as it is confirmed in Table 2.2.

There is an obvious trend in the data of Table 2.2 from lower to higher energies. The topological entropy rises almost linearly with the momentum of the free particle. This is however somewhat misleading: The strong proliferation of orbits does not reflect that the system becomes "more chaotic". The increase in energy leads to shorter times of the periods, such that more orbits have accumulated below a fixed time $T$. Similarly the escape rate shows that a particle escapes faster at higher energies. Somewhat surprising is the behaviour of the Hausdorff dimension. There does not seem to be an overall trend, although intuitively one might expect the fractal dimension to shrink as the orbits tighten closer to the triangle of muffin tins. But as it is a measure in phase space, one needs to take into account the momentum dimension, which increases as the trajectories get closer to the centers of the muffin tins, where the momenta become large due to the Coulomb singularity. Thus the dimension of the repellor in phase space may increase.

# Chapter 3

# Quantum Mechanics

Having proved and characterized the chaoticity of the classical dynamics, we develop in this chapter a general method to determine the quantum mechanical properties of a general muffin tin potential in two dimensions and then try to find particular characteristics of quantum chaos. We first discuss the two-dimensional scattering on the example of a single muffin tin and then determine the S-matrix of the full system as a function of the phase-shifts of the single scatterers. We then discuss the eigenphases, the time-delay function and the resonances in more detail and discuss the numerical results.

## 3.1 Scattering in two dimensions

We start from the Schrödinger equation

$$\left(-\frac{\hbar^2}{2m}\Delta + V(\vec{q})\right)\Psi(\vec{q}) = E\,\Psi(\vec{q}). \tag{3.1}$$

The Laplace operator $\Delta := \frac{\partial^2}{\partial q^{1\,2}} + \frac{\partial^2}{\partial q^{2\,2}}$ replaces the kinetic term of the classical Hamiltonian. As usual we scale the equation to get rid of the constants. With the definitions

$$\mathcal{V}(\vec{q}) := \frac{2m}{\hbar^2}V(\vec{q}) \quad , \quad \mathcal{E} := \frac{2m}{\hbar^2}E =: k^2 \tag{3.2}$$

we have the simpler form

$$(\Delta - (\mathcal{V}(\vec{q}) - \mathcal{E}))\,\Psi(\vec{k},\vec{q}) = 0. \tag{3.3}$$

This equation is formally solved by the integral equation (see, e.g., [63])

$$\Psi(\vec{k},\vec{q}) = e^{i\vec{k}\vec{q}} + \int d^2q'\, G^{0+}(\vec{q},\vec{q}')\,\mathcal{V}(\vec{q}')\Psi(\vec{k},\vec{q}'), \tag{3.4}$$

known as the Lippmann-Schwinger equation, where the free (retarded) Green's function is the solution of

$$(\Delta + \mathcal{E})\, G^{0+}(\vec{q}, \vec{q}\,') = \delta(\vec{q} - \vec{q}\,'). \tag{3.5}$$

The solution in any dimension can be written in terms of Hankel functions. In 2 dimensions this reads

$$G^{0+}(\vec{q}, \vec{q}\,') = \frac{m}{2i\hbar^2} H_0^+(k|\vec{q} - \vec{q}\,'|) \tag{3.6}$$

We denote the Hankel functions of the first and second kind by $(+)$ and $(-)$ respectively.

Since we are looking for a scattering solution, the boundary condition is given by the requirement for the asymptotic behaviour of the wave function at large distances from the interaction region. We use the asymptotic expansion of the Hankel function for large arguments

$$H_0^+(k|\vec{q} - \vec{q}\,'|) \sim \sqrt{\frac{2}{\pi k}} \frac{e^{i(k|\vec{q}-\vec{q}\,'|-\pi/4)}}{\sqrt{|\vec{q} - \vec{q}\,'|}}. \tag{3.7}$$

Especially for the case of very large distance from the interaction region and fixed energy, one can apply the following approximations for the modulus in eq. (3.7)

$$\begin{array}{rcl} q \gg q' \;:\; |\vec{q} - \vec{q}\,'| & \approx & q \\ q \gg kq'^2 \;:\; k|\vec{q} - \vec{q}\,'| & \approx & kq - k\frac{\vec{q}\,'\vec{q}}{q}. \end{array} \tag{3.8}$$

Then eq. (3.4) attains the asymptotic form

$$\Psi(\vec{k}, \vec{q}) \sim e^{i\vec{k}\vec{q}} + \left[\sqrt{\frac{2}{i\pi k}} \int d^2q'\, e^{-i(\vec{k}'\vec{q}')}\, \mathcal{V}(\vec{q}\,')\Psi(\vec{k}, \vec{q}\,')\right] \frac{e^{ikq}}{\sqrt{q}}. \tag{3.9}$$

Here we have set $\vec{k}' := k\vec{q}/q$. Thus for $q \to \infty$ the solution is a superposition of a free plane wave (the incoming wave) and a radial outgoing part as the scattered wave. The contents of the square bracket in eq. (3.9) can be seen as the scattering amplitude $f(k, \theta', \theta)$ with

$$\Psi(\vec{k}, \vec{q}) \sim e^{i\vec{k}\vec{q}} + f(k, \theta', \theta)\frac{e^{ikq}}{\sqrt{q}}, \tag{3.10}$$

where $\theta$ and $\theta'$ are the polar angles of $\vec{k}$ and $\vec{k}'$ respectively. Notice that we will use $k$ here as the natural momentum variable, which is the same as $p$ in chapter 2, when $\hbar = 1$.

To find a solution we expand the wave function into a useful basis. We shall study this first in the case of a radially symmetric potential and proceed then to a non-symmetrical one like a muffin tin potential.

## 3.2 Radially Symmetric Potentials

As a result of the continuous radial symmetry, the angular momentum is conserved and the solution separates into a radial and an angular dependence. We can expand the solution in terms of the eigenfunctions of the angular momentum operator. In two dimensions these are just the trigonometric functions $e^{il\theta}$ for a given angular momentum $l$ and we thus get as an ansatz

$$\Psi(\vec{k},\vec{q}) = \sum_{l=-\infty}^{\infty} c_l R_l(kq) e^{il\bar{\theta}}, \tag{3.11}$$

where $\bar{\theta}$ is the angle between $\vec{k}$ and $\vec{q}$, i.e., $\bar{\theta} = \theta' - \theta$. It is equal to the scattering angle, because $\vec{q}$ becomes parallel to the outgoing wave vector asymptotically (the potential being centered at the origin). This is the partial wave expansion in two dimensions. For the radial part we use an ansatz with Bessel and Hankel functions

$$R_l(kq) = J_l(kq) - it_l(k) H_l^{(+)}(kq), \tag{3.12}$$

where the coefficients $t_l$ will turn out to be the diagonal elements of the T-matrix [63]. Inserting this into the above eq. (3.11), it splits into the two required parts: Expanding the two-dimensional plane wave into Bessel functions (see eq. (A.4)) and comparing it with the first part, we find that

$$c_l = i^l. \tag{3.13}$$

Using this relation and the asymptotic form of the Hankel function (eq. (A.5))

$$H_l^+(kq) \sim \sqrt{\frac{2}{i\pi k}} \frac{e^{i(kq - l\pi/2)}}{\sqrt{q}} \tag{3.14}$$

we recover the required asymptotic behaviour (3.10) for the wave function by setting

$$f(k,\theta',\theta) = f(k,\bar{\theta}) = -\sqrt{\frac{2i}{\pi k}} \sum_l t_l(k) e^{il\bar{\theta}} \tag{3.15}$$

for the scattering amplitude. It depends only on k and on the scattering angle $\bar{\theta}$ as a consequence of the rotational symmetry. We can also rewrite this in terms of Hankel functions of the first and second kind

$$R_l(kq) = \frac{1}{2}\left(H_l^{(-)}(kq) + s_l H_l^{(+)}(kq)\right) \tag{3.16}$$

by using $2J_l(z) = H_l^{(-)}(z) + H_l^{(+)}(z)$. Instead of the T-matrix we have here the diagonal form of the S-matrix via

$$s_l(k) := 1 - 2it_l(k) \tag{3.17}$$

and can now use the unitarity of the S-matrix to introduce the scattering phase shift in the final expression for the solution

$$\Psi(\vec{k},\vec{q}) = \sum_{l=-\infty}^{\infty} \frac{i^l}{2} \left( H_l^{(-)}(kq) + e^{2i\eta_l(k)} H_l^{(+)}(kq) \right) e^{il\bar{\theta}}. \tag{3.18}$$

The scattering phase shifts, i.e., the S-matrix, carry the whole scattering information and will thus be a central object later on. E.g., the total cross section as the square of the scattering amplitude $f(k,\theta,\theta')$ integrated over the outgoing angle $\theta'$

$$\sigma_{\text{tot}}(k) = \int d\theta' |f(k,\theta,\theta')|^2 = \int d\bar{\theta} |f(k,\bar{\theta})|^2 \tag{3.19}$$

can be expressed by the phase shifts (in general the total cross section is dependent on the incoming angle, but it is independent in radially symmetric cases). Using eq. (3.15) and the relation

$$t_l = \frac{1-s_l}{2i} = e^{i\eta_l} \frac{e^{-i\eta_l} - e^{i\eta_l}}{2i} = -e^{i\eta_l} \sin(\eta_l) \tag{3.20}$$

the cross section becomes

$$\sigma_{\text{tot}}(k) = \frac{4}{k} \sum_l \sin^2(\eta_l). \tag{3.21}$$

The main structure of the cross section is generally determined by the poles of the S-matrix in the complex energy or momentum plane. In special cases, they can be understood as physical bound states or resonances with a finite life time, but this is not always the case. Nevertheless we will talk of bound states in the case of poles on the positive imaginary momentum axis and of resonances in the case of poles in the fourth quadrant of the complex momentum plane (see, e.g., [72]). For a billiard the situation is different and the bound states are all located at the positive real axis. A pole of the S-matrix in the k-plane is equivalent to the condition

$$\cot \eta_l = i \tag{3.22}$$

for one of the phase shifts, which can be seen by eq. (3.20).

### 3.2.1 Finite Range Potentials

Due to the sharp boundary of the muffin tin, we can solve the Schrödinger equation inside and outside the muffin tin separately and choose the boundary conditions by glueing them together. Thus for the outside region we require the solution to follow the asymptotics of a scattering wave

$$\psi_{q>R}(\vec{k},\vec{q}) = \sum_{l=-\infty}^{\infty} i^l \left( J_l(kq) - it_l(k) H_l^{(+)}(kq) \right) e^{il\theta}, \tag{3.23}$$

according to the ansatz in eq. (3.12).

Inside the region, the potential is non-trivial and the ansatz

$$\psi_{q<R}(\vec{k},\vec{q}) = \sum_{l=-\infty}^{\infty} c_l R_l(kq) e^{il\theta} \tag{3.24}$$

leads to the following differential equation for the radial part of the wave function

$$\left(\frac{\partial^2}{\partial q^2} + \frac{1}{q}\frac{\partial}{\partial q}\right) R_l(kq) - \left(\mathcal{V}(q) - \mathcal{E} + \frac{l^2}{q^2}\right) R_l(kq) = 0. \tag{3.25}$$

To fulfill the final boundary condition on the rim of the muffin tin for the determination of the matrix elements $t_l(k)$, we can compare the two series (3.23) and (3.24) term by term. To retain a continuous and differentiable function we need to require

$$\psi_{q<R}(\vec{k},\vec{R}) = \psi_{q>R}(\vec{k},\vec{R}) \tag{3.26}$$

$$\frac{\partial}{\partial q}\psi_{q<R}(\vec{k},\vec{q})|_{q=R} = \frac{\partial}{\partial q}\psi_{q>R}(\vec{k},\vec{q})|_{q=R}. \tag{3.27}$$

Thus we have

$$t_l(k) = -i\left\{\frac{kJ_l'(kR) - J_l(kR)\,L_l(k)}{kH_l'^{(+)}(kR) - H_l^{(+)}(kR)L_l(k)}\right\}, \tag{3.28}$$

where we have used a short-hand notation for the logarithmic derivative

$$L_l(k) := \frac{\frac{\partial}{\partial q}R_l(kq)|_{q=R}}{R_l(kR)}. \tag{3.29}$$

The prime denotes the derivative with respect to the argument of the function. For the scattering phase shift this translates into the equation

$$\tan(\eta_l) = \left\{\frac{kJ_l'(kR) - J_l(kR)\,L_l(k)}{kN_l'(kR) - N_l(kR)\,L_l(k)}\right\}. \tag{3.30}$$

This is the form we shall use from now on. Before analyzing the truncated Coulomb potential we shall discuss a few features of two other examples to give an intuition for scattering properties in two dimensions. They can furthermore serve as integrable models in comparison to the chaotic muffin tin model.

As a first example we shall discuss the **square well potential.** We assume a constant attractive potential of depth $V(q) = -V_0$ for $\vec{q}$ inside the muffin tin. The differential equation (3.25) reduces to the Bessel differential equation with shifted energy $\tilde{\mathcal{E}} := \mathcal{E} -$

$\frac{2mV_0}{\hbar^2} = \tilde{k}^2$. Allowing only regular solutions at the origin, the solutions are the J-Bessel functions themselves and the equation for the phase shift turns out to be

$$\begin{aligned} \tan(\eta_l) &= \left\{ \frac{kJ_l'(kR)J_l(\tilde{k}R) - \tilde{k}\, J_l(kR)\, J_l'(\tilde{k}R)}{kN_l'(kR)J_l(\tilde{k}R) - \tilde{k}\, N_l(kR)\, J_l'(\tilde{k}R)} \right\} \\ &= \frac{J_l(kR)}{N_l(kR)} \left\{ \frac{kJ_l'(kR)/J_l(kR) - \tilde{k}\, J_l'(\tilde{k}R)/J_l(\tilde{k}R)}{kN_l'(kR)/N_l(kR) - \tilde{k}\, J_l'(\tilde{k}R)/J_l(\tilde{k}R)} \right\}. \end{aligned} \tag{3.31}$$

For $k \to \infty$, $k \approx \tilde{k}$ and the numerator in eq. (3.31) vanishes asymptotically. Thus the phase shift approaches a multiple of $\pi$. This is equivalent to saying that for high energies the T-matrix vanishes and the potential has less influence on the particle. By convention one usually defines the asymptotic phase shift to be vanishing

$$\eta_l(k) \to 0 \text{ for } k \to \infty. \tag{3.32}$$

When the energy approaches the threshold of zero energy, $\tilde{k} \approx \sqrt{V_0}$, the bracket in eq. (3.31) remains finite and the prefactor becomes the determining factor

$$\frac{J_l(kR)}{N_l(kR)} \approx \frac{\pi}{l} \left( \frac{kR}{2} \right)^{2l}, \tag{3.33}$$

as long as $l \neq 0$. Thus eq. (3.33) approaches zero as $k \to 0$. Again, $\eta_l$ becomes a multiple of $\pi$. But since we have fixed the high energy behaviour and the phase is completely continuous, the Levinson theorem holds

$$\eta_l(0) = m\pi, \tag{3.34}$$

where $m$ is the number of bound states for the quantum number $l$. In Fig. 3.1 we have plotted a few scattering phases for a very weak potential without any bound states.

One can see the resonances, whenever the phase exhibits a strong increase. Deepening the potential, one can watch these resonances wandering towards the threshold and eventually becoming a bound state. It is quite an interesting question to study the motion of resonances in the complex plane as a function of the potential strength, but very little is known.

The case $l = 0$ is somewhat special in two dimensions as the fraction in eq. (3.33) vanishes only logarithmically

$$\frac{J_0(kR)}{N_0(kR)} \approx \frac{\pi}{2} \left( \frac{1}{\ln(kR)} \right). \tag{3.35}$$

As a consequence the partial cross section for $l = 0$ diverges like $1/(k \ln^2(kR))$ as can be seen in Fig. 3.2. One can also see in Fig. 3.2 that the resonances are too short-lived to be detected in the cross section.

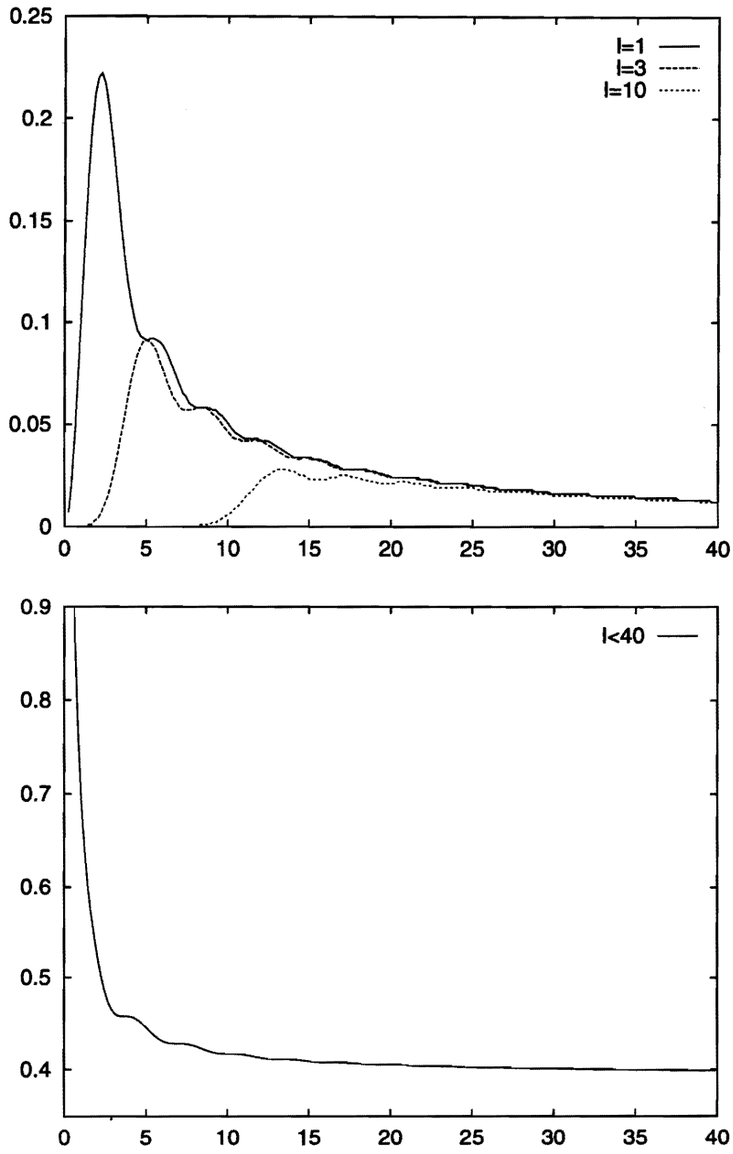


Figure 3.1: Scattering phase shift of the square well potential as a function of $k$. Above the phase shifts for the angular momenta $l = 1, 3, 10$ are shown separately, below one can see the sum up to l=40

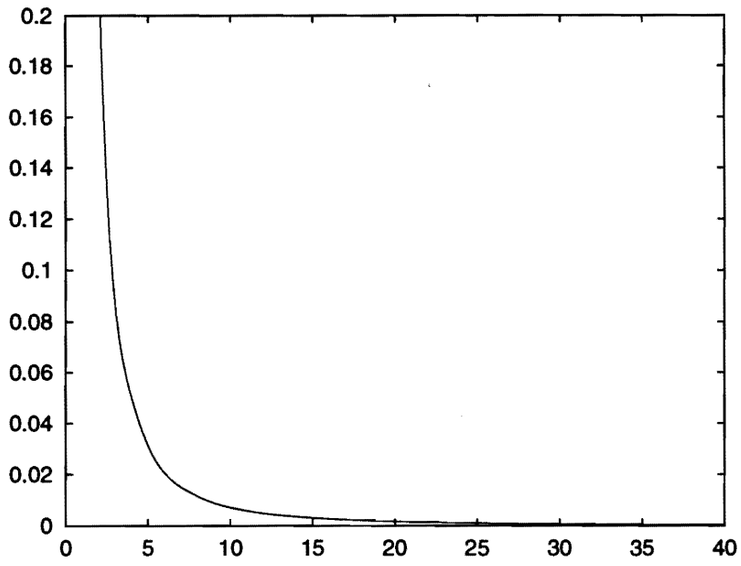


Figure 3.2: Scattering cross-section for the weak attractive square well potential

As for the **hard disc** (an infinitely high cylinder), our next example, the situation is somewhat different. Although it is not a true potential, one can use the same method for the reason that it has this sharp boundary. Requiring Dirichlet boundary conditions for the wave function on the rim, the logarithmic derivative becomes infinite and for the phase we get

$$\tan(\eta_l) = \frac{J_l(kR)}{N_l(kR)}. \tag{3.36}$$

The asymptotic behaviour of the phase for $k \to \infty$ is very different from the usual potential in that it never vanishes,

$$\eta_l(k) \approx -kR + (l+1)\pi/2 + (1/4)\pi \pmod{\pi}. \tag{3.37}$$

The "potential" is never switched off as the energy increases. For fixed energy though, only a finite number of phases differs from zero, since from the asymptotic behaviour for large order of the Bessel functions we find

$$\frac{J_l(kR)}{N_l(kR)} \approx \frac{1}{2}\left(\frac{ekR}{2l}\right)^{2l} \text{ for } l \to \infty, \tag{3.38}$$

which becomes very small for $kR > l$. The semiclassical argument reflected in this estimate is that only impact parameters smaller than the target size contribute. In Fig. 3.3 a few phases demonstrate this behaviour.

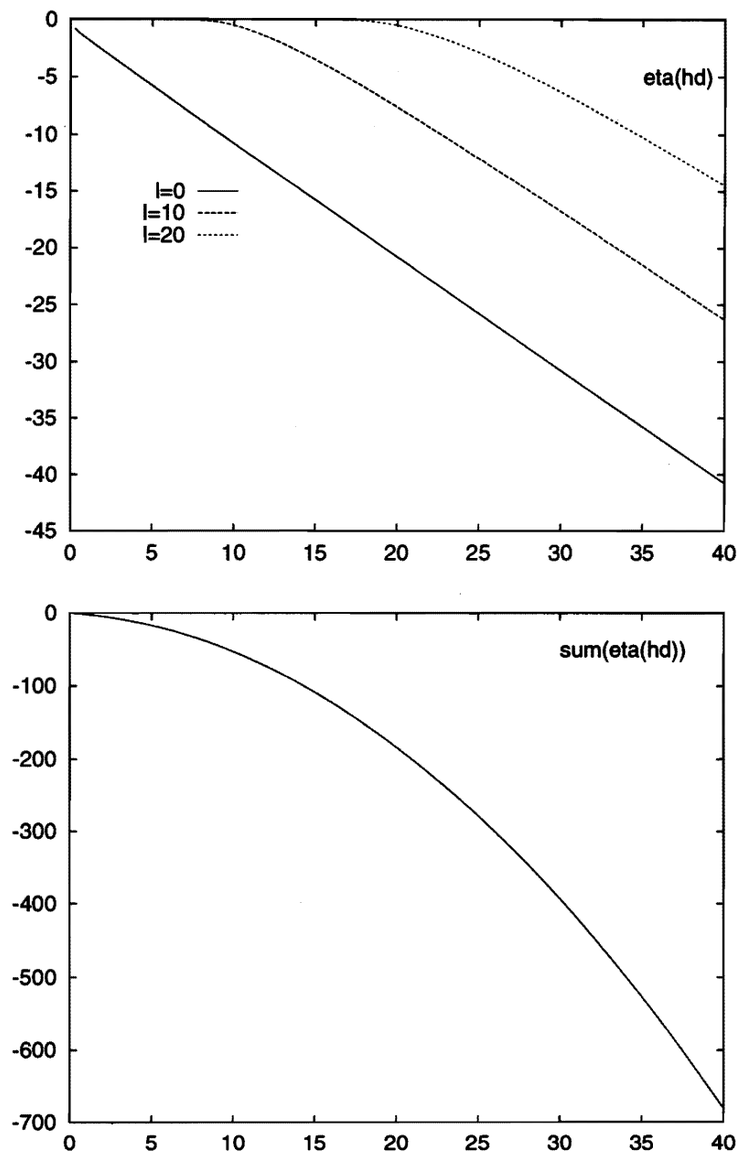


Figure 3.3: Scattering phase shift of the hard disc. One can see how the phases only set in for $l > kR$ ($R = 1$), above one can see the angular momenta 0,10 and 20 and below the sum up to l=40

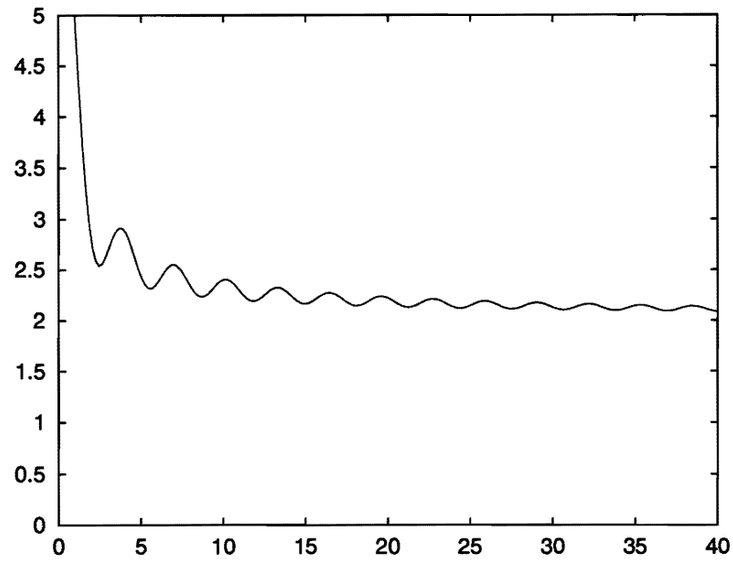


Figure 3.4: Scattering cross-section for the hard disc

For $k \to 0$ the situation is quite similar to the square well, only that in this case there can be no bound states. The cross section diverges again for the same reason. It does not vanish for high energies but approaches the classical size of the object, which is the diameter (see Fig. 3.4). This is different from the three dimensional case, where the high energy limit and the classical cross section differ by a factor of 2.

The S-matrix contains poles but they can hardly be understood as metastable states in case of the hard disc. The wiggles in the cross section can rather be seen as an interference effect.

Finally the **Coulomb potential** might be viewed as something in between the two examples, a potential that never switches off completely. To determine its properties, we observe that eq. (3.25) turns into the Whittaker equation for the reduced radial function

$$r_l(kq) := \sqrt{q} R_l(kq). \tag{3.39}$$

It is explicitly solved in terms of confluent hypergeometric functions. The general solution is a superposition of the two linearly independent solutions, one of which is irregular at the origin. Since we are interested in the region $q < R$, the wave function has to be regular at the origin and we are left with

$$\begin{aligned} R_l^C(kq) &= Cq^l e^{-ikq} F(-l + \tfrac{1}{2} - \kappa, -2l + 1; 2ikq) \\ &= \hat{C} \tfrac{1}{\sqrt{q}} M_{\kappa,l}(2ikq), \end{aligned} \tag{3.40}$$

where $\kappa = mZ/(\hbar^2 k)$ and $C, \hat{C}$ are some constants. In the case of the full Coulomb problem the behaviour of this solution is well studied, for positive as well as for negative

energies. For $\mathcal{E} < 0$ , $k$ is purely imaginary. The energy is discretized by the requirement for the solution to be square integrable. This can only be obtained by truncating the series expansion of the hypergeometric function, which happens whenever

$$l + \frac{1}{2} - \kappa = n \tag{3.41}$$

is a natural number. Therefore the energy values for bound states turn out to be

$$E_n = -\frac{mZ^2}{2\hbar^2(n + l + \frac{1}{2})^2}. \tag{3.42}$$

For positive energies the same solution becomes an infinitely ranged oscillating function as the wave number is real. This scattering function has the property of a phase shift logarithmically increasing with $q$ as a result of the infinite range (and slow decay) of $V(q)$. We do not have to worry about this as we truncate the potential at $q = R$. Further more we have to remember that we have lifted the Coulomb potential by an overall constant $\frac{Z}{R}$. This is equivalent to saying that inside the muffin tin we have an "effective" energy $\mathcal{E}' := \mathcal{E} - \frac{2mZ}{\hbar^2 R} = k'^2$. Thus the inside wave function for the Coulomb muffin tin finally reads

$$\psi_{q<R}(\vec{k}, \vec{q}) = \sum_{l=-\infty}^{\infty} c_l R_l^C(k'q) e^{il\theta}. \tag{3.43}$$

The logarithmic derivative can be calculated by using eq. (A.10) for the Whittaker function to be ($R = 1$)

$$L_l(k) = 2ik' \left( \frac{1}{2} - \frac{\kappa - 1/2}{2ik'} \right) + \left( \frac{1}{2} + l - \kappa \right) \frac{M_{\kappa+1,l}(2ik')}{M_{\kappa,l}(2ik')}. \tag{3.44}$$

An asymptotic behaviour is difficult to determine because of the oscillations of the Whittaker function. But for high energies, the potential comes closer to the shape of a $\delta-$function potential (cf. the Jacobi metric in chapter 2). The phase shifts decay for the $\delta-$potential as can be seen, e.g., by approximating it with a potential $V_\mu(q) = \sqrt{\mu/\pi} e^{-\mu q^2}$ and then letting $\mu \to \infty$. This is a limiting representation of the $\delta$-function. In the numerical calculation one can see the decay as well (Fig. 3.5). The routine is only able to produce reliable results up to $k \approx 30$. Down to the threshold, the behaviour is similar to that of the square well. In Fig. 3.5 we have chosen the same parameters as in chapter 2 ($Z = 8, m = R = \hbar = 1$) and find three bound states, two of which are degenerate (in fact they correspond to the three lowest eigenvalues (3.42) of the full potential, slightly shifted). Again, the resonances have a too short life-time to be seen in the cross section, except the first one (Fig. 3.6).

Notice that in all three cases, there is no special relation or dynamics among the eigenphases to different angular momenta. In fact they come arbitrary close to each other. This will be different for the chaotic case.

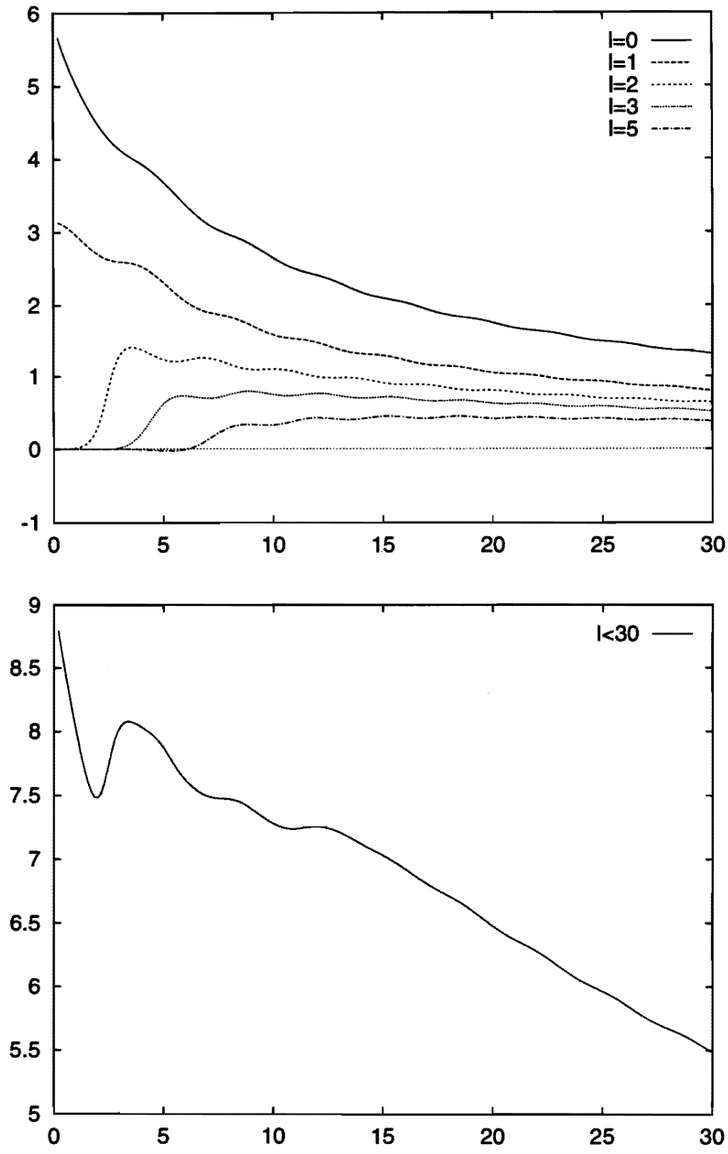


Figure 3.5: The Coulomb phase shift for selected angular momenta and below the sum up to $l = 30$. $l = 0$ and $l = 1$ show 2 bound states and 1 bound state respectively

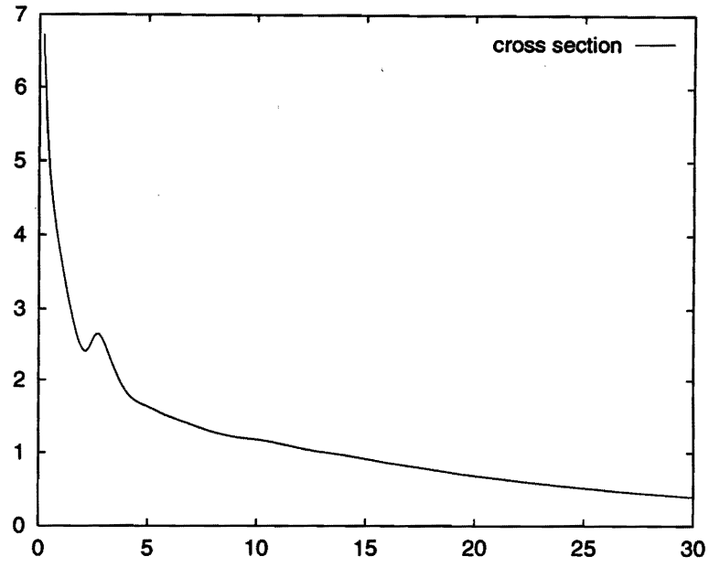


Figure 3.6: Scattering cross-section for the Coulomb potential

## 3.3 Muffin Tin Potentials

In the non-symmetrical case there is no such natural basis of functions, but we can use the angular momentum basis as well as any other basis for an expansion like the following

$$\begin{aligned}\Psi(\vec{k},\vec{q}) &= \sum_{l=-\infty}^{\infty} d_l \left[ J_l(\vec{k},\vec{q}) - i \sum_{l'} T_{ll'} H_{l'}^{(+)}(\vec{k},\vec{q}) \right] \\ &= \sum_{l=-\infty}^{\infty} \frac{d_l}{2} \left[ H_l^{(-)}(\vec{k},\vec{q}) + \sum_{l'} S_{ll'} H_{l'}^{(+)}(\vec{k},\vec{q}) \right].\end{aligned} \tag{3.45}$$

We have introduced a new notation for the J-Bessel function (and similarly the Hankel function) by defining

$$J_l(\vec{k},\vec{q}) := J_l(kq) e^{il\bar{\theta}}, \tag{3.46}$$

where $\bar{\theta}$ is the angle between $\vec{k}$ and $\vec{q}$. The T-matrix is not diagonal anymore, but the asymptotic behaviour is still reproduced in a similar manner as in eq. (3.15), the sum being replaced by a double sum. But as the S-matrix is still unitary, because of the probability conservation in elastic scattering, it is diagonalizable by the eigenvalue equation

$$\sum_{l'} S_{ll'} A_{l'\lambda} = s_\lambda A_{l\lambda} = e^{2i\eta_\lambda} A_{l\lambda}. \tag{3.47}$$

Since the matrix is unitary, the eigenvectors, labeled by the index of the eigenvalues

$\lambda$, obey the orthogonality relation

$$\sum_l A^\dagger_{l\lambda} A_{l\lambda'} = \sum_l A^*_{\lambda l} A_{l\lambda'} = \delta_{\lambda\lambda'} \tag{3.48}$$

and the completeness relation

$$\sum_\lambda A_{l\lambda} A^*_{\lambda l'} = \delta_{ll'}. \tag{3.49}$$

The full matrix can therefore be transformed via the similarity transformation

$$S_{ll'} = \sum_\lambda A_{l\lambda} s_\lambda A^*_{\lambda l'}. \tag{3.50}$$

Thus we can insert into the expansion (3.45) a Kronecker symbol and get

$$\begin{aligned} \Psi(\vec{k},\vec{q}) &= \sum_{l,l'} d_l \delta_{l,l'} \Psi_{l'}(\vec{k},\vec{q}) \\ &= \sum_{l,l'\lambda} d_l A_{l\lambda} A^*_{\lambda l'} \Psi_{l'}(\vec{k},\vec{q}) \\ &= \sum_\lambda \tilde{d}_\lambda \tilde{\Psi}_\lambda(\vec{k},\vec{q}) \end{aligned} \tag{3.51}$$

using the definitions

$$\tilde{d}_\lambda := \sum_l d_l A_{l\lambda} \tag{3.52}$$

and

$$\tilde{\Psi}_\lambda(\vec{k},\vec{q}) = \sum_{l'} \frac{1}{2} A^*_{\lambda l'} \left( H^{(-)}_{l'}(\vec{k},\vec{q}) + s_\lambda H^{(+)}_{l'}(\vec{k},\vec{q}) \right). \tag{3.53}$$

This form is now the analogous expansion to the partial wave expansion above. It contains a diagonal representation of the S-matrix and thus a direct connection to a generalized phase shift.

The muffin tin potential is non-symmetric in general. Our aim is now to reduce the integral equation (3.4) to an algebraic equation by relating the full phase shift to the single scatterer phase shifts. In principle this will enable us to determine the wave function of the system, but we shall restrict ourselves to finding the resonance energies and the eigenphases of the S-matrix.

The derivation of the equation is an extended KKR-method, named after the authors Korringa, Kohn and Rostocker [68], who first developed these ideas for periodic potentials. For the case of two dimensions periodic arrangements have been studied in [65]. John and Ziesche [66] extended the principles to general muffin tin potentials in 3 dimensions, where the muffin tins are arbitrarily distributed in configuration space (see also [67]). We are going to derive the analogous condition for two dimensions.

Take for example a scenario pictured in Fig. 1.1. Each circle in the two dimensional configuration space represents a region of non-vanishing interaction, whereas everywhere

else the potential is identically zero. The different shadowing implies that the potentials may vary in type and strength. We assume that for each muffin tin as a single scatterer, the S-matrix is known, i.e. all scattering phase shifts are given. For simplicity all muffin tins are taken to be circular symmetric, although this is not a necessary restriction to the method. Their S-matrix is thus diagonal in an angular momentum basis. The center of the circle $i$ with radius $R_i$ lies on the point $\vec{s}_i$. The notation is the same as in chapter 2.

Therefore we can start with an ansatz by expanding again in terms of partial waves. According to eq. (3.53) our ansatz for the generalized partial wave expansion is a superposition of scattering solutions centered at the single scatterers

$$\Psi_\lambda = \sum_{i=1}^{N} \sum_{l=-\infty}^{\infty} a_{il} \left( H_l^{(-)}(\vec{k}, \vec{q}_i) + e^{2i\eta_\lambda} H_l^{(+)}(\vec{k}, \vec{q}_i) \right). \tag{3.54}$$

We have dropped the tilde and the arguments of the wave function. The solution is expressed in terms of the local coordinates $\vec{q}_i = \vec{q} - \vec{s}_i$. In the direct surrounding of a muffin tin, the solution can also be expressed in terms of a superposition of local scattering solutions. Thus in the vicinity of muffin tin with label $j$, we can expand

$$\Psi^j = \sum_{l'=-\infty}^{\infty} b_{jl'} \left( H_{l'}^{(-)}(\vec{k}, \vec{q}_j) + e^{2i\eta_{l'}^j} H_{l'}^{(+)}(\vec{k}, \vec{q}_j) \right), \tag{3.55}$$

with coefficients $b_{jl'}$ to be determined below.

In the immediate surrounding of the muffin tin $j$ the two represenetations resemble the same function, i.e.,

$$\Psi_\lambda = \Psi^j. \tag{3.56}$$

Now we exploit the addition theorems for Hankel functions again (cf. eq. (A.3)) and rewrite equation (3.54) in terms of the basis in (3.55). That is to say, we need to transform the Hankel functions in terms of the local coordinates $\vec{q}_i$ into the local coordinates $\vec{q}_j$. We therefore split $\vec{q}_i = \vec{q}_j - (\vec{s}_i - \vec{s}_j)$. The addition theorem is valid under the restriction $q_j \leq |\vec{s}_j - \vec{s}_i|$, i.e., that we remain in the space between the muffin tins, but the eigenphases we are interested in are of course valid also in the far distance. Splitting the Hankel functions into Bessel- and Neumann-functions, we get for eq. (3.54)

$$\begin{aligned} \Psi_\lambda &= \sum_{il} \sum_{l'} 2\, a_{il} e^{i\eta_\lambda} \left( (J_{ll'}^{ij}(k) \cos(\eta_\lambda) - \sin(\eta_\lambda) N_{ll'}^{ij}(k))\, J_{l'}(\vec{k}, \vec{q}_j) \right. \\ &- \left. \delta_{ij}\delta_{ll'} \sin(\eta_\lambda) N_{l'}(\vec{k}, \vec{q}_j) \right). \end{aligned} \tag{3.57}$$

We have adopted here the following definitions for the coefficient matrices

$$\begin{aligned} J_{ll'}^{ij}(k) &:= J_{l-l'}(k|\vec{s}_i - \vec{s}_j|) e^{i(l-l')\phi_{ij}} \\ N_{ll'}^{ij}(k) &:= (1 - \delta_{ij}) N_{l-l'}(k|\vec{s}_i - \vec{s}_j|) e^{i(l-l')\phi_{ij}}, \end{aligned} \tag{3.58}$$

where $\phi_{ij}$ is the angle of the relative vector $\vec{s}_{ij} := \vec{s}_i - \vec{s}_j$ with respect to the $x$-axis of the configuration space. Note that these matrices are hermitian: The interchange of $i$ and $j$ yields a factor $(-1)^{l-l'}$ via

$$e^{i(l-l')\phi_{ji}} = e^{i(l-l')(\phi_{ij}+\pi)} = (-1)^{l-l'} e^{i(l-l')\phi_{ij}}, \tag{3.59}$$

which is exactly compensated by changing the sign in the order of the special function

$$J_{l-l'}(kq) = (-1)^{l-l'} J_{l'-l}(kq). \tag{3.60}$$

Only a complex conjugation remains in the exponential of eq. (3.59). Rewriting equation (3.55) in a similar manner we have

$$\Psi^j = \sum_{l'} 2\, b_{jl'} e^{i\eta^j_{l'}} \left(\cos(\eta^j_{l'}) J_{l'}(kq_j) - \sin(\eta^j_{l'}) N_{l'}(kq_j)\right) e^{il'\phi_{q_j}}. \tag{3.61}$$

Comparing the coefficients in front of the Neumann functions in eq. (3.57) and (3.61) we can eliminate the constants $b_{jl'}$ by

$$b_{jl'} = \delta_{ij}\delta_{ll'} e^{i(\eta_\lambda - \eta^j_{l'})} \frac{\sin(\eta_\lambda)}{\sin(\eta^j_{l'})} a_{il}. \tag{3.62}$$

Thus replacing these in the coefficients for the Bessel-functions and removing an overall factor $2e^{i\eta_\lambda}\sin(\eta_\lambda)$ we find that the determination of the vector $a_{il}$, i.e., eq. (3.56) reduces to solving the equation

$$\sum_{il} \left[J^{ij}_{ll'}(k)\cot(\eta_\lambda) - N^{ij}_{ll'}(k) - \delta_{ij}\delta_{ll'}\cot(\eta^i_l)\right] a_{il} = 0. \tag{3.63}$$

For this equation to have non-trivial solutions, the determinant of the matrix must vanish. Expressing the matrices as bold face letters and dropping thus the indices

$$\begin{aligned} \mathbf{J}(k) &:= J^{ij}_{ll'}(k) \\ \mathbf{N}(k) &:= N^{ij}_{ll'}(k) \\ \mathbf{C}(k) &:= \delta_{ij}\delta_{ll'}\cot(\eta^i_l), \end{aligned}$$

the secular equation reads

$$\boxed{\det\left|\mathbf{J}(k)\cot(\eta_\lambda) - \mathbf{N}(k) - \mathbf{C}(k)\right| = 0}. \tag{3.64}$$

This way we find all the solutions $\cot(\eta_\lambda)$, i.e. all the eigenphases of the S-matrix, for a given momentum $k$.

Before we go on we would like to point out a few properties of the matrix in eq. (3.64). First of all, the matrix is in principle (bi-)infinite dimensional. But as the indices $l, l'$ describe the relative angular momenta to the individual single scatterers, it is reduced

to an effectively finite dimensional one by the above mentioned semiclassical argument that only angular momenta maximally of the order of $l \approx kR$ contribute, where $k$ is the momentum and $R$ the (maximal) radius of a muffin tin. The numerical confirmation can be found by a similar estimate as in eq. (3.38). It becomes relevant far away from the diagonal $l = l'$. For the case of N muffin tins the matrix in eq. (3.64) is effectively $N \times (2l+1)$-dimensional.

The next remark is concerned with the physical meaning of the matrix. Using the relation $\cot(\eta_\lambda) - i = 2i(\exp(2i\eta_\lambda) - 1)^{-1} = 2i(s_\lambda - 1)^{-1}$, we can rewrite eq. (3.63) to

$$\left(\mathbf{1} - 2i\left[i\mathbf{H}^{(+)}(k) - \mathbf{C}(k)\right]^{-1}\mathbf{J}(k)\right)a = s_\lambda a. \tag{3.65}$$

We have combined the above defined matrices analogous to the definition of Hankel function to define

$$\mathbf{H}^{(+)}(k) = \mathbf{J}(k) + i\mathbf{N}(k) \tag{3.66}$$

Thus the left-hand side of the equation is a representation of the S-matrix. Furthermore, the square bracket can be identified as the inverse of the T-matrix. This matrix is constructed by the scattering information of a single muffin tin (in form of the inverse of the reactance matrix $k_l^i = -\tan(\eta_l^i) = (s_l^i - 1)/(s_l^i + 1)$) and their geometric arrangement. To find the eigenphases, we need to find the eigenvalues of the left hand side. The only poles, i.e., resonances, this representation can exhibit, are given, whenever

$$\det|(i\mathbf{H}^{(+)}(k) - \mathbf{C}(k))| = 0, \tag{3.67}$$

since the Bessel function is holomorphic in the complex plane. This condition is equivalent to setting $\cot(\eta_\lambda) = i$ in eq. (3.64) as mentioned above in eq. (3.22).

The search for eigenphases can be reformulated into a variational principle, which provides a few useful information. Multiplying in eq. (3.63) the transpose of the vector $a_{il}$ from the left, we can express the eigenphases by

$$\cot(\eta_\lambda) = \frac{a^\dagger(\mathbf{N}(k) + \mathbf{C}(k))a}{a^\dagger\mathbf{J}(k)a}. \tag{3.68}$$

The eigenvectors are eigenvectors to the unitary matrix in eq. (3.65) and therefore form an orthonormal basis and live on the unit sphere. On the other hand a hermitian matrix as the one in the eq.s (3.64) and (3.68) extremizes on the unit sphere exactly for eigenvectors [69]. Thus a variation of eq. (3.68) with respect to the vectors $a$ should vanish for eigenvectors.

The denominator in eq. (3.68) is strictly positive for eigenvectors as can be seen by

$$\begin{aligned}\sum_{il}\sum_{jl'}(a_{jl'})^\dagger J^{ij}_{l'l}a_{il} &= \sum_{il}\sum_{jl'}\sum_{l''}(a_{jl'})^\dagger J^{0j}_{l'l''}J^{i0}_{l''l}a_{il} \\ &= \sum_{l''}\left|\sum_{il}J^{i0}_{l''l}a_{il}\right|^2 > 0\end{aligned} \tag{3.69}$$

as long as the vector $a$ does not vanish (they are of unit length). We have used the addition theorem for Bessel functions again and defined in analogy to (3.58)

$$J^{i0}_{ll'}(k) := J_{l-l'}(k|\vec{s}_i|)e^{i(l-l')\phi_i}. \tag{3.70}$$

Eq. (3.68) and eq. (3.69) lead to an interesting fact. The only poles that can arise in eq. (3.68) for real positive values of $k$ have to come from poles of at least one of the $\cot(\eta^i_l)$. Therefore $\eta_\lambda$ reaches a multiple of $\pi$ (or zero) only simultaneously with at least one of the $\eta^i_l$. One could say that the $\eta^i_l$ define corridors in which the $\eta_\lambda$ have to reside.

## 3.4 Scattering Phases and the Number of States

For bounded systems the density of states is related to the Green's operator via

$$d(E) = -\frac{1}{\pi}\mathrm{Im}\,\mathrm{Tr}G(E) = \int d^2q\,\rho(\vec{q},E), \tag{3.71}$$

where we have added the explicit dependence on energy in the argument of the Green's function this time. In this representation of the Green's operator the trace denotes the integration over the whole available coordinate space, i.e., the integral over the local density of states. Thus we obtain the full density of states as a sum over delta-functions that peak at the energy eigenvalues.

For open systems, this quantity is infinite, since the spectrum is continuous. Nevertheless some structure in the energy dependence of the Green's function is left, created by the states with finite life-time, the resonances. To exhibit this structure for real positive energies, we need to regularize the Green's function. The most common and intuitive method is to surround the system by a box with radius $D$, subtract the free Green's function inside the box and finally let the size of the box approach infinity. One can show that such a procedure leads to the relation [70, 71] (in the mathematical literature known as Krein's trace formula)

$$-\lim_{D\to\infty}\mathrm{Im}\,\mathrm{Tr}\left(G^+_D(E) - G^{+0}_D(E)\right) = \frac{1}{2i}\,\mathrm{Tr}\left(\mathbf{S}^{-1}\frac{\partial \mathbf{S}}{\partial E}\right), \tag{3.72}$$

where $\mathbf{S}$ denotes the S-matrix of the whole system. As long as there are no bounded states imbedded in the continuous spectrum, this quantity does not allow the interpretation as the density of states anymore. In the context of the time-dependent scattering formulation, one can see that it causes a retardation of the phase of the outgoing wave function. For this reason it is called the time-delay, although this is more a qualitative name rather than a quantitative measure for the actual delay time of a scattering wave packet (see, e.g., [63]).

To express the sum over eigenphases in terms of the single scatterer data, we use the KKR-representation of eq. (3.65). First we notice that

$$\ln\det\left(\frac{\mathbf{S}-\mathbf{1}}{2i}\right) = \ln\det(e^{i\eta_\lambda}\sin(\eta_\lambda)) = i\sum_\lambda \eta_\lambda + \sum_\lambda \ln\sin(\eta_\lambda). \tag{3.73}$$

On the other hand we have

$$\begin{aligned}
\ln\det\left(\frac{\mathbf{S}-\mathbf{1}}{2i}\right) &= \ln\det(\mathbf{J}(k)) - \ln\det\left((\mathbf{C}(k) - i\mathbf{H}^{(+)}(k)\right) \\
&= \ln\det(\mathbf{J}(k)) - \ln\det\left((\mathbf{C}(k) - i\mathbf{1} - i\tilde{\mathbf{H}}^{(+)}(k)\right) \\
&= \ln\det(\mathbf{J}(k)) + \ln\det(\mathbf{C}(k) - i\mathbf{1}) \\
&\quad - \ln\det\left(\mathbf{1} + i\mathbf{T}(k)\tilde{\mathbf{H}}^{(+)}(k)\right) \\
&= \ln\det(\mathbf{J}(k)) + i\sum_{i,l}\eta_l^i + \sum_{i,l}\ln\sin(\eta_l^i) \\
&\quad - \ln\det\left(\mathbf{1} + i\mathbf{T}\tilde{\mathbf{H}}^{(+)}(k)\right),
\end{aligned} \tag{3.74}$$

where the definition of the new notations are

$$\begin{aligned}
\tilde{\mathbf{H}}^{(+)}(k) &:= (1-\delta_{ij})\left[J_{ll'}^{ij}(k) + iN_{ll'}^{ij}(k)\right] \\
\mathbf{T}(k) &:= -(\mathbf{C}(k) - i\mathbf{1})^{-1}.
\end{aligned} \tag{3.75}$$

Taking the imaginary part of the two equations one finds that

$$\sum_\lambda \eta_\lambda + \mathrm{Im}\sum_\lambda \ln\sin(\eta_\lambda) = \sum_{i,l}\eta_l^i + \mathrm{Im}\sum_{i,l}\ln\sin(\eta_l^i) + \mathrm{Im}\ln\det\left(\mathbf{1} + i\mathbf{T}\tilde{\mathbf{H}}^{(+)}(k)\right). \tag{3.76}$$

The second term on the left only contributes, when the argument of the logarithm vanishes. According to the observation below eqs. (3.68) and (3.69) that the eigenphases of the full system and the single scatterer reach $\pi$ simultaneously, this contribution cancels the second term on the right hand side. Thus we end up with an expression for the sum over eigenphases of the following form

$$\boxed{\sum_\lambda \eta_\lambda = \sum_{l,i}\eta_l^i + \mathrm{Im}\ln\det\left(\mathbf{1} + i\mathbf{T}\tilde{\mathbf{H}}^{(+)}(k)\right)}. \tag{3.77}$$

This quantity is the analogue to the counting function for the number of states in bounded systems, $N(E)$. If there were bound states embedded in the continuum, which is quite possible since the formalism is valid for very general situations, their number would be counted by $\frac{1}{\pi}\sum_\lambda \eta_\lambda$. The number of resonances though is not reflected here, as the phase does not always rise by $\pi/2$ as is often assumed in the heuristic discussions of resonance phenomena. The number of resonances has to be counted in the complex momentum plane, i.e., by a function $N(K)$ that counts the number in a circle of given

radius $K$. There is very little known about this function and no analytical expression. A few asymptotic estimates were given by mathematicians only recently [34, 35, 36].

An interesting point to notice in eq. (3.77) is the splitting into a part that only depends on the eigenphases of the individual muffin tins and a part that contains the geometry of the specific arrangement. It has the form of the determinant of some transfer matrix, which is an often encountered structure in quantum chaos. We shall see in the next chapter that these parts can naturally be associated with the smooth and the oscillating part in the semiclassical approximation.

### 3.4.1 Statistics of Eigenphases

The question in this general setting is now to mark specific characteristics of quantum chaoticity. Therefore we use three Coulomb potentials as this has been shown to be classically chaotic in the second chapter. The method is to study the statistical properties of a given spectrum. In general the method allows to take any potential inside the muffin tins, especially hard discs as well. These have been studied extensively before [61, 47]. But some of the analysis on eigenphases done here has not been discussed for the hard disc system and should be interesting. We use the literature on the resonances of the hard discs as a check for our numerical calculations.

The natural spectrum given in a scattering system is the spectrum of eigenphases. The most commonly discussed measures are the level spacing distribution of nearest neighbour levels as a short range property and the number variance or the spectral rigidity for long range correlations. These functions have widely been studied for energy levels of bounded systems but not so much for eigenphases. In Fig. 3.9 one can see an example of a spectrum of 153 eigenphases taken at the momentum $k = 30$. We have plotted the number of eigenphases below some given value $\eta$. There seem to be only phases between 0 and $\pi/2$. They could not cross either of the boundaries 0 and $\pi$ because the eigenphases of each muffin tin do not cross it either (cf. Fig. 3.5). This is about the maximum number of eigenphases we can achieve for a given momentum $k$, because this corresponds to an angular momentum of about $l = 25$ ($R = 1$), above which the routine for the Whittaker function is not reliable anymore. The dimension of the matrix is thus $3(2l + 1) = 153$.

Fig. 3.7 and 3.8 we show a few phases as a function of the momentum for the symmetric and the asymmetric triangle respectively. We show a small sector at small momentum only, because it is quite messy around 0, as many eigenphases only start to deviate from zero. The essential features can be seen here: Whereas in the symmetric case a few of the phases exhibit repulsion and a few cross each other, the asymmetric picture shows only level repulsion. The crossing of levels is due to the group of discrete symmetries left in the equilateral triangle. Therefore the S-matrix is still reducible and the spectra of the different representations overlap. In the absence of symmetries, there is no degeneracy in the levels and thus level repulsion.

To find general features for chaotic systems and make more quantitative statements

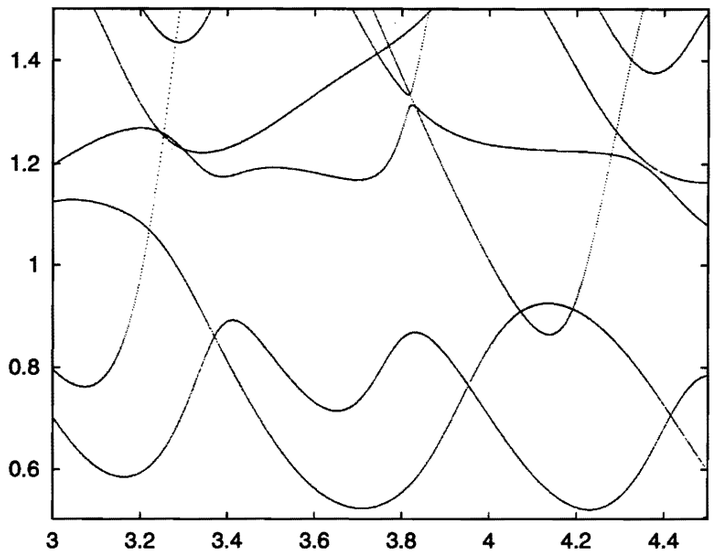


Figure 3.7: Dynamics of eigenphases as a function of the momentum $k$ for a symmetric triangle

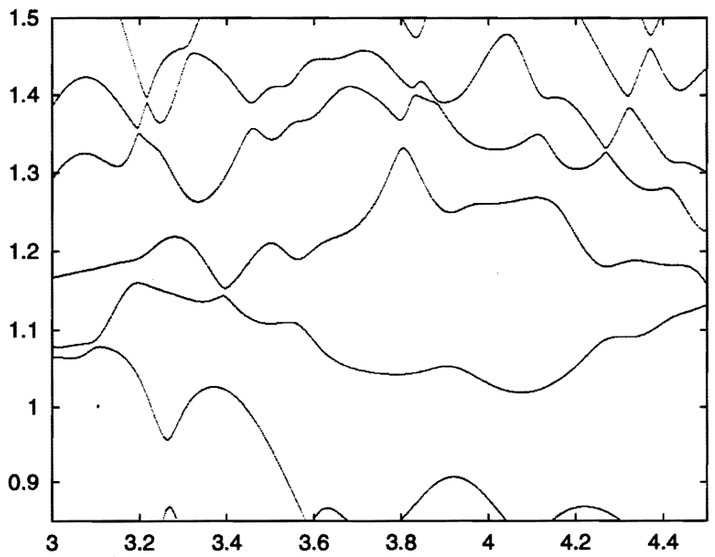


Figure 3.8: Dynamics of eigenphases as a function of $k$ for an asymmetric triangle

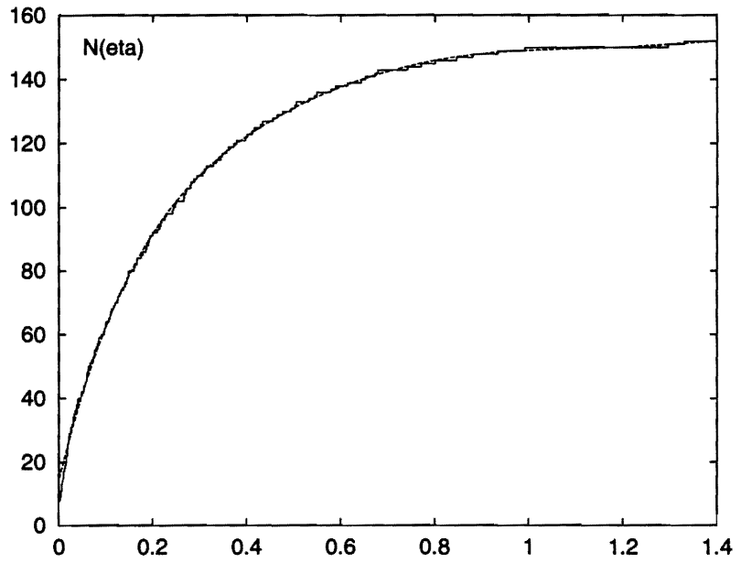


Figure 3.9: An example for the staircase function $N(\eta)$ of eigenphases at $k = 30, l = 25$. The dashes line shows the polynomial fit. Most of the eigenphases calculated are found near 0, because they just start to become relevant.

of this observation one needs to unfold the spectrum to achieve a comparable scale for different systems. This is done by transforming the mean density of eigenvalues to unity. In bounded system the asymptotic behaviour of the mean density of states is given by Weyl's law (or what is called the Thomas-Fermi approximation for potentials) and the unfolding is a well defined procedure. In this case there is no such analogue and we have to fit the mean behaviour. The dashed line in Fig. 3.9 shows a fit with a polynom of degree seven. Defining the unfolded spectrum via

$$\eta_i' := \bar{N}(\eta_i) \tag{3.78}$$

fulfills the requirement, since the mean spacing of eigenphases

$$< \Delta\eta' >=< \eta_i' - \eta_{i-1}' >=< \bar{N}(\eta_i) - \bar{N}(\eta_{i-1}) >= 1 \tag{3.79}$$

equals unity by construction (we have changed the counting index to $i$). The unfolded spectrum is compared to the line $y = x$ in Fig. 3.10. Next to it in Fig. 3.11 we have plotted a spectrum of 400 random numbers chosen from the interval $[0, 400]$. Although the spectrum of eigenphases looks quite random at the first place, there is an obvious difference to the truly random numbers. To see this we will use the above statistical measures, which were introduced by the theory of random matrices (RMT). We shall give a brief idea of this theory to discuss its results for our specific case.

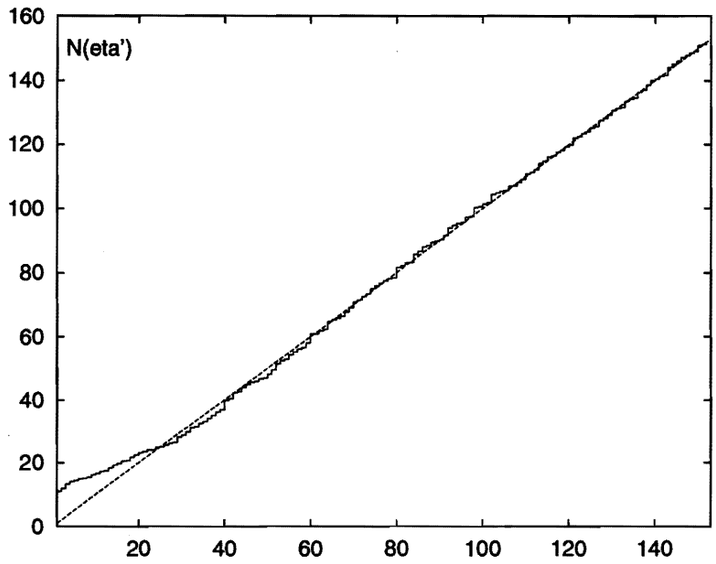


Figure 3.10: The same staircase function, now unfolded. The dashed line is the mean behaviour, which by construction is the function $y = x$

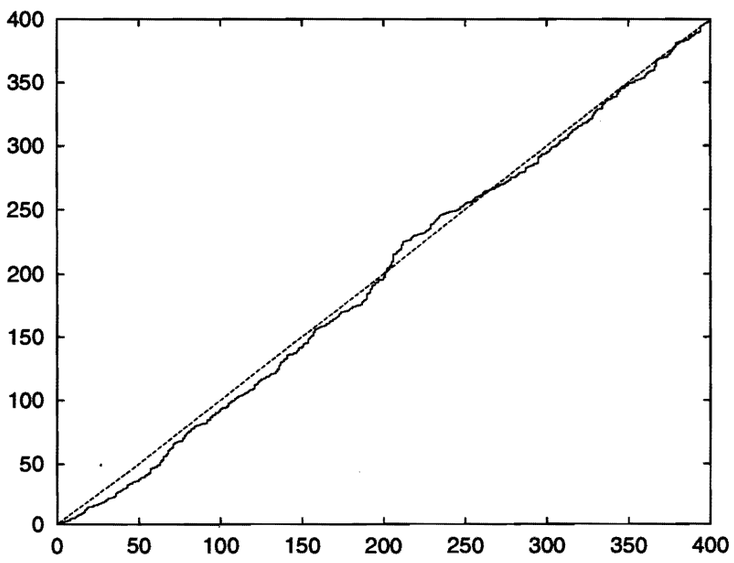


Figure 3.11: For a comparison: a random spectrum calculated by 400 random numbers between 0 and 400. It oscillates much more from its mean behaviour, which is given by the line y=x

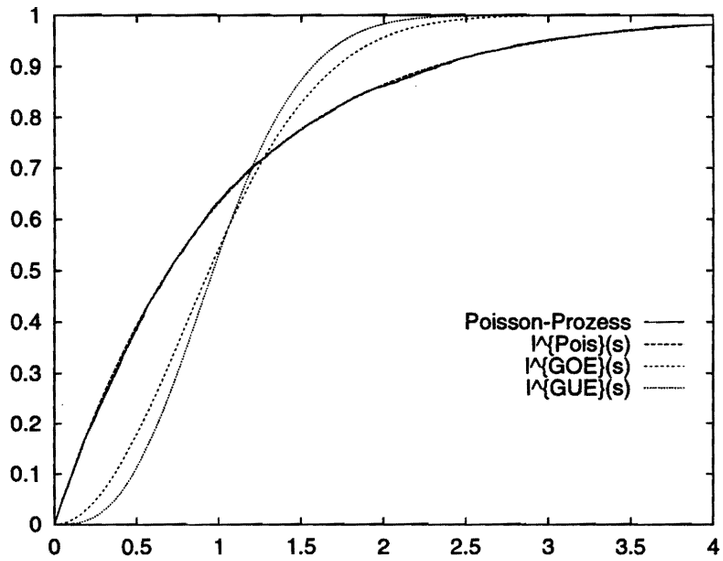


Figure 3.12: Integrated nearest-neighbour statistics $I(s)$ for 5000 random numbers. It follows the Poissonian statistics quite nicely.

The aim of RMT was to obtain results about complicated quantum mechanical systems using a minimum knowledge about the underlying dynamics. The system was assumed to be complex enough that an ensemble of matrices with random entries gives a good account of the situation. To model the Hamiltonian one needs to take an ensemble of hermitian matrices (called a Gaussian ensemble, since the entries are taken to obey a Gaussian distribution) or for the S-matrix it is a set of unitary matrices (called a circular ensemble, because the eigenvalues all lie on a circle). One can further distinguish the results by using the knowledge of a few basic symmetries. In a situation that is invariant under time reversal, the results have to be independent under the group of orthogonal transformations. For broken time reversal symmetry, like, e.g., in the presence of a magnetic field, this is replaced by unitary transformations. According to the situation, the ensembles to be applied are called orthogonal ensembles (GOE or COE) and unitary ensembles (GUE or CUE) respectively. We shall compare our results to those if appropriate.

The first quantity we will look at is the level spacing distribution of neighbouring levels. Let $P(s)ds$ be the probability of two neighbouring eigenphases to be separated by a distance between $s$ and $s + ds$. The theoretical predictions made by RMT can be described very well by the distributions

$$P^{\mathrm{GOE}}(s) = P^{\mathrm{COE}}(s) \approx \frac{\pi}{2} s\, e^{-(\pi/4)s^2}, \tag{3.80}$$

and for the case of broken time reversal symmetry by

$$P^{\mathrm{GUE}}(s) = P^{\mathrm{CUE}}(s) \approx \frac{32}{\pi^2} s^2 \, e^{-(4/\pi)s^2}. \tag{3.81}$$

The level spacing statistics for the Gaussian and for circular ensembles coincide. In contrast to this expectation for chaotic systems, the level spacing for integrable systems is expected to follow a Poissonian statistics

$$P^{\mathrm{Pois}}(s) = e^{-s}. \tag{3.82}$$

The argument for this expectation is as follows. The integrable case is characterized by the existence of a number of symmetries, all of which yield a spectrum according to their quantum numbers. These spectra overlap independently. Therefore degeneracies are much more possible ($P^{Pois}(0) = 1$) than in the RMT distributions ($P^{\mathrm{GOE/GUE}}(0) = 0$). The latter phenomenon is called level repulsion.

The numerical examination of this quantity is very much dependent on the choice of the binsize. Therefore we will look at the integrated probability

$$I(s) = \int_0^s P(s')ds' \tag{3.83}$$

to get rid of this freedom of choice. The formulas then translate to

$$\begin{aligned} I^{\mathrm{GOE}}(s) &\approx 1 - e^{-(\pi/4)s^2} \\ I^{\mathrm{GUE}}(s) &\approx \mathrm{erf}\left(\tfrac{2s}{\sqrt{\pi}}\right) - \tfrac{4s}{\pi} e^{-(4/\pi)s^2} \\ I^{\mathrm{Pois}}(s) &= 1 - e^{-s}. \end{aligned} \tag{3.84}$$

In Fig. 3.12 we have taken 5000 random numbers. One can see, how well it approaches the curve expected for a Poissonian process. The main feature being that small distances are the most probable ones, as $I(s)$ has its strongest increase there. The other curves are the predictions for the GOE and GUE.

Fig. 3.13 displays the behaviour of the eigenphases for the slightly asymmetric configuration shown in Fig. 2.4 in chapter 2. It is quite surprising in the first moment that it seems to be Poissonian as well and there is no level repulsion, which is generally expected in quantum chaotic systems. This is independent of the energy, since it is similar for smaller energies (see Fig. 3.14). It is a consequence of the almost conserved discrete symmetry of this particular situation. Whereas in the classical case the lengths spectrum of periodic orbits immediately lost all resemblance to the symmetric situation after slightly destroying the symmetry, the quantum mechanics still seems to recover it. The degeneracy of eigenphases due to the fact that the S-matrix is still reducible in the symmetric triangle is still present. In Fig. 3.15 the triangle is distorted to angles with $20, 60$ and $100$ degrees and one can see in Fig. 3.8 how the level repulsion sets in. But even then, the

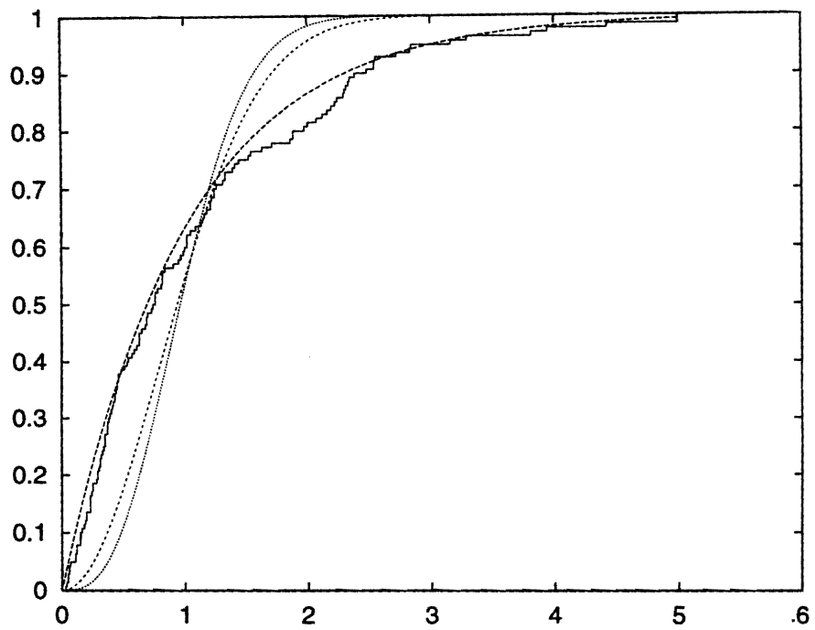


Figure 3.13: Integrated nearest-neighbour statistics $I(s)$ for eigenphases. Here, 153 eigenphases are included, evaluated at the momentum $k = 30$. The configuration is only slightly asymmetric and hence the level repulsion is still weak.

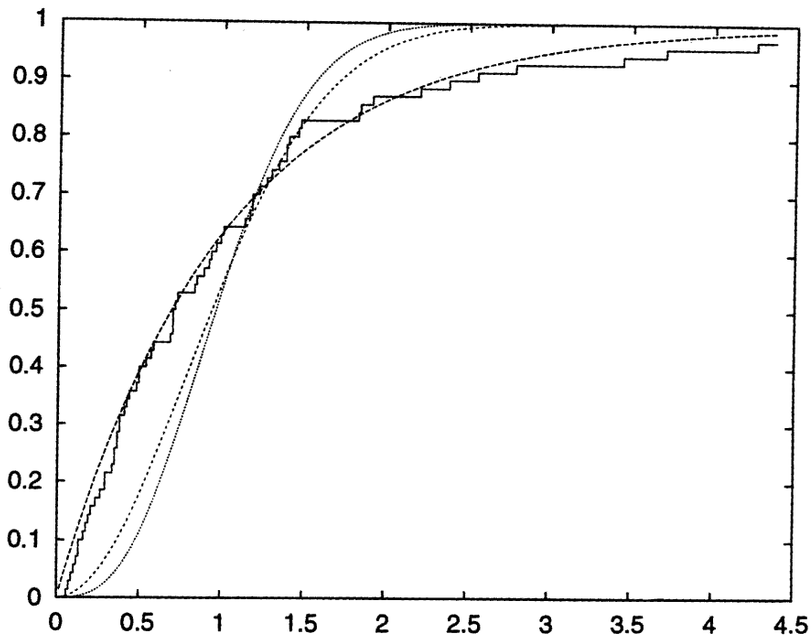


Figure 3.14: $I(s)$ for eigenphases at $k = 20$, where the effective dimension of the S-matrix is only 70

behaviour of the random matrix ensemble is not quite reproduced. This might as well be a problem of the poor statistics based only on 150 phases.

The next quantity we shall look at, the number variance $\Sigma^2(L)$, provides a measure for long-range correlations in the spectrum. It is defined as the average deviation of the number of levels $n(\eta, L)$ in an interval of length $L$ around some point $\hat{\eta}$ from the mean number (which should be $L$), i.e.,

$$\Sigma^2(L) :=< (n(\eta, L) - L)^2 > . \tag{3.85}$$

It measures the deviation of the spectrum from the straight line as a function of the length of the interval under consideration. The numerical calculation is of course dependent on the interval $\delta$ of averaging and $\hat{\eta}$ as can be seen from the definition

$$< f(\eta) >:= \frac{1}{\delta} \int_{\hat{\eta}-\delta/2}^{\hat{\eta}+\delta/2} f(\eta) d\eta. \tag{3.86}$$

Especially for a small number of phases like here the usually required relation $\hat{\eta} \gg \delta \gg L$ is hard to realize. Fig. 3.16 displays the number variance for the slightly asymmetric situation with $\hat{\eta} = 100$ and $\delta = 50$. The behaviour for random processes is given by the dashed line. One can see strong deviation from the completely random spectrum, it looks

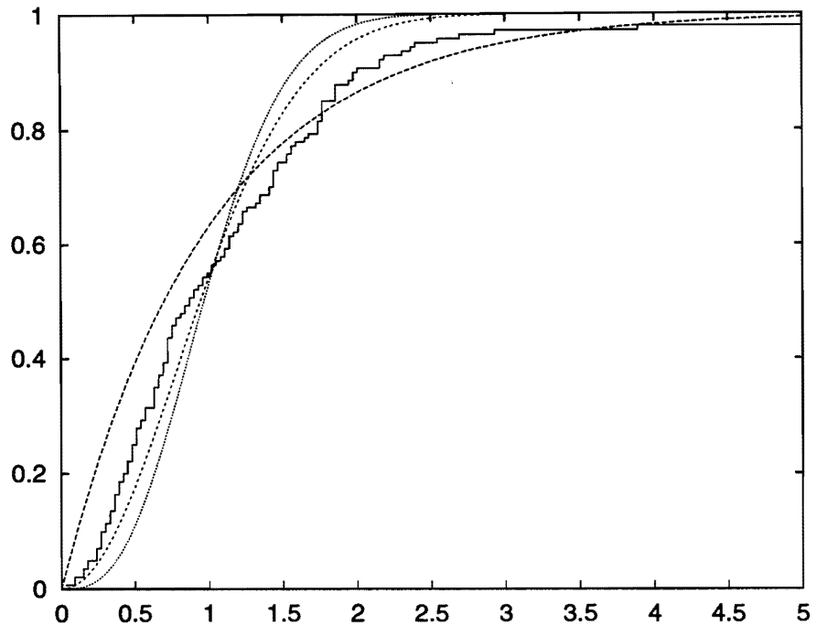


Figure 3.15: Here the configuration is even more asymmetric, the relation of the magnitude of the angles of the triangle is 1:3:5. The level repulsion at small distances is apparent.

even as if it saturates above some certain $L_{max}$. This, however, is probably too fast to conclude. In Fig. 3.17 $\hat{\eta}$ has been changed to 80 and the saturation has gone. This can be explained by looking at the unfolded spectrum once more. Whereas the saturation for higher values means that the deviation from the straight line is very small, for lower values, the fit has left out a long range wiggle, which comes into play in this measure and the number variance blows up. This sensitivity is again a consequence of the small number of eigenphases. For the almost symmetric configuration (Fig. 3.18), again, there is some sort of saturation to be expected. This shows that the long range behaviour is independent of the short range correlations, i.e., that the similarity to a Poissonian statistics on small length scales does not imply Poissonian behaviour on the long range.

Concluding, one could say that generally the spectrum seems to be much more rigid than a random spectrum and shows level repulsion, but these measures are very sensitive to the unfolding procedure and thus are difficult to be taken quantitatively.

### 3.4.2 Resonances and the Argument of $\det(\mathbf{1} + i\tilde{\mathbf{T}}\tilde{\mathbf{H}})$

As for the resonance it does not make much sense to apply these statistical methods, since there are only a few. Qualitatively, the resonances become less stable as the energy increases as can be seen in Fig. 3.19. There does not seem to be any regularity, not even

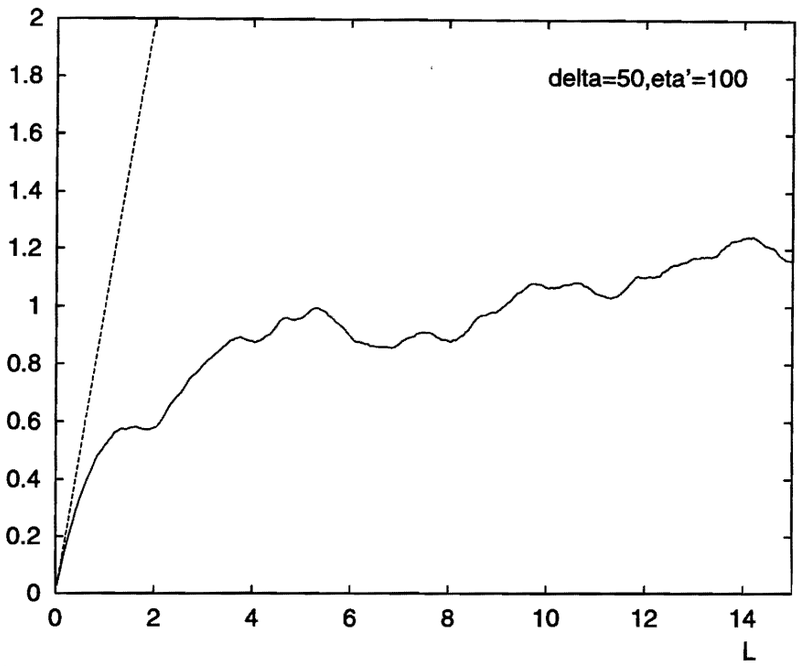


Figure 3.16: $\Sigma^2(L)$ for the eigenspectrum of the asymmetric configuartion with parameters $\delta = 50$ and $\hat{\eta} = 100$

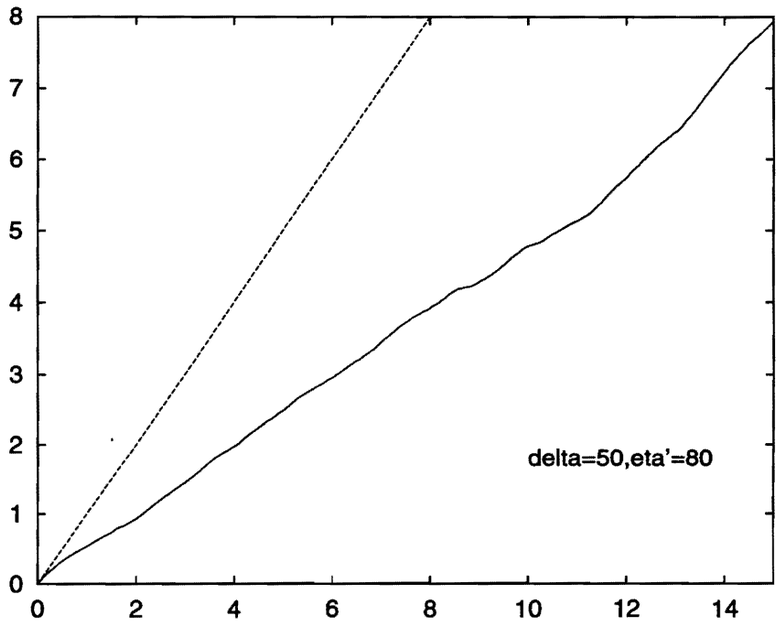


Figure 3.17: $\Sigma^2$ as before, but $\hat{\eta}$ is changed to 80

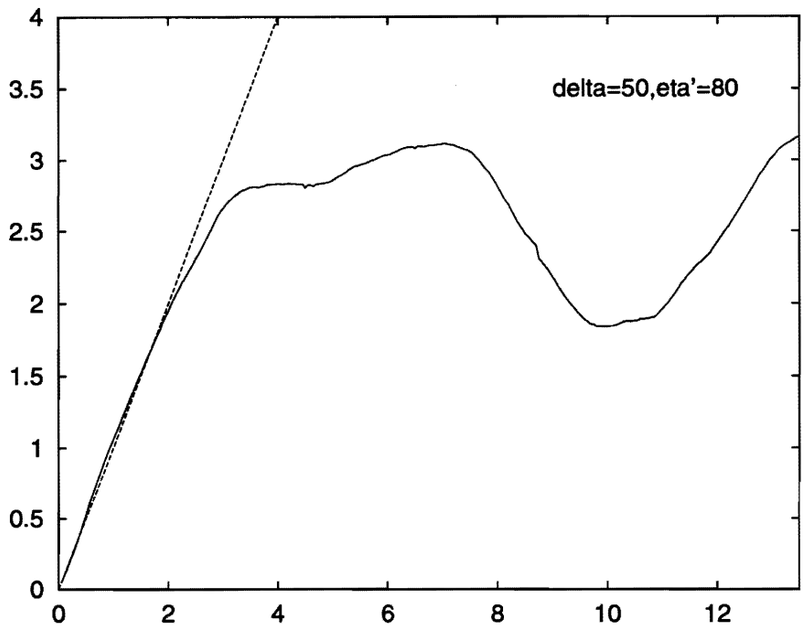


Figure 3.18: $\Sigma^2$ for the almost symmetric triangle with $\delta = 50$ and $\hat{\eta} = 80$

in the symmetric triangle, at least no obvious one. There seems to be no clustering but rather an equidistant distribution in most cases. This would correspond to an expected level repulsion, where the measure would be the distance in the complex momentum plane. The number of resonances $N(K)$ below a certain radius $K$ in the momentum plane grows linearly with $K$. Estimates in [34] expect a polynomial increase

$$N(K) \leq C_1 K^n + C_2 \tag{3.87}$$

as the leading behaviour and nothing is known about the constants. Here $n$ is the dimension of the configuration space. Our Fig. 3.20 rather suggests a slower increase of the form $N(K) \approx C_1 K^1 + C_2 = C_1 K^{n-1} + C_2$, if anything can be conjectured from such a few resonances only.

The argument of the determinant of $(\mathbf{1} + i\mathbf{T}\tilde{\mathbf{H}})$ is plotted in Fig. 3.21. The main feature is its decay, corresponding to the decay of the life-time of the resonances. The reason and its consequences for the semiclassical theory will be discussed in the next chapter. Generally one expects this oscillatory part to have a root at the real part of the resonances in analogy to the bounded case. We see that this is not the case. This can be explained by the level repulsion of the eigenphases: The resonance being a pole in one of the eigenphases would yield its strong increase, but it is inhibited to rise because of the repulsion (see Fig. 3.8) and thus this feature is averaged out.

$\mathrm{Arg}\det(\mathbf{1} + i\mathbf{T}\tilde{\mathbf{H}})$ is the mathematical analogue to the fluctuating part of the spectral

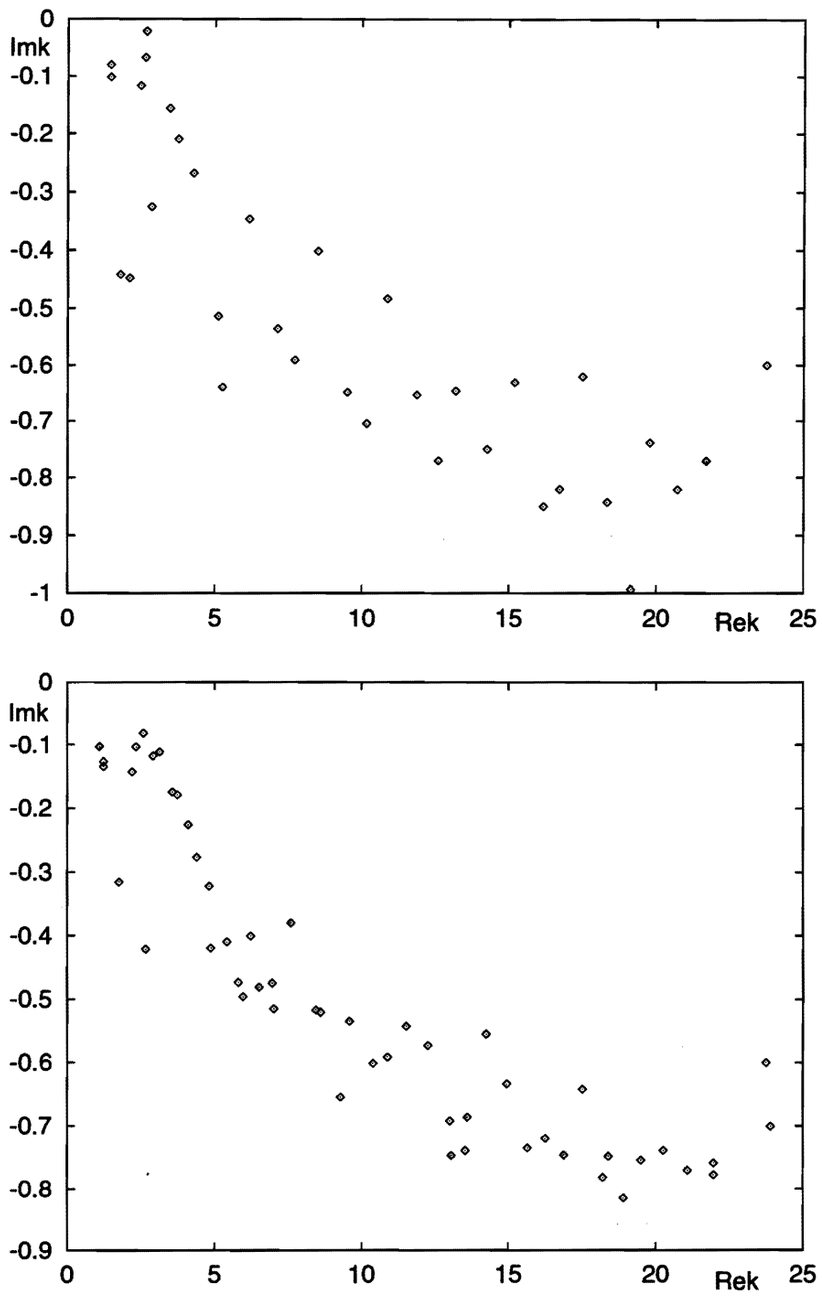


Figure 3.19: The distribution of resonances in the complex $k$-plane, symmetric (above) and slightly asymmetric case (below).

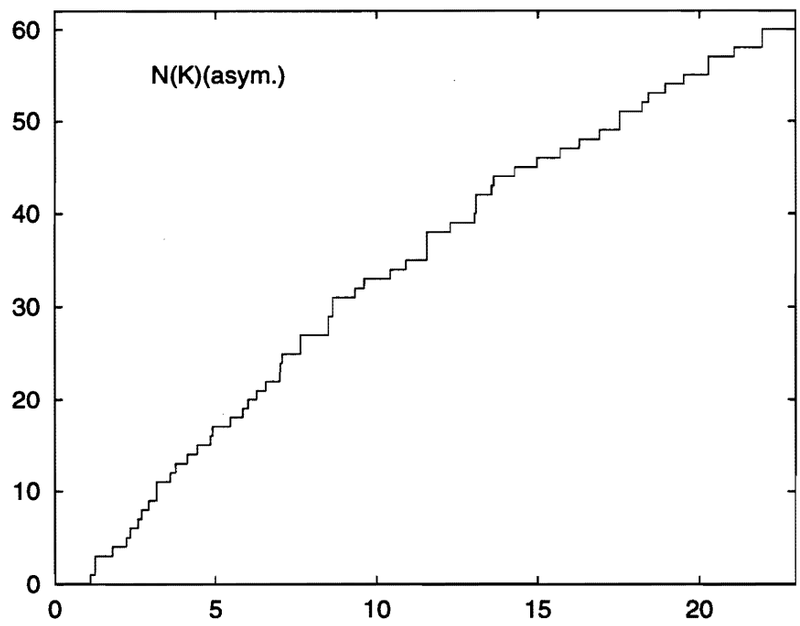


Figure 3.20: The number of resonances below a radius $K$ in the complex momentum plane for the asymmetric configuration

staircase function of bounded systems. Therefore we shall discuss in a scattering situation the conjecture of the preceding chapter of the unique characterisation for a quantum chaotic system that these oscillations follow a Gaussian distribution [17, 16]. To be more precise, it has been conjectured that $N_{osc}(E)$, normalized by the spectral rigidity, $\Delta_\infty(E)$ in the following way,

$$W(E) := \frac{N_{osc}(E)}{\sqrt{\Delta_\infty(E)}} \tag{3.88}$$

approaches limiting distribution that marks uniquely its character as classcially integrable or chaotic systems. That is to say that the distribution $f(w)$ of values of the function in eq. (3.88) is a Gaussian distribution

$$f(w) = \frac{1}{\sqrt{2\pi}} \exp(-w^2/2) \tag{3.89}$$

for all scaling chaotic systems in the limit of high energies and a non-universal (in general not even symmetric) distribution for classically integrable systems. For high energies the spectral rigidity can be understood as the second moment of $N_{osc}(E)$, i.e.,

$$\Delta_\infty(E) \approx < \frac{1}{2L} \int_{E-L}^{E+L} N_{osc}^2(E')\, dE' > \tag{3.90}$$

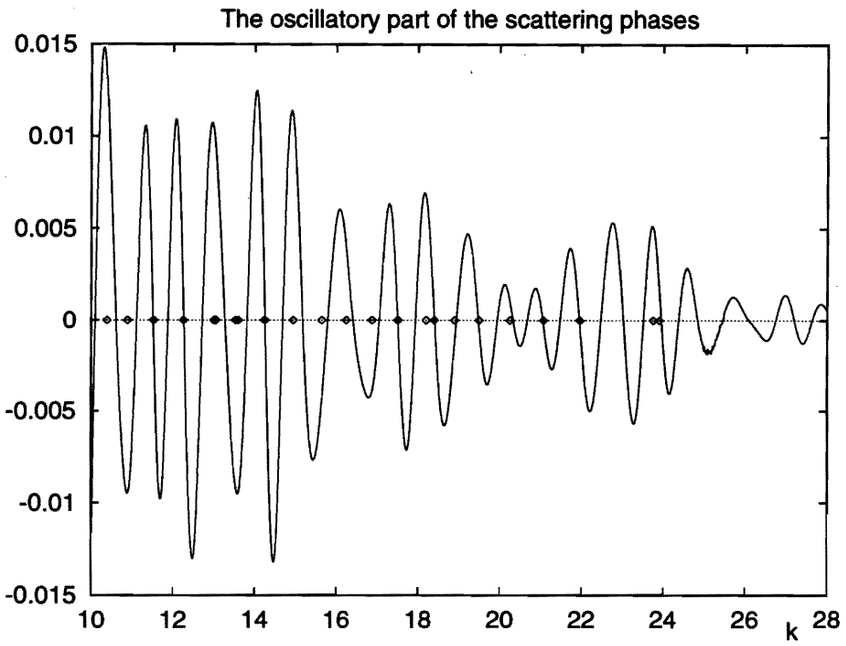


Figure 3.21: The argument of the KKR-determinant, $\eta_{osc}(k)$, and the points mark the real part of the resonances

such that it plays the role of normalizing the distribution to a universal scale, similarly to the unfolding of the spectrum. This formula is valid under a few restrictions on $E$ and $L$ (see [15]).

To see what the situation is like for $\eta_{osc} = \arg(\det(\mathbf{1} + i\mathbf{T}\tilde{\mathbf{H}}))$ in this scattering system, we normalize it by the square root of its second moment, which we compute numerically. It decays roughly like $1/k$. The cumulative distribution function found is plotted in Fig. 3.22 and Fig. 3.23, evaluated at 2000 points. We have used the integrated distribution as this has a smoother appearance. It can easily be calculated to be

$$F(w) = \int_{-\infty}^{w} f(w')dw' = \frac{1}{2}(1 + \mathrm{erf}(w)) \tag{3.91}$$

The figure shows that is not quite Gaussian in either cases, but it is fairly symmetric, the mean value is zero (as it $F(0) = 1/2$) and it seems to resemble the normal distribution very well around 0. We shall give an explanation for these features and why it will never resemble a complete Gaussian in the case of scattering systems on the basis of a semiclassical analysis in the next chapter. Additionally we have plotted the distribution for a simple sinusoidial curve. This is done to illustrate, that such a distribution function is not a simple consequence of the symmetric oscillation.

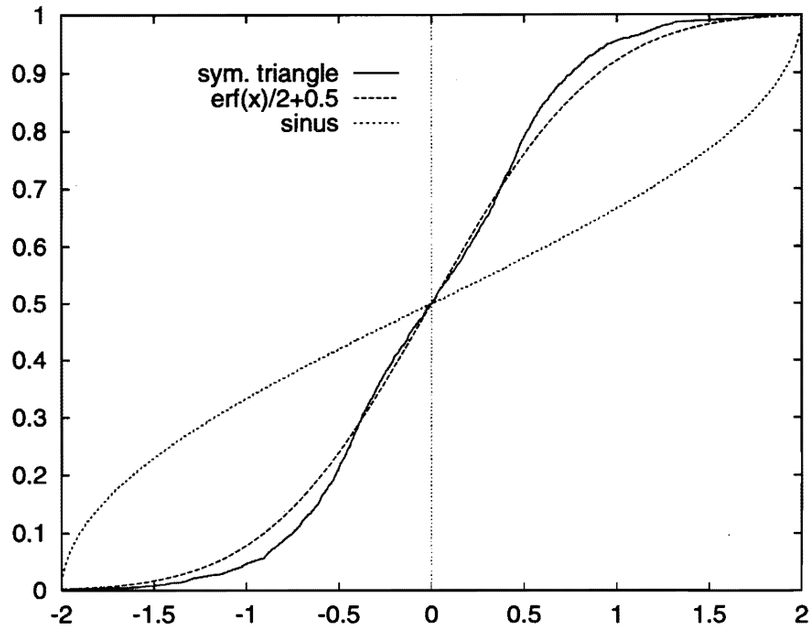


Figure 3.22: The distribution function for the normalized $\eta_{osc}$ in the symmetric case. For comparison an integrated Gaussian distribution and a simple sinusoidial distribution

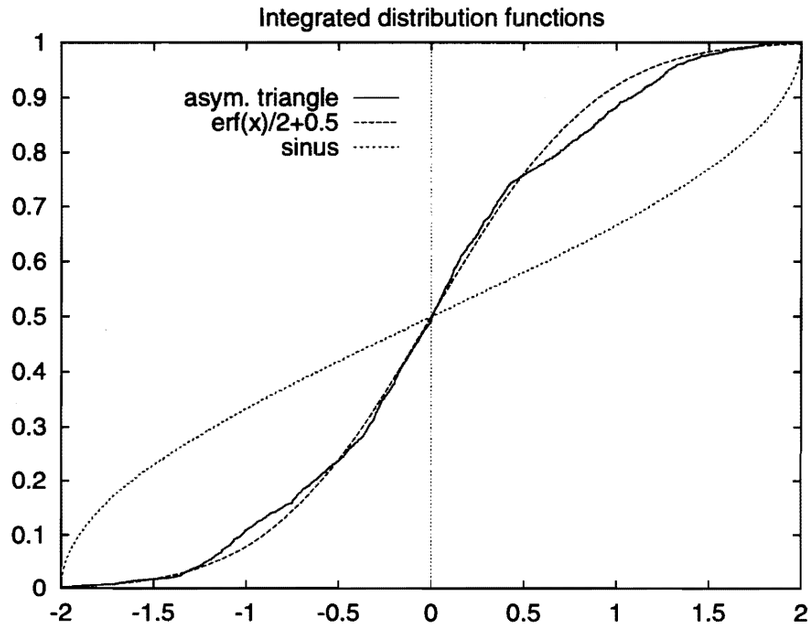


Figure 3.23: The cumulative distribution function for $\eta_{osc}$ for the asymmetric configuration

# Chapter 4

# Semiclassical Analysis

Ever since quantum mechanics has been celebrated as the correct theory to describe microscopic phenomena, the question of the relation to classical mechanics has been raised. In the presence of an exact theory one might ask, why (semiclassical) approximations should be of any interest. In fact there are numerous reasons of which we shall mention a few. First of all, a lot of intuitive understanding of quantum mechanical phenomena is given by quantization rules based on classical quantities. For a second reason we may recall that on many occasions, the calculation of semiclassical approximations is easier than the exact theory. This is especially the case in high energy regions, which generally corresponds to the limit, where $\hbar$ is small compared to other quantities involved. Finally it has often proved to be a fruitful exploration in the direction of new mathematics.

In this chapter, we shall demonstrate that also in our system semiclassical analysis has advantages in the points mentioned above.

The best semiclassical quantization rule known today is the EBK-quantization [21], which generalizes the WKB-method by including topological properties of the system. Nevertheless this kind of rule requires the existence of invariant tori in phase space, i.e., an integrable classical flow as described in the introduction. This has already been recognized by Einstein in 1917 [73]. Thus this kind of quantization breaks down in the chaotic case. For a completely unstable classical flow Gutzwiller has found that the trace of the Green's function can be approximated semiclassically by an infinite sum over classical periodic orbits. The relation of periodic orbits to energy eigenvalues is more intriguing than for integrable situations, as there is no simple association of orbits to eigenvalues. As for the situation of scattering, the periodic orbit sum recovers the time-delay function.

Therefore we shall first derive the trace formula for irregular scattering in general. The derivation is very similar to that in the bounded case. We then compare this general form with a periodic orbit sum derived directly from the KKR-determinant, to see whether there are any form of corrections to the trace formula for muffin tin potentials. After that the connection to the dynamical zeta function is shown and the surprising transition to the classical zeta function in the specific case of Coulombic muffin tins is discussed. We

then introduce the class of almost periodic functions and draw the link to quantum chaos. We find a few nice applications in correlation functions and distribution functions. Finally we study the periodic orbit sum to the extend it is possible for the Coulomb centers.

## 4.1 The Trace Formula and the KKR-Determinant

The Green's function, as we have seen before can be taken as a central object to study quantum mechanics. The semiclassical approximation of the Green's function in energy representation reads in two dimensions [21]

$$G^{sc}(\vec{q},\vec{q}';E) = \frac{1}{i\hbar}\sum_{cl.p.o.}\frac{1}{\sqrt{2\pi i\hbar}}\sqrt{|D|}\exp\left\{\frac{i}{\hbar}S(\vec{q},\vec{q}';E) - i\frac{\pi}{2}\mu\right\}. \tag{4.1}$$

It is a sum over all classical paths from $\vec{q}$ to $\vec{q}'$. The argument of the exponential contains the classical action of the paths defined in eq. (2.2) and a topological index $\mu$ that counts the number of conjugate points along the path, called the Maslov index [21, 49]. The prefactor as the amplitude of the oscillating function is given by the determinant of the 3 by 3 matrix

$$D = \det\begin{pmatrix} \frac{\partial^2 S}{\partial\vec{q}\partial\vec{q}'} & \frac{\partial^2 S}{\partial\vec{q}\partial E} \\ \frac{\partial^2 S}{\partial E\partial\vec{q}'} & \frac{\partial^2 S}{\partial E^2} \end{pmatrix}. \tag{4.2}$$

This formular can be derived, e.g., from the Feynman path integral by stationary phase approximation [74]. For the free motion of a particle in two dimensions one can see that it reduces to

$$G^{0sc}(\vec{q},\vec{q}';E) = \frac{m}{i\hbar^2}\frac{1}{\sqrt{2\pi}}\frac{\exp\left(ik|\vec{q}'-\vec{q}|-\pi/4\right)}{\sqrt{k|\vec{q}'-\vec{q}|}}, \tag{4.3}$$

since there is only one trajectory between two points in configuration space and no conjugate point. This recovers exactly the high energy limit of the exact form for the free Green's function as evaluated in eq. (3.7).

The semiclassical approximation of the Green's function has the same analytical structure as the exact one. Thus we again need to regularize it as in chapter 3 before taking the trace

$$(g^{sc}(E) - g^{0sc}(E)) := \lim_{D\to\infty}\mathrm{Im}\int dq^2(G^{sc}_D(\vec{q},\vec{q};E) - G^{0sc}_D(\vec{q},\vec{q};E)). \tag{4.4}$$

The diagonal elements of the semiclassical form are classical trajectories that start at $\vec{q}$ and return to the same point $\vec{q}$. Therefore one has to divide the sum over classical paths into two cases: the orbit of zero length and the non-trivial orbits that contribute a true loop in configuration space. It turns out that this splits the semiclassical trace formula

into a smooth part according to the orbit of zero length and an oscillatory part including all *periodic* orbits

$$(g^{sc}(E) - g^{0sc}(E)) = \overline{(g^{sc}(E) - g^{0sc}(E))} + g^{sc}_{osc}(E). \tag{4.5}$$

The first term on the right hand side reduces to a phase space integral and is thus known as the Weyl term in the case of billiards or the Thomas-Fermi term in the context of potentials. It provides the mean behaviour of the trace. The regularization applies only to the mean behaviour, since the free Green's function does not contain any non-trivial periodic orbits. The second term constitutes the oscillatory part here represented by a sum over periodic orbits. The imaginary part yields the density of states (in the presence of bounded states) or more generally the time-delay function $t_d(E)$

$$t_d(E) := \frac{d}{dE}\eta(E) := \frac{d}{dE}\sum_{\lambda=-\infty}^{\infty}\eta_\lambda(E) = -\left(g(E) - g^0(E)\right). \tag{4.6}$$

This is the general theory developed by Gutzwiller. It has been tested in many billiard systems [21]. Its derivation relies on the strict hyperbolicity of the system as it requires the periodic orbits to be isolated. In some systems modifications have been discussed due to families of non-isolated orbits. These usually cover a finite area in phase space and are thus not isolated. These families arise for example in billiards with two parallel boundaries [77], where the so called bouncing ball orbits yield a non-vanishing contribution, by discontinuities in the curvature of the boundary [78, 61] or through corners of the billiard [79].

To see whether there are any further contributions in our case, we derive a periodic orbits sum directly from KKR-determinant in eq. (3.77). We have claimed in chapter 3 that this splitting in two parts in eq. (3.77) corresponds exactly to the splitting into a smooth and an oscillatory part in eq. (4.5). We shall prove this by discussion of each part separately. We keep in mind that the Gutzwiller trace resembles the time-delay, whereas the argument of the KKR-determinant represents the sum over eigenphases. Therefore the latter periodic orbit sum should be related to the Gutzwiller sum through integration of the time-delay with respect to the energy as we shall see later.

### 4.1.1 Thomas-Fermi term

The regularizing free Green's function does not yield any non-trivial closed orbit and thus contributes fully to the smooth part $\bar{t}_d(E)$ of eq. (4.6) as mentioned above. For small distances the classical action of a particle in a potential can be approximated by

$$S(\vec{q}' \to \vec{q}; E) \approx |\vec{q}' - \vec{q}|\sqrt{2m\left(E - V(\frac{\vec{q}' + \vec{q}}{2})\right)} \tag{4.7}$$

and thus looks like a free motion with a shifted energy. For small arguments the full Green's function is therefore approximated by the free Green's function, which is the zeroth order Hankel function, where the energy in the argument is shifted. Using the behaviour of the Hankel function for small arguments [64]

$$H_0^+(z) \to \frac{2i}{\pi}\left(\ln(\frac{z}{2})+\gamma\right)+1 \text{ for } z \to 0 \tag{4.8}$$

we find that the regularized local density term for scattering on a potential

$$\overline{(\rho_{sc}-\rho_{sc}^0)}(\vec{q}',E) = \lim_{|\vec{q}'-\vec{q}|\to 0} \mathrm{Im}\frac{1}{\pi}\left(G_{sc}^{0+}(\vec{q}',\vec{q};E-V\left(\frac{\vec{q}'+\vec{q}}{2}\right)\right) - G_{sc}^{0+}(\vec{q}',\vec{q};E)\Big) = 0 \tag{4.9}$$

vanishes because it is independent of its argument according to (4.8) and (3.6). Therefore the regularized Thomas-Fermi term, which is the *integrated* mean behaviour of the time-delay, is maximally a constant. This seems to be somewhat surprising and unfamiliar in the context of quantum chaos. But this is because scattering on potentials has not been discussed for so long. It is consistent with our result of the exact quantum mechanical calculation in chapter 3 (the smooth part of the integrated regularized Thomas-Fermi density is represented by the high energy limit of the sum of scattering phases of the individual muffin tin). It is confirmed by calculating its derivative with respect to $E$ (or $k$). It approaches zero, for the square well as much as for the Coulombic muffin (cf. Figs. 3.1 and 3.5).

The Thomas-Fermi term itself can then be calculated using the semiclassical approximation for the scattering phases [80] ($b$ is the impact parameter)

$$\begin{aligned}
\eta_l^{sc} &= \frac{1}{\hbar}\left\{\int_{r_0}^{R}\sqrt{2m(E-V(q))-\frac{l^2}{q^2}}dq + l\arccos\left(\frac{l}{\sqrt{2mER}}\right) - \sqrt{2mER^2-l^2}\right\} \\
&= k\left\{\int_{r_0}^{R}\sqrt{1-\frac{V(q)}{E}-\frac{b^2}{q^2}}dq + b\arccos\left(\frac{b}{R}\right) - \sqrt{R^2-b^2}\right\} \\
&= k\tilde{\eta}(b)
\end{aligned} \tag{4.10}$$

and evaluating the sum by a stationary phase integral. The sum is first rewritten into an integral by the Poisson summation formula

$$\sum_{l=-\infty}^{\infty} \to k\sum_{m=-\infty}^{\infty}\int_{-R}^{R} dbe^{i2\pi mkb}, \tag{4.11}$$

where we have replaced $l = pb = \hbar kb = (\sqrt{2mE})b$ and taken into account again that only angular momenta contribute, for which the impact parameter is in the range of the radius

of the muffin tin. Therefore we can truncate the integral to the interval $[-R, R]$. For the Coulombic potential a quite lengthly calculation yields

$$\lim_{E\to\infty} \sum_l \eta_l = 0. \tag{4.12}$$

Note that this is only true for well behaved potentials. The situation is different for hard obstacles like hard discs. Here the local density vanishes everywhere except in a region of the area of the hard disc, where the full Green's function is identical zero. Thus the integral over the configuration space is an integral over the volume of the hard disc and the leading term in the Thomas-Fermi approximation yields

$$\bar{t}^{sc}_{d_{hd}}(E) = -\frac{m}{2\pi\hbar^2}\pi R^2, \tag{4.13}$$

which is independent of the energy. For three discs there is an additional factor of 3. The integrated density is then quadratic in $k$ and thus reproduces exactly the leading behaviour of the sum of eigenphases of the hard disc shown in Fig. 3.3 in chapter 3. General estimates on the high energy behaviour of the sum of scattering phases are being put on firm mathematical grounds only recently [34, 33]. One can show generally that the leading order for scattering from hard obstacles is in fact proportional to the volume of the obstacle, just like the Weyl formula for the mean number of levels inside the obstacle.

Furthermore asymptotic expansions are given for scattering on surfaces of non-euclidean metrics. At first site this construction might be applicable to the case of a potential by the transformation of the dynamics to a geodesic flow in a system with Jacobian metrics, used in chapter 2. This flow would clearly be non-euclidean. But the decisive difference is that the Jacobian metric is energy dependent and the asymptotic expansions derived in [33] are valid for an energy independent metric and are thus not suitable.

### 4.1.2 Periodic Orbit term

Taking the trace of the semiclassical approximation for the non-trivial orbits yields a sum over all periodic orbits in phase space

$$g^{sc}_{osc}(E) = \frac{1}{i\hbar}\sum_{p.o.} \frac{T_0}{\sqrt{|2 - \mathrm{Tr}\mathbf{M}|}} \exp\left(\frac{i}{\hbar}S(E) - \frac{i\pi}{2}\nu\right) \tag{4.14}$$

by using a stationary phase approximation. The index $\nu$ in the exponent has now changed to the maximal number of conjugate points along the periodic orbit (as this number is dependent on the starting point for non-periodic orbits (see, e.g., [75, 76])) and the amplitude can be written as a function of the trace of the stability matrix $\mathbf{M}$, introduced in chapter 2, times the primitive period $T_0$ of the orbit. This formula contains only classical quantities except $\hbar$. We have shown in chapter 2 that in the case of 3 Coulombic muffin tins there are no conjugate points. Furthermore the trace of the monodromy matrix is

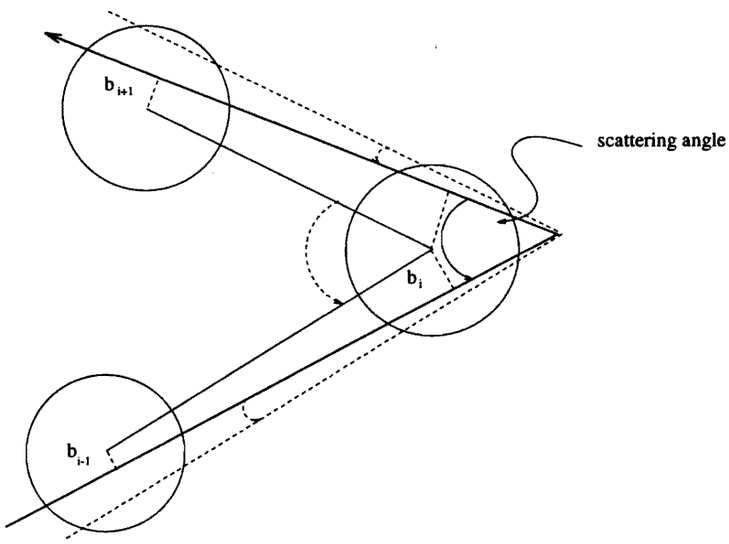


Figure 4.1: Illustration for the stationary phase condition with a non-trivial scattering angle. The scattering angle (full line) results as difference between $(\alpha_{i-1,i} - \alpha_{i,i+1})$ and $(\arcsin(\frac{b_i - b_{i-1}}{s_{i-1,i}}) - \arcsin(\frac{b_{i+1} - b_i}{s_{i,i+1}}))$ (dashed lines).

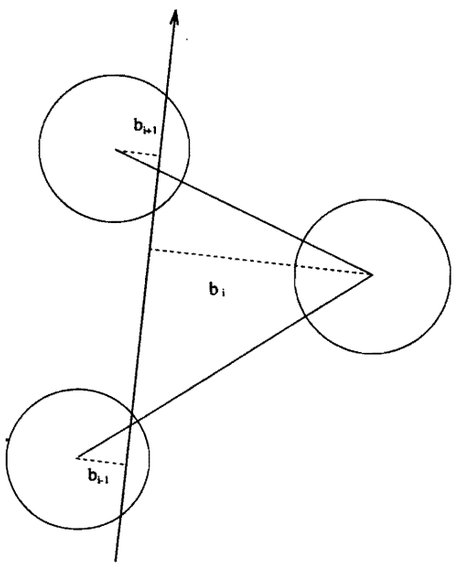


Figure 4.2: The stationary phase condition for vanishing scattering angle. The straight line does not hit the intermediate muffin tin.

always positive and larger than 2 and thus there are only direct hyperbolic periodic orbits. Using the relation (2.32) we can therefore simplify the periodic orbits sum to

$$g_{osc}(E) = \frac{1}{i\hbar}\sum_{\gamma}\sum_{r=1}^{\infty}\frac{T_\gamma}{2\sinh(ru_\gamma/2)}\exp\left(\frac{i}{\hbar}rS_\gamma(E)\right). \tag{4.15}$$

The periodic orbits can be split into primitive periodic orbits, here labeled with $\gamma$, and their multiples, which are counted in the second sum with the variable $r$.

Now we shall evaluate the second part in eq. (3.77). We have claimed that

$$\mathrm{Im}\log\det\left(\mathbf{1}+i\mathbf{T}\tilde{\mathbf{H}}\right) \cong \eta_{osc}^{sc}(E). \tag{4.16}$$

To see this, one can first expand the left hand side into the logarithmic series. Applying the relation $\log\det(1+M) = \mathrm{Tr}\log(1+M)$ one has

$$\begin{aligned}\log\det\left(\mathbf{1}+i\mathbf{T}\tilde{\mathbf{H}}\right) &= \sum_{n=1}^{\infty}\frac{(-1)^n}{n}\mathrm{Tr}(i\mathbf{T}\tilde{\mathbf{H}})^n \\ &= \sum_{n=1}^{\infty}\frac{1}{2^n n}\sum_{l_1}\cdots\sum_{l_n}\sum_{i_1}\cdots\sum_{i_n}(e^{2i\eta_1}-1)\ldots(e^{2i\eta_n}-1)\tilde{H}_{l_1 l_2}^{i_1 i_2}\ldots\tilde{H}_{l_n l_1}^{i_n i_1}.\end{aligned} \tag{4.17}$$

Here we have applied the short-hand notation $\eta_j := \eta_{l_j}^{i_j}$. Multiplying out the brackets in the last equation one gets for each order $n$ a multiple sum over $2^n$ products over $n$ Hankel functions and a number of $e^{2i\eta_l}$ and $(-1)'s$. First there are the sums over the $i_j$. They allow all combinations of different muffin tins in the product, except double appearance of the same index, because of the factor $(1-\delta_{ij})$ in $\tilde{\mathbf{H}}$ (cf. eq. 3.75). Thus it is a sum over all combinations of symbols of length $n$ consisting of the numbers $\{1,2,3\}$ without repetition, which resembles already exactly the code used in chapter 2 to determine the periodic orbits. Therefore it is a sum over all codewords and we next have to see what contribution to each codeword is given by the remaining sum over angular momenta.

The sum over $l_i$ will again be replaced by an integral over the impact parameter $b_i$, which will be evaluated by the stationary phase method. We will then see that the summands containing at least one $(-1)$ as a factor will not contribute as they have no stationary point within the region of integration. Thus we start with those that yield non-vanishing integrals.

For one angular momentum, the sum looks as follows

$$\sum_{l_i} e^{2i\eta_{l_i}} H_{l_{i-1}-l_i}^{(+)}(ks_{i-1,i})H_{l_i-l_{i+1}}^{(+)}(ks_{i,i+1})e^{i(l_{i-1}-l_i)\alpha_{i-1,i}+i(l_i-l_{i+1})\alpha_{i,i+1}}. \tag{4.18}$$

Here $\alpha_{i,j}$ denotes the angle of the line connecting the centers of the muffin tins $i$ and $j$ with the $x$-axis and $s_{ij} = |\vec{s}_i - \vec{s}_j|$ just like the notion used in chapter 2. Using the Debye asymptotic expansion for the Hankel function eq. (A.7), replacing the scattering phase by

its semiclassical approximation of eq. (4.10) and applying the Poisson formula the sum turns into the integral

$$\frac{e^{-i\pi/2}}{2\pi}k\sum_{m_i}\int_{-R_i}^{R_i}db_i\frac{e^{ik\xi}}{((s_{i-1,i}^2-(b_{i-1}-b_i)^2)(s_{i,i+1}^2-(b_i-b_{i+1})^2))^{1/4}}, \tag{4.19}$$

where we have used the abbreviation for the phase

$$\begin{aligned}\xi \;:=\; & 2\pi m b_i + 2\eta(b_i) + \sqrt{s_{i-1,i}^2-(b_{i-1}-b_i)^2} + \sqrt{s_{i,i+1}^2-(b_i-b_{i+1})^2} \\ & -(b_{i-1}-b_i)\arccos\left(\frac{b_{i-1}-b_i}{s_{i-1,i}}\right) - (b_i-b_{i+1})\arccos(\frac{b_i-b_{i+1}}{s_{i,i+1}}) \\ & +(b_{i-1}-b_i)\alpha_{i-1,i} + (b_i-b_{i+1})\alpha_{i,i+1}.\end{aligned} \tag{4.20}$$

This integral is to be evaluated by the stationary phase method, i.e., at points, where the derivative of $\xi$ with respect to $b_i$ vanishes. But this condition yields

$$\begin{aligned}& \mathrm{sgn}(b_i)\left[2\arccos\left(\frac{b_i^2-R}{R\sqrt{Z^2+4Eb_i^2}}\right)-\pi\right]+\arcsin\left(\frac{b_i}{R}\right) \\ =\;& \arcsin\left(\frac{b_{i-1}-b_i}{s_{i-1,i}}\right)-\arcsin\left(\frac{b_i-b_{i+1}}{s_{i,i+1}}\right)+\alpha_{i-1,i}-\alpha_{i,i+1}\end{aligned} \tag{4.21}$$

which coincides exactly with the periodic orbit condition in chapter 2 that two consecutive angles match (cf. eqs. (2.27) and (2.29)). It can also be visualized in Fig. 4.1. The left-hand side is effectively the scattering angle. This fact is generally known, as the derivative of the semiclassical eigenphase with respect to the impact parameter is just the scattering angle [80]

$$2\frac{d}{db}\tilde{\eta}^{sc} = \theta(b). \tag{4.22}$$

Therefore this would work with any potential, but it is the particular property of the Coulomb potential that these orbits actually exist at any given energy. In potentials bounded from below or above, they will cease to exist above a certain energy.

Passing from the the one-dimensional integral in eq. (4.19) to the n-dimensional, the stationary phase condition requires a classical scattering at all muffin tins and we find thus that only classical periodic orbits contribute. The phase, evaluated at the stationary phase point then yields exactly the classical action of the associated periodic orbit.

We are left with the terms, where a $(-1)$ in (4.18) replaces the factor $e^{2i\eta_i}$. The stationary phase condition yields no scattering angle at the intermediate disc $i$ (see Fig. 4.2) and the condition reads simply

$$\arcsin\left(\frac{b_{i-1}-b_i}{s_{i-1,i}}\right)-\alpha_{i-1,i} = \arcsin(\frac{b_i-b_{i+1}}{s_{i,i+1}})-\alpha_{i,i+1}. \tag{4.23}$$

But going from muffin tin $i-1$ to $i+1$ with zero scattering angle at muffin tin $i$, or equivalently fulfilling condition (4.23) results just in a straight line. Because of the special configuration of the potential that the muffin tins are located on a convex triangle, the straight line has an impact parameter larger than $R_i$ and is therefore not within the region of integration. Therefore there is no stationary point in the n-dimensional integral in the case with at least one $(-1)$ in the product and it vanishes in this approximation. Thus only the periodic orbits contribute.

The evaluation of the $n$-dimensional stationary phase integral [81]

$$\int_{-R_1}^{R_1} db_1 \ldots \int_{-R_n}^{R_n} db_n \times \prod_{i=1}^{n} \frac{\exp(ik(2\eta(b_i) + \sqrt{s_{i,i+1}^2 - (b_i - b_{i+1})^2} - (b_i - b_{i+1})\arccos(\frac{b_i - b_{i+1}}{s_{i,i+1}})))}{(s_{i,i+1}^2 - (b_i - b_{i+1})^2))^{-1/4}} \tag{4.24}$$

produces a determinant of second order derivatives of the phase that has the form

$$F_{i,j} = a_i\delta_{ij} + b_i\delta_{i,j-1} + c_i\delta_{i,j+1}, \tag{4.25}$$

i.e., there are only elements on the diagonal, the two off-diagonals and in the upper right and lower left corner (the periodic condition implies the identification $n+1=1$). The factors can be calculated to give

$$\begin{aligned} a_i &= \frac{d}{db_i}\theta(b_i) + \frac{1}{L_{i-1}} + \frac{1}{L_i} \\ b_i &= -\frac{1}{L_i} \\ c_i &= -\frac{1}{L_{i-1}}. \end{aligned} \tag{4.26}$$

Here we have used the abbreviation

$$L_i := \sqrt{s_{i,i+1}^2 - (b_i - b_{i+1})^2}. \tag{4.27}$$

$L_i$ denotes just the distance a particle travels between the rims of two consecutive muffin tins. This type of $n \times n$ determinant can be decomposed into the trace over a $2n$-fold product $2 \times 2$ matrices

$$\hat{\mathbf{M}}_f^i = \begin{pmatrix} 1 & L_i \\ 0 & 1 \end{pmatrix} \tag{4.28}$$

and

$$\hat{\mathbf{M}}_s^i = \begin{pmatrix} -1 & 0 \\ -\frac{d\theta(b_i)}{db_i} & -1 \end{pmatrix}, \tag{4.29}$$

which can be associated with our stability matrices in chapter 2. This time they look different, because they are written corresponding to a different basis. The coordinates have been changed from $dq, d\dot{q}$ to $dq, d\theta$, where $\theta$ is the direction of the momentum (cf. [54]). But the trace is independent of the basis. It can directly be calculated for $n = 2$ and proven for $n > 2$ by induction that

$$\mathrm{Tr}\hat{\mathbf{M}} - 2 = \det F \prod_{i=1}^{n} L_i. \tag{4.30}$$

Taking all factors into account, we find that the expansion of the logarithm of the KKR-determinant in eq. (3.77) reads

$$\log\det\left(\mathbf{1} + i\mathbf{T}\tilde{\mathbf{H}}\right) \cong \sum_{n=1}^{\infty} \frac{1}{n} \frac{e^{iS_n(E)/\hbar}}{\sqrt{\mathrm{Tr}\mathbf{M}_n - 2}}. \tag{4.31}$$

Finally we have to split the orbit sum into primitive periodic orbits and multiple traversals. We find that the same primitive orbit $\gamma$ of codelength $m$ is counted $m$ times in the sum over all codewords, because it includes all cyclic permutations. Dividing these out and denoting by $r$ the multiple traversals we get

$$\eta^{sc}_{osc}(E) = \mathrm{Im} \sum_{\gamma} \sum_{r=1}^{\infty} \frac{e^{irS_\gamma(E)/\hbar}}{r\sqrt{\mathrm{Tr}\mathbf{M}^r_\gamma - 2}}. \tag{4.32}$$

The sum has exactly the same form as the Gutzwiller sum and there are no further contributions other than the periodic orbits. Furthermore no ghost-orbits appear. These are orbits that arise from a stationary phase point but are classically impossible, e.g., by passing through some inaccessible region of phase space [82]. Thus the KKR-sum (4.32) can be calculated by integration of the Gutzwiller sum (4.15), assuming that the prefactors do not depend much on the energy but only the classical action in the exponent (This is the assumption made in the stationary phase argument throughout the calculation before and is therefore consistent).

The Gutzwiller formula has been the starting point for an immense effort in research over the last 15 years. A number of systems have been explored to evaluate this formula to find convincingly good results. These systems though have all been exceptional in one particular point: The classical action, and thus the stability exponent, was a simple function of the energy, i.e., it was a scaling system in some power of the energy. This advantage was needed to be able to calculate the periodic orbits once at a fixed energy and use them for all other energies. The more generic case of a non-scaling system, like the general muffin tin model, requires in principle to calculate the periodic orbits for each energy separately. This amounts to an unpracticable mass of numerical input, especially since the topological structure of the periodic orbits might in general be different at different energies.

Although the Coulombic muffin tins are not an exactly scaling system, there are a few properties that still raises the hope to be able to use the periodic orbit sum in a certain approximation: For high energies, as could be seen in chapter 2, the classical action becomes essentially a function linear in the momentum and the stability of each orbits seems to be a constant. Furthermore the symbolic dynamics of the periodic orbits is independent of the energy and thus can be used at any scale. In the context of Maslov indices the situation is even simpler than in the case of the periodic orbit sum of a typical billiard, because of the absence of conjugate points.

The rest of the chapter is thus devoted to rather general results and new perspectives on the periodic orbits theory in general. It will be applied to the case of the Coulombic muffin tin only were appropriate and possible.

First we shall spend a small section on the dynamical zeta functions, because they show a nice connection between quantum and classical mechanics. Furthermore they lead us to the important question of convergence of the periodic orbit sum in eq. (4.32).

A general difficulty of the periodic orbits sums is their convergence. In general they can not even be expected to be conditionally convergent as they are supposed to reproduce the analytical structure of the trace of the Green's operator. A lot of methods have been developed to achieve better convergence to make numerical studies possible (see e.g. [60, 59]. We want to discuss this topic in a different context that is hardly been discussed in connection with quantum chaos yet, but may be very fruitful. This is the theory of almost periodic functions. One advantage is that different convergence properties can be associated with different classes of almost periodicity and some properties can be read off simply by their affiliation to one of the classes. To this end we shall give a short account on the theory and cite the most useful results.

## 4.2 Dynamical Zeta Function

There is another way of integrating the periodic orbit sum in eq. (4.15). First we notice that it can be rewritten expanding the amplitude in a geometrical series

$$\begin{aligned} g^{sc}_{osc}(E) &= \frac{1}{i\hbar}\sum_{\gamma}\sum_{n=1}^{\infty} T_\gamma \frac{\exp\left(\frac{i}{\hbar}nS_\gamma - nu_\gamma/2\right)}{\left(1-\exp\left(-nu_\gamma\right)\right)} \\ &= \frac{1}{i\hbar}\sum_{\gamma}\sum_{n=1}^{\infty}\sum_{m=0}^{\infty} T_\gamma \exp\left(\frac{i}{\hbar}nS_\gamma - nu_\gamma/2 - nmu_\gamma\right) \\ &= \frac{1}{i\hbar}\sum_{\gamma}\sum_{m=0}^{\infty} T_\gamma \frac{\exp\left(\frac{i}{\hbar}S_\gamma(E) - u_\gamma/2 - mu_\gamma\right)}{1-\exp\left(\frac{i}{\hbar}S_\gamma(E) - u_\gamma/2 - mu_\gamma\right)} \end{aligned} \tag{4.33}$$

Under the same assumption as above that the classical action is scaling the sum can be written as the logarithmic derivative of an infinite product

$$g_{osc}(E) = -\frac{\partial}{\partial E}\log Z(E) \tag{4.34}$$

where we have used the relation $T_\gamma = \frac{\partial S_\gamma}{\partial E}$ and defined

$$\begin{aligned} Z(E): &= \prod_\gamma \prod_{m=0}^{\infty} (1 - \exp(\frac{i}{\hbar} S_\gamma(E) - u_\gamma/2 - m u_\gamma)) \\ &= \prod_{m=0}^{\infty} Z_m(E) \\ &= \prod_{m=0}^{\infty} \tilde{\zeta}_{1/2}^m(E)^{-1}. \end{aligned} \tag{4.35}$$

This is in fact an infinite product over Ruelle-type zeta functions, discussed in chapter 2, evaluated at the value $\beta = 1/2$ with an additional index $m$ and the argument being the spectrum of classical actions rather than periods. As mentioned in chapter 2, the roots of the Ruelle-type zeta function are the classical resonances (in mode space). Here the roots of this zeta functions give the resonances of the quantum mechanics (in energy space). In principle it should be possible to find a system, where one Ruelle-type zeta function would interpolate between both quantum mechanical and classical resonances. This would require a scaling action, vanishing of all Maslov indices and only direct hyperbolic orbits.

The zeta function above is given in its Euler product representation. Expanding the product we arrive at its representation as a sum

$$Z_m(E) = 1 + \sum_{n=1}^{\infty} \mathcal{A}_n e^{i\mathcal{S}_n}, \tag{4.36}$$

where we have used the following definitions

$$\mathcal{A}_n = \prod_{i=1}^{n} (-1)^n e^{-(m+1/2)u_{\gamma_i}} \tag{4.37}$$

and

$$\mathcal{S}_n = \sum_{i=1}^{n} S_i(E). \tag{4.38}$$

In the case the classical action is scaling in the form $S_\gamma = p\, l_\gamma$, where $p$ is the momentum and $l_\gamma$ is the length, the letter sum can be written as the momentum times a sum over lengths $L_n$, sometimes called the pseudo-lengths. Taking the momentum as the variable (instead of the energy) and rotating the function by the definition $s := -ip$, eq. (4.36) turns into a Dirichlet series

$$Z(s) = 1 + \sum_{n=1}^{\infty} A_n e^{-L_n s}. \tag{4.39}$$

For these Dirichlet series explicit formulas are known about the abscissa of absolute and the abscissa of conditional convergence [60]. Thus one can sometimes use this resummation of the periodic orbit sum as an analytical continuation to extend the region of numerical evaluation beyond the region of absolute convergence, since it might still be conditionally convergent [47].

This form of generalized Dirichlet series brings us directly to our next topic.

## 4.3 Almost Periodic Functions

This subject was started up at the beginning of this century [83]. The original interest was to study properties of the Riemann zeta function as a function of the complex variable $s = \sigma + i\,t$. In its representation as a series over positive integers, it can be rewritten in the following way ($\sigma > 1$)

$$\zeta(s) := \sum_{n=1}^{\infty} \frac{1}{n^s} = \sum_{n=1}^{\infty} \frac{1}{n^\sigma} e^{-i(\log n)t}. \tag{4.40}$$

It was then generally asked, what kind of general features can be found for series of the form

$$\sum_{n=1}^{\infty} a_n e^{-i\lambda_n t}, \tag{4.41}$$

where $a_n$ is a complex number (independent of $t$), $\lambda_n$ an arbitrary set of real numbers and $t$ is a real variable.

First we shall explain the meaning of *almost periodic*: The functions $f(t)$ that are represented by (convergent) Fourier series with harmonic frequencies are all periodic, i.e., there exists a number $T$, such that for all real $t$ we have

$$|f(t+T) - f(t)| = 0. \tag{4.42}$$

Of course, with $T$ all numbers $T_n = nT$ obey condition (4.42) as well. Thus we have an infinite number of periods. For almost periodicity one requires a condition that is slightly weaker. The more one changes the condition, the bigger the class of functions. We will give the two conditions and their corresponding classes that are most important for our purposes.

### 4.3.1 Uniformly Almost Periodic Functions

This is the class originally studied by H. Bohr [83], sometimes called the proper almost periodic functions. Here a function $g(t)$ is almost periodic, if for all $\varepsilon > 0$ there is an infinite set of numbers $\{\tau_n\}$ relatively dense on the real line, such that

$$|g(t+\tau_n) - g(t)| < \varepsilon \tag{4.43}$$

for all real values of $t$. The numbers being relatively dense only expresses the fact that there is a maximal difference $L(\epsilon)$ between two neighbouring numbers $\tau_n$ and $\tau_{n+1}$. This maximal difference in general approaches infinity as $\varepsilon$ goes to zero. The analogy to eq. (4.42) is obvious. The meaning of (4.43) is that each value of an uniformly almost periodic function will almost be reached again, infinitely often ($\tau_n, n \to \infty$) and arbitrarily close ($\varepsilon \to 0$). This striking feature is called almost periodicity.

One of the main theorems of Bohr was to show that the class of functions obeying condition (4.43) coincides with the set of all series of the form (4.41) as long as the series converges *uniformly.* Uniform convergence is quite a strong condition. If, for example, all the frequencies $\lambda_n$ are linearly independent, i.e., there is no rational linear combination of a finite subset of $\{\lambda_n\}$ that adds up to zero, then uniform convergence is equivalent to absolute convergence. In this case a necessary and sufficient condition for (4.41) to be uniformly almost periodic is

$$\sum_{n=1}^{\infty} |a_n| < \infty. \tag{4.44}$$

In general this is not necessary for the series to converge uniformly. Nevertheless, these functions are always bounded,

$$\sup_{t \to \pm\infty} |g(t)| < B < \infty. \tag{4.45}$$

One can calculate the coefficient $a$ to a given frequency $\lambda$ via

$$a = \lim_{T\to\infty} \frac{1}{2T} \int_{-T}^{T} g(t) e^{-i\lambda t} dt =: M\{g(t)e^{i\lambda t}\}. \tag{4.46}$$

This kind of averages always exist and is only different from zero, if $\lambda = \lambda_n$. Therefore the Dirichlet series (4.41) is also called the Fourier series of the function. As a consequence of the uniform convergence we can extend the mean value in (4.46) to a product of two functions or its autocorrelation

$$M\{g(t+\delta)g(t)\} = \lim_{T\to\infty} \frac{1}{2T} \int_{-T}^{T} g(t+\delta)g^*(t)dt = \sum_{n=1}^{\infty} |a_n|^2 e^{i\lambda_n \delta} \tag{4.47}$$

The result is again an almost periodic function in $\delta$. For practical numerical purposes, it is important to know, how fast this limes converges as $T \to \infty$. Assume, we require an accuracy sharper than $2\gamma > 0$. Then the estimate given by Bohr is

$$|M\{g(t+\delta)g(t)\} - \frac{1}{2T} \int_{-T}^{T} g(t+\delta)g^*(t)dt| < \gamma + \frac{BL(\gamma)}{T}, \tag{4.48}$$

where the constants are given as above. Thus, we simply have to choose $T > \frac{BL(\gamma)}{\gamma}$ to meet the required accuracy. Unfortunately it is not as simple to find the value of $L(\gamma)$, but some hints are given by numerical estimates. It is important to know however that this approximation is invariant under shifts on the real axis, i.e., instead of calculating the interval of the autocorrelation around 0 as in the definition, it can be done around any point on the real axis. Because of this independence it is why truly universal quantities,

in which one is interested in quantum chaos, can be defined like, e.g., autocorrelation functions as we shall discuss below.

A lot of questions have been raised concerning these functions [97]. One of them is the question of the existence of a mean motion, i.e., whether there is a mean frequency around which the function oscillates or the question of the distribution of zeros. There has also been some work on the distribution functions and we shall come back to these at the end of the chapter.

### 4.3.2 $B^p$-Almost Periodic Functions

The generalization occurs here by changing the norm in eq. (4.42) and(4.43) to a seminorm $D_{B^p}[\cdot]$. It is defined by

$$D_{B^p}[f(x)] := \left[\limsup_{T\to\infty} \frac{1}{2T} \int_{-T}^{T} |f(x)|^p dt\right]^{1/p} . \tag{4.49}$$

The subscript $B$ is a reference to Besicovitch, who studied these functions in detail [84]. In this case, a locally $L^p$ function $f(t)$ is said to be $B^p$-almost periodic, if to any $\varepsilon$ corresponds a set $\{\tau_n\}$ uniformly dense on the real line, for which

$$D_{B^p}[f(t+\tau_n) - f(t)] < \varepsilon \tag{4.50}$$

and additionally for every $c > 0$

$$\left[\limsup_{T\to\infty} \frac{1}{2T} \int_{-T}^{T} \limsup_{N\to\infty} \frac{1}{2N+1} \sum_{n=-N}^{n=N} \int_{t}^{t+c} |f(x+\tau_n) - f(x)|^p \, dx \, dt\right]^{1/p} < \varepsilon. \tag{4.51}$$

Uniform density is a certain restriction of relative density, but this is a more technical detail. This definition has a far less obvious meaning. The main point is that the comparison between actual values of the function is replaced by a comparison of certain values of integrated regions.

What we are interested in is that this class is larger than the preceding one. For the case of $p = 2$ these functions can again be represented by Dirichlet series, for which the following condition holds: Any series of the form (4.41) with

$$\sum_{n=1}^{\infty} |a_n|^2 < \infty \tag{4.52}$$

is a $B^2$-function. This series then is a Fourier representation of the function. The mean value, defined as above, for such a function exists as well and can be used to calculate the Fourier series. For a short review see [85].

A connection between both classes is given by the generalization to **analytic almost periodic functions**. Replacing the variable $it$ by a complex variable $s = \sigma + it$, the real part of the variable acts as an additional parameter like $\sigma$ in the example of the Riemann zeta function. Analytic almost periodicity is then nothing else than almost periodicity in the variable $t$ for a fixed value of $\sigma$. This parameter changes the convergence properties of the Fourier coefficients and thus can interpolate between *u.a.p.* and $B^2$-functions. We shall see the use of this below.

## 4.4 Correlation Functions

For the application we shall recall some experimental motivation. In scattering cross sections of nuclear reactions already 30 years ago wild, seemingly random oscillations have been observed that could not be explained with conventional resonance theory [86, 87]. Very recently in measurements of the magneto-resistance of mesoscopic devices, which is strongly linked to the level density of the system, similar oscillations have been observed, experimentally as well as numerically [88, 89, 90, 91]. These were proven not to be background noise, since they are completely reproducible. The fact that oscillations of the same order of magnitude and the same degree of irregularity have been observed in very different experiments gave rise to the notion of universal fluctuations [92]. Our aim here is to show that a well defined characterization scheme of universal behaviour is possible on the basis of almost periodic functions.

To find regularities in these fluctuations and look for specific properties, one discusses the autocorrelation function of the fluctuating part [86, 93]. Take, e.g., the autocorrelation function of the fluctuating part of the time-delay. Semiclassically, we know that the momentum $p$ is the natural variable, when the classical action scales in $p$ as assumed throughout (It would also work with the energy, but the calculations become more difficult). Then we define

$$\begin{aligned} C_{\Delta p,\hat{p}}(\epsilon) &:= < {t_d}^{osc}\left(p+\frac{\epsilon}{2}\right), {t_d}^{osc}\left(p-\frac{\epsilon}{2}\right) >_{\Delta p,\hat{p}} \\ &= \frac{1}{2\Delta p}\int_{\hat{p}-\Delta p}^{\hat{p}+\Delta p} dp\, {t_d}^{osc}\left(p+\frac{\epsilon}{2}\right) {t_d}^{osc}\left(p-\frac{\epsilon}{2}\right) \end{aligned} \tag{4.53}$$

One of the universal properties proposed for this correlation function is its Lorentzian decay for small $\epsilon$ [86, 93]

$$C_{\Delta p,\hat{p}}(\epsilon) \sim \frac{\gamma^2}{\epsilon^2+\gamma^2}. \tag{4.54}$$

But experimental as well as numerical studies on various models [94, 95, 96] show that in the contrary, it deviates very early from a Lorentzian, shows many zeros and does not necessarily decay.

First of all we notice that the averaging procedure in the definition (4.53) has been chosen as a box average cutting the integral at $\hat{p}\pm\Delta p$. This varies sometimes in the literature. Furthermore the autocorrelation function is clearly dependent on $\hat{p}$ and $\Delta p$. Universality can only be discussed, when we know how strongly it depends on these quantities. We therefore recall from the previous section the definition of the mean value calculation of uniformly almost periodic functions. The only difference is that the argument there is a complex function. A simple calculation however shows that

$$C_\infty(\epsilon) := \lim_{\Delta p\to\infty} C_{\Delta p,\hat{p}}(\epsilon) = \frac{1}{2}\mathrm{Re}M\{g_{osc}(p+\epsilon)g_{osc}(p)\}. \tag{4.55}$$

In this limit the autocorrelation function becomes independent of $\hat{p}$ and we may also shift the arguments about $\epsilon/2$, because of the independence of the mean value under shift on the real axis. The advantages are that this definition is independent of any parameters and the autocorrelation function is simply given by the diagonal part of the double sum of periodic orbits as given by eq. (4.47). The remainder term that arise, when taking only finite $\Delta p$, can be estimated by eq. (4.48) and vanishes like $1/\Delta p$ .

Finally we have to justify, how far this procedure is applicable to the time-delay, i.e., what class of almost periodicity the semiclassical expression of $t_d^{osc}$ belongs to. We study the convergence properties by comparing the mean increase of the Fourier coefficients with the increase of its number below a certain length $l$ [54, 59]. We have for the Fourier coefficients

$$a_\gamma \cong \frac{l_\gamma e^{-u_\gamma/2}}{1-e^{-u_\gamma}} = \frac{l_\gamma e^{-\lambda_\gamma l_\gamma/2}}{1-e^{-\lambda_\gamma l_\gamma}}. \tag{4.56}$$

Neglecting the fast decay of the denominator, using the mean behaviour of the Lyapunov exponent and the mean growth rate of the number of periodic orbits (cf. chapter 2) we find that

$$\sum_\gamma |a_\gamma|^2 \cong \int_{l_1}^\infty dN(l)e^{-\bar{\lambda}l} \cong \int_{l_1}^\infty l dl e^{(\tau-\bar{\lambda})l} < \infty \tag{4.57}$$

The last inequality is valid because of the finite classical escape rate for scattering systems, which yields $\tau-\bar{\lambda} = -\Gamma < 0$, as can be confirmed in the tables in chapter 2. Therefore the time-delay is a $B^2$ almost periodic function and probably not a uniformly almost periodic one (because of $\tau > \bar{\lambda}/2$ in general, it is not absolute convergent). Therefore we have to use analytical continuation first to make the sum absolute convergent to be on the save side. Again we use $s := -ip$ and let $\sigma = \mathrm{Re}s > 0$, such that

$$\sum_\gamma |a_\gamma e^{-\sigma l_\gamma}| < \infty. \tag{4.58}$$

Applying the autocorrelation function to this absolute convergent sum and letting $\sigma \to 0$ at the end, we get finally the expression

$$C_\infty(\epsilon) = \frac{1}{2}\sum_\gamma \sum_{r=1}^\infty |a_{\gamma,r}|^2 \cos(r l_\gamma \epsilon). \tag{4.59}$$

This representation of the correlation function has a few consequences. It is an absolute convergent sum and thus an uniform almost periodic function itself. The mean value is zero, since its Fourier coefficient to the constant term is zero. Since it will never stop oscillating and even return to each value arbitrary close and arbitrary often, it has an infinite number of zeros and *correlations on all scales.* This is the reason why Gutzwiller himself very recently called almost periodicity the fractal property of quantum chaos [98]. All these properties modify the conjecture on a Lorentzian behaviour.

This procedure has been studied and proves to work very well in two cases [99]: The case of three hard discs and the scattering on the modular domain of the upper half plain in the hyperbolic metric [100]. In both cases the diagonal approximation resembles very well the exact correlation function and shows nicely the invariance under shifts on the real axis by calculating the integral at various regions on the real axis (i.e, for different values of $\hat{p}$ and $\Delta p$.

Having this form of the autocorrelation function at hand, one can also say a few words about the form factor for scattering systems. Normalizing the autocorrelation function by $\tilde{C}_\infty(\epsilon) := C_\infty(\epsilon)/C_\infty(0)$, which is equivalent to unfolding the fluctuating part of the time-delay by its mean behaviour. Then the form factor $K(\tau)$ is defined as the Fourier transform

$$K(\tau) := \int_{-\infty}^{\infty} e^{i\tau\epsilon}\tilde{C}_\infty(\epsilon)\, d\epsilon. \tag{4.60}$$

As the Fourier series of the autocorrelation function converges absolute, we can calculate

$$K(\tau) = \frac{2\pi}{C_\infty(0)} \sum_\gamma \sum_{r=1}^{\infty} |a_{\gamma,r}|^2\, \delta(\tau - r l_\gamma). \tag{4.61}$$

To study the long time behaviour, i.e., where $\tau$ is large, we integrate once over $\tau$ to get rid of the $\delta$-functions, extract the mean growth of the number of periodic length and find in a similar estimate as above in eq. (4.57) that

$$K(\tau) \approx \frac{2\pi}{C_\infty(0)} \tau e^{-\Gamma\tau}. \tag{4.62}$$

In contrast to the case of bounded systems, where the form factor saturates in general at 1, it decays for scattering systems at the rate of the classical escape rate. This has been conjectured [101] but never been put on a firm ground.

To summarize, the main ingredient to the calculations above is that the remainder term to the diagonal approximation of the double sum can be estimated to be small enough, when taking a finite but large averaging interval.

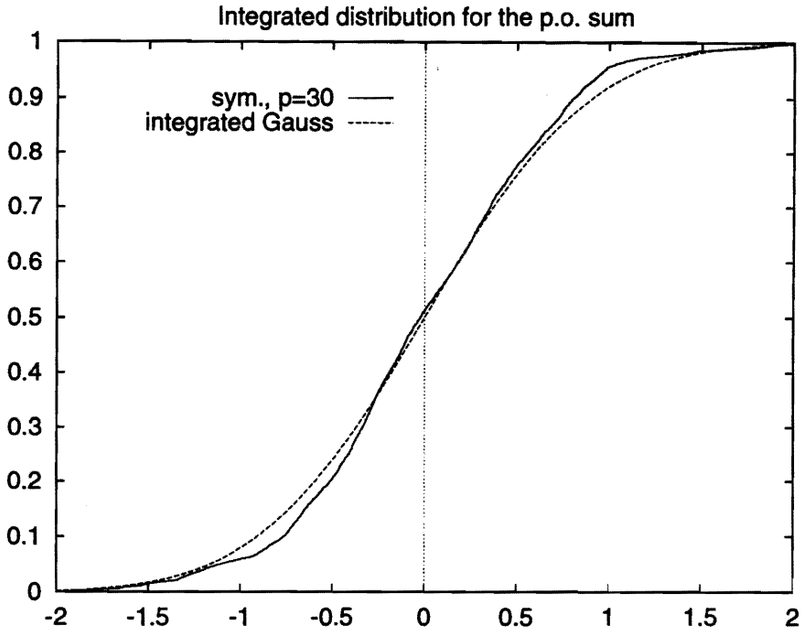


Figure 4.3: The integrated distribution function for an almost periodic function, here the example evaluated at p=30 (see the distribution of the exact $\eta_{osc}$ in chapter 3)

## 4.5 Distribution Functions

In the preceding chapter we have stated that the distribution function can be proven not to be Gaussian. This can be done by its semiclassical representation as an almost periodic function.

$\eta_{osc}^{sc}$ for our system is not almost periodic since it is not scaling, such that the arguments brought up here are not applicable to this case. But nevertheless, we have plotted the distribution in Fig. 3.22 and Fig. 3.23 and see that the deviations from the Gaussian as well as the similarities with the Gaussian behave, as if the function were almost periodic, as we shall see below.

In scaling systems $\eta_{osc}^{sc}$ is a $B^2$-almost periodic function. A smoothing out procedure or the continuation into the complex plane yields an *u.a.p.* function. Distribution functions for *u.a.p.* functions have been studied very early already. Especially the work of Wintner [102] is very useful in our context. He studies the case of all $l_\gamma$ being linear independent. This is the situation generally given for chaotic systems, when we neglect for a moment the multiple traversals (remember that there are only 107 multiples under the first 16510 primitive orbits in our system and since the series converges absolutely, shorter length are dominant).

The first thing that can be noted is the boundedness of the function. Therefore the

distribution will not exceed a given upper and lower boundary $B$ , which is one reason, why it can not be truly Gaussian in the tails. Wintner could even derive an exact formular for the integrated distribution function $F_{u.a.p.}(w)$, which reads (cf. eq. (3.91))

$$F_{u.a.p.}(w) = \frac{1}{\pi} \int_0^\infty \frac{\sin(w\xi)}{\xi} \prod_\gamma^\infty J_0(a_\gamma \xi) d\xi. \tag{4.63}$$

This form exhibits very interesting general features. First of all the distribution function is independent of the length spectrum. The deeper reason is that the linear independence translates into a statistical independence, which is then used for an ergodic averaging. Furthermore the derivative of this function is very similar to a Gaussian in many respects as it is symmetric around 0, i.e., $F(0) = 1/2$, all even order derivatives of $F$ at 0 vanish and at the edges $\pm B$ of its domain, which are the upper bounds of the function, it decays like $e^{-1/(w-B)^2}$ and $e^{-1/(w+B)^2}$ respectively. This formula could only be derived for *u.a.p.*s, such that one can not switch off the regularization of the periodic orbits sum at the end.

Thus it is not a Gaussian, but these properties suggest that in the case of bounded systems, where $N_{osc}^{sc}$ is not a $B^2$-almost periodic function, a suitable extension of almost periodicity could give a proof of the conjecture. It will be a delicate extension though, since it was shown in a recent paper [103] that the distribution function of a $B^1$-almost periodic function (in an extended sense) does not even have to be symmetric anymore (in this paper they studied the flucuating part $N_{osc}(E)$ of the spectral staircase of a classically integrable system).

Assuming for our system that the periodic orbit sum for finite $k$ resembles the limiting distribution function to a certain extend, we have plotted it for $k = 30$ in Fig. 4.3. It recovers the main characteristics of the exact distribution function surprisingly well

## 4.6 Discussion of the Periodic Orbit Sum

Evaluating the periodic orbits sum we have to recall the results about the classical quantities in chapter 2. We concentrate on the momentum region $10 < k < 30$. Below $k = 10$ a linear dependence of the classical action cannot be a reasonable approximation and above $k = 30$ we have no calculation of the exact quantum mechanical expression to compare with. Thus taking the calculated values for the action at the fixed point $k$ (in the examples it will always be $k = 10$ and $k = 30$) we define a "length" $l_\gamma := S_\gamma/k$ ($\hbar = 1$) for each periodic orbit. The stabilities are taken to be constant (see Fig. 2.4 and Fig. 2.6).

Thus constructing an almost periodic approximation for our periodic orbit sum we conclude from the values of $\tau$ and $\bar{\lambda}$ in Tab. 2.1 that we have a $B^2$- almost periodic function only. Thus we have to regularize it in the usual way ($s := -ip$) and continue it into the complex plane.

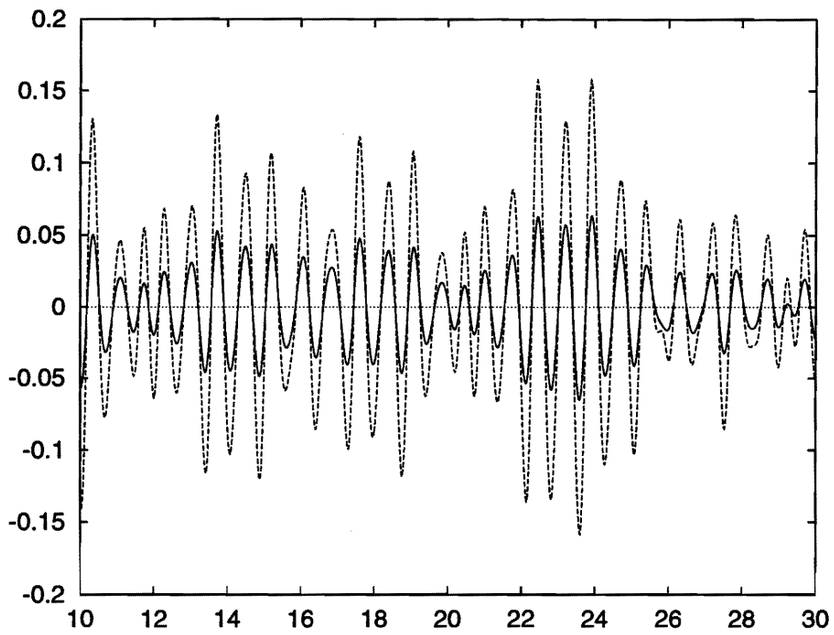


Figure 4.4: An example of the convergence of periodic orbit sum for $\eta_{osc}(k)$. Only the height of the amplitude is influenced by continuation into the region of absolute convergence (we have used the asymmetric length spectrum here). The imaginary part of $p$ is changed from $\mathrm{Im}p = 0.2$ (dashed) to $\mathrm{Im}p = 0.3$ (full)

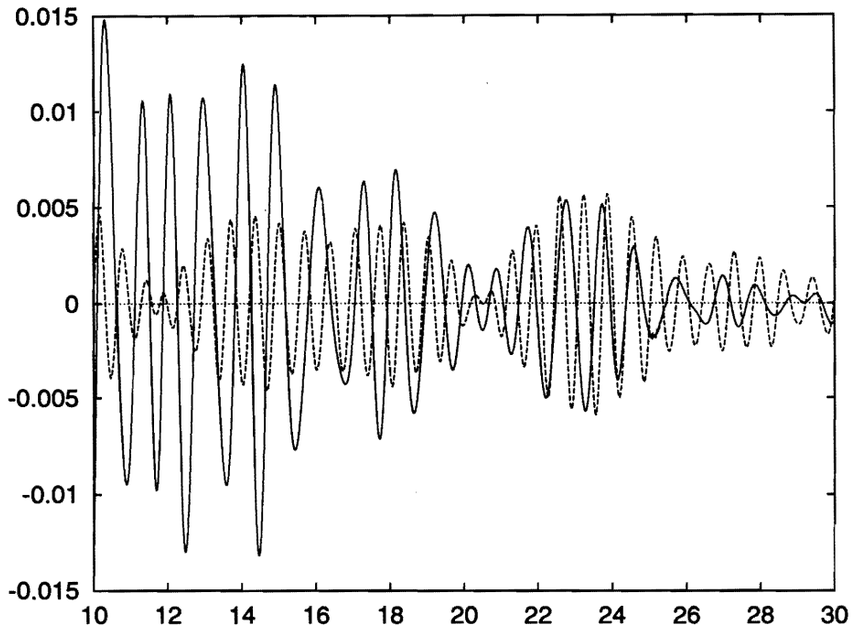


Figure 4.5: Comparison of the continuated periodic orbit sum (dashed) and the exact part (full) for the evaluation at p=10

In Fig. 4.4 we have evaluated the periodic orbit sum for the asymmetric lengths spectrum for different values of the attenuation factor Re $s$. Surprisingly the effect is that only the overall amplitude is changed and the oscillations seem to stay roughly the same. This has to do with the fact that there are strong correlations in the length spectrum as they are essentially a multiple of three basic lengths (Fig. 2.4). Using this observation that only the amplitude changes, one might try to compare this form with the exact oscillation, ignoring the mismatch in the magnitude, only testing the oscillation. In Fig. 4.5 and Fig. 4.6 we have plotted the regularized periodic orbit sum evaluated at $k = 10$ and $k = 30$ respectively. It does not seem to be a good approximation.

The deviation can be understood from Fig. 4.7, where we have compared the two approximations and see that they do not agree. Even in this short range the mean frequency for $k = 10$ is slightly but essentially larger then for $k = 30$. The reason is that the classical action actually has the form $S = A \cdot k + B/k$ and is only asymptotically scaling in $k$. Thus for any finite $k$ the approximation made above produces a lengths spectrum that is too large, for $k = 10$ even larger than for $k = 30$. Therefore both approximations oscillate too fast, although the overall long range oscillations are resembled quite well.

What remains is the discussion of the limit $k \to \infty$. On the one hand the oscillations will not cease, because the individual lengths of the periodic orbits approach a finite limes. This is the multiple of the geometric length of the distance between the centers of two

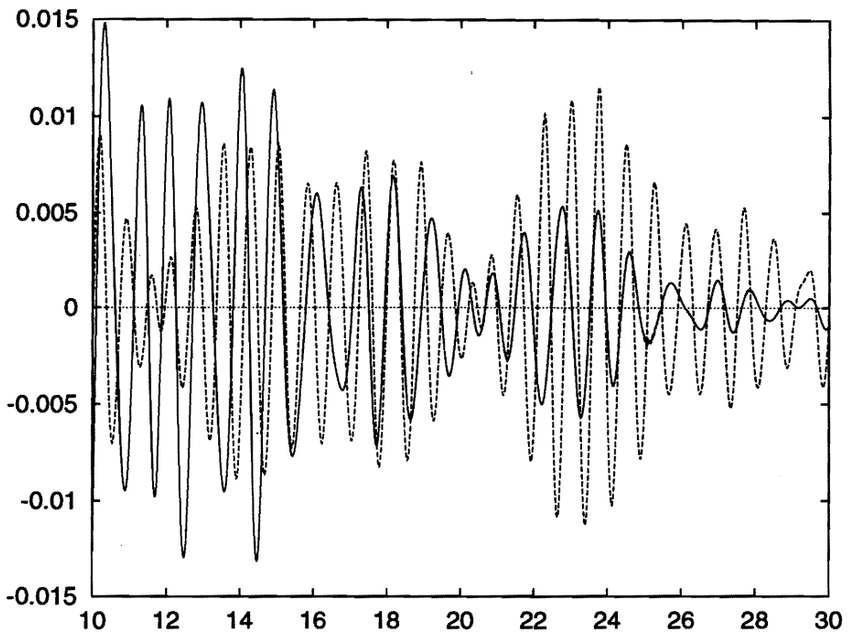


Figure 4.6: Comparison of the continuated periodic orbit sum (dashed) and the exact part (full) for the evaluation at p=30

muffin tins. On the other hand, the stabilities will increase to infinity and thus attenuate the amplitude to zero. The Fig. 2.6 is deceptive in that it suggests a finite limes. But all periodic orbits will come closer and closer to the centers of the muffin tins and the curvature is infinite , when the both limits $|\vec{q} - \vec{s}_i| \to 0$ *and* $E \to \infty$ are taken at the same time. Thus $\eta_{osc}$ will vanish as the Fig.3.21 in the preceding chapter already suggests. What goes along with this decay of oscillations is that the resonances are pushed deeper and deeper into the complex plane, thus the eigenphases detect less of it on the real energy axis. In this indirect way, the stability of the orbits have an effect on the stability of the resonances. Therefore a quantitative analysis seems to be not feasible on this basis, but the general features of the quantum mechanics can be understood from purely classical arguments quite well.

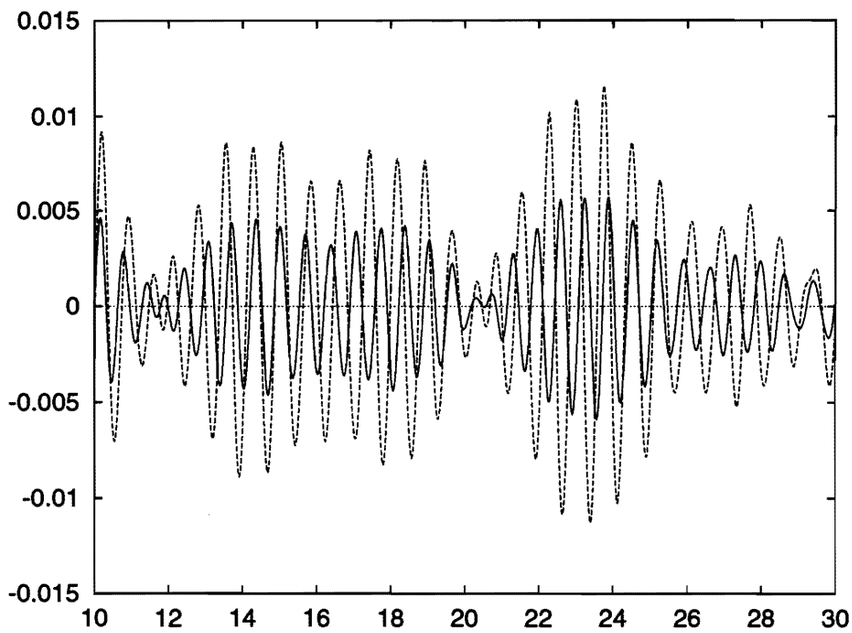


Figure 4.7: Comparison of the two approximations to the action of the periodic orbits at $p = 10$ (full) and $p = 30$ (dashed). The frequencies are slightly different, enough to destroy the similarity.

# Chapter 5

# Summary and Outlook

The aim of the work was to study how far classical and quantum chaotic scattering can be classified and discussed in a potential system that may serve as a model for a realistic physical system. We chose a 2-dimensional muffin tin with 3 tins, all of which endowed with a (finite range) attractive Coulomb interaction. They are all of same strength but their position is varied in different calculations from symmetric to asymmetric configurations.

In the classical analysis we were able to show that the dynamical system associated with the Hamiltonian equations is chaotic. More precisely, we could find a symbolic dynamics to label all periodic orbits in the system. Their number increases exponentially as a function of the length at the rate of the topological entropy. They were all found to be hyperbolic and thus isolated in phase space. The stability has been determined by transforming the problem to the geodesic flow on a curved Riemann surface and solving the Jacobi equation. This method is applicable to all potential systems and represents an elegant way to determine monodromy matrices and Lyapunov exponents in general. Finally we have determined characterizing numbers of the chaotic dynamics by the method of calculating the topological pressure. The real part of the abscissa of convergence of the Ruelle-type zeta function as a function of some parameter $\beta$ allows to calculate these quantities just like in thermodynamics, where many quantities can be calculated from the free energy in statistical physics.

With respect to quantum mechanics we have first developed 2-dimensional scattering theory in general and discussed it on a few integrable cases. We then derived a method in analogy to the KKR method to solve the problem of N arbitrarily located muffin tins. This method renders a secular equation to determine the resonances and the eigenphases of the S-matrix. In application to the Coulomb case we have determined the first resonances for different geometries of muffin tin arrangements and the eigenphases as a function of the energy. The eigenphases at fixed energy were taken to study the signs of quantum chaos as there is the level repulsion phenomenon and the saturation of the number variance. Due to bounds given by the numerical evaluation of the Coulomb wave function, the

number of eigenphases and resonances that could be determined was not very high. We shortly discussed an analogue for scattering systems of the Gaussian conjecture that was put forward as a unique identification of quantum chaos in scaling bounded systems. We have found that here, as probably for all potential scattering systems, the typical chaotic oscillations fade out for high energies and a modification of the conjecture has to be applied.

The semiclassical analysis was based on the trace formula, which has been formulated for scattering systems in a regularized form. We have shown that the Gutzwiller trace formula coincides with a semiclassical approximation of the exact quantum mechanical expression of the muffin tin potential and therefore no further contributions appear. Especially for the Coulomb case the periodic orbit sum simplifies extremely because of the missing Maslov indices. Nevertheless numerical examination is not possible because of the non-homogeneity of the potential. Therefore only qualitative statements were possible like the relation of the increasing instability of the periodic orbits to increasing instability of resonances. As an outlook to overcome this problem of scaling we propose to look at different quantities, like, e.g., eigenphases. To study these semiclassically one could derive a semiclassical expression for the quantity

$$\det(S - \lambda), \tag{5.1}$$

which should work along the lines of the semiclassical approximation undertaken with the KKR-determinant in the last chapter. The roots would yield the spectrum of eigenphases. Preliminary calculations show, that the approximation would involve periodic orbits of the PSM (cf. Introduction) rather than the periodic orbits of the dynamics itself. This requires a completely different classical analysis.

Finally we have cited the theory of almost periodic functions and shown that it can be exploited to obtain some general results on semiclassical periodic sums, their convergence properties and especially their correlation functions. This theory seems to carry a lot of possibilities to improve the understanding of quantum chaotic phenomena by giving it a rigorous mathematical background. Next to the Gaussian conjecture, e.g., the rigidity of quantum chaotic spectra might eventually be proven to be a consequence of almost periodicity in some extended definition or the connection to RMT may be found in a deeper analysis of these functions.

# Acknowledgements

I would like to thank Prof. Frank Steiner for his confidence, constant encouragement and the numerous inspiring discussions over the whole period of the work.

Among the uncountable stimulating discussions within the group, I would like to thank in particular Jens Bolte, Guido Beneke, Arnd Bäcker, Jens Marklof, Thomas Hesse and Roman Schubert for the fruitful and motivating exchange about all sort of things.

The 'Studienstiftung des deutschen Volkes' has supported me generously over the whole time of my studies. Many things would not have been possible without this support.

Thanks are due to my family, in particular my brother Jasper, whose company I have enjoyed so much in this time.

Above all, I would like to thank for the seemingly never ending support and patience of Franziska, to whom this work is dedicated.

# Appendix A

# Some Formulae on Special Functions

Since we use certain properties about special functions quite frequently, some of which are very common and some are less well known, we list a few of them here in the appendix (see, e.g., [64]).

The differential equation

$$z^2\frac{d^2w}{dz^2} + z\frac{dw}{dz} + (z^2 - \nu^2)w = 0 \tag{A.1}$$

coincides with the 2-dimensional radial Schrödinger equation (3.25) with the variable $z = kq$ and the angular momentum $\nu = l$. Two linear independent solutions are the Bessel functions $J_\nu(z)$ and Neumann functions $N_\nu(z)$ and linear combinations of those, like the Hankel functions $H_\nu^{(\pm)}(z) = J_\nu(z) \pm iN_\nu(z)$.

For all of these functions the addition theorem by Neumann

$$\mathcal{C}_\nu(u \pm v) = \sum_{k=-\infty}^{\infty} \mathcal{C}_{\nu\mp k}(u)J_k(v), \tag{A.2}$$

holds. It is valid under the restriction that $|v| < |u|$. Furthermore, Graf's addition theorem allows to split modulus and phases of the argument to yield for the Hankel functions the following identity

$$H_\nu^{(+)}(|v+u|)e^{i\nu\phi_{v+u}} = \sum_{k=-\infty}^{\infty} H_{\nu-k}^{(+)}(|u|)J_k(|v|)e^{i[(\nu-k)\phi_u + k\phi_v]} \tag{A.3}$$

with the same restrictions for $u$ and $v$. To expand the free Green's function we use especially the case $\nu = 0$.

As a special result of general expansions of functions in terms of Bessel functions we need the two-dimensional plane wave expansion

$$e^{i\vec{k}\vec{q}} = e^{ikq\cos\theta} = \sum_{l=-\infty}^{\infty} i^l e^{il\theta} J_l(kq). \tag{A.4}$$

The asymptotic expansions for large argument and fixed order are known to be

$$J_\nu(z) \approx \sqrt{\frac{2}{\pi z}} \cos(z - (\nu + 1/2)\pi/2) \tag{A.5}$$

and

$$N_\nu(z) \approx \sqrt{\frac{2}{\pi z}} \sin(z - (\nu + 1/2)\pi/2) \tag{A.6}$$

a combination of which yields the expansion for Hankel functions. For an expansion in large order and argument, one has to apply Debye's asymtotic expansion, which reads for the Hankel function

$$H_\nu^{(\pm)}(x) \approx \sqrt{\frac{2}{\pi}} \frac{\exp \pm i\sqrt{x^2 - \nu^2} \mp i\nu \arccos(\nu/x) \mp i\pi/4}{(x^2 - \nu^2)^{1/4}}. \tag{A.7}$$

Including the $1/r$-potential in the Schrödinger equation the radial equation turns after some calculation into the Whittaker equation

$$\frac{d^2w}{dz^2} + [\frac{\kappa}{z} - \frac{1}{4} + \frac{1/4 - \nu^2}{z^2}]w = 0. \tag{A.8}$$

The regular solution $M_{\kappa,\nu}$ we are interested in is linked to the ${}_1F_1$ confluent hypergeometric function by

$$M_{\kappa,\nu}(z) = e^{-z/2} z^{1/2+\nu} {}_1F_1(\frac{1}{2} + \nu - \kappa, 1 + 2\nu, z). \tag{A.9}$$

as cited in the chapter 3. The recurrence relation of the hypergeometric functions carry over to the Whittaker function and the one we have exploited in eq. (3.44) reads

$$zM'_{\kappa,\nu}(z) = \left(\frac{1}{2}z - \kappa\right) M_{\kappa,\nu}(z) + \left(\frac{1}{2} + \nu + \kappa\right) M_{\kappa+1,\nu}(z). \tag{A.10}$$

# Bibliography


[1] V.I. Arnol'd and A.Avez, *Ergodic Problems of Classical Mechanics*, (Benjamin, New York, 1968)

[2] A.J. Lichtenberg and M.A. Lieberman, *Regular and Chaotic Dynamics*, (Springer, New York, 1992)

[3] H. Poincaré, *Les Méthodes Nouvelles de la Méchanique Céleste*, (Gauthier-Villars, Paris, 1892)

[4] L. Boltzmann, J. f. d. reine u. angew. Math. **100**, 26 (1887)

[5] Y. Sinai, Sov. Math. Dokl. **4**, 1818 (1963)

[6] P. Walters, *Ergodic Theory: Introductory Lectures*, (Springer, Berlin, 1975)

[7] V.I. Arnol'd, *Mathematical Methods in Classical Mechanics*, (Springer, New York, 1978)

[8] M.L. Mehta, *Random Matrices and the Statistical Theory of Energy Levels*, (Academic Press, New York, 1967) and a new and revised version 1990

[9] O. Bohigas, M.-J. Giannoni and C. Schmit, Phys. Rev. Lett. **52**, 1 (1984)

[10] O. Bohigas, *Random Matrix Theories and Chaotic Dynamics*, in Proc. 1989 Les Houches School on Chaos and Quantum Physics, eds M.-J. Giannoni, A. Voros and J. Zinn-Justin, (Elsevier, Amsterdam, 1991)

[11] O. Bohigas and H.A. Weidenmüller, Ann. Rev. Nucl. Part. Sci **38**, 421 (1988)

[12] F. Haake, *Quantum Signatures of Chaos*, (Springer, Berlin, 1991)

[13] R. Aurich and F. Steiner, Physica **D43**, 155 (1990); Proc. Roy. Soc. London **A437**, 693 (1992)

[14] J. Bolte, G. Steil and F. Steiner, Phys. Rev. Lett. **69**, 2188 (1992)

[15] J. Bolte, Int. J. Mod. Phys. **B7**, 4451 (1993)

[16] R. Aurich, J. Bolte and F. Steiner, Phys. Rev. Lett. **73**, 1356 (1994)

[17] F. Steiner, *Festschrift Universität Hamburg 1994: Schlaglichter der Forschung zum 75. Jahrestag (ed. R. Ansorge)*, 543 (Dietrich Reimer Verlag, Hamburg, 1994)

[18] P. Gaspard and P. Alonso, Phys. Rev. **A47**, R3486 (1993); CHAOS **3**, 601 (1993)

[19] B. Burmeister, Diploma thesis, Universität Hamburg (1995)

[20] M. Sieber and F. Steiner, Phys. Lett. **A148**, 415 (1990)

[21] M.C. Gutzwiller, *Chaos in Classical and Quantum Mechanics*, (Springer, New York, 1990)

[22] see articles in CHAOS **2**, special issue on *Periodic Orbit Theory*, (1991)

[23] M.C. Gutzwiller, J. Math. Phys. **8**, 1979 (1967)

[24] R. Aurich, M. Sieber and F. Steiner, Phys. Rev. Lett **61**, 483 (1988); R. Aurich and F. Steiner, Physica **D39**, 169 (1989)

[25] M.C. Gutzwiller, J. Math. Phys. **12**, 343 (1971)

[26] R. Aurich and F. Steiner, Physica **D32**, 451 (1988)

[27] M. Berry and M. Tabor, Proc. Roy. Soc. London **A349**, 101 (1976); Proc. Roy. Soc. London **A356**, 375 (1977)

[28] U. Smilansky, *The Classical and Quantum Theory of Chaotic Scattering* in Proc. 1989 Les Houches School on Chaos and Quantum Physics, eds M.-J. Giannoni, A. Voros and J. Zinn-Justin, (Elsevier, Amsterdam, 1991)

[29] C. Jung and H.-J. Scholz, J. Phys. **A20**, 3607 (1987)

[30] S. Bleher, E. Ott and C. Grebogi, Phys. Rev. Lett. **63**, 919 (1989); Y. Lai, R. Blümel, E. Ott and C. Grebogi, Phys. Rev. Lett. **68**, 3491 (1992)

[31] M. Knauf and M. Klein, *Classical Chaotic Planar Scattering on a Coulombic Potential*, Lecture Notes in Physics **13** (Springer, Berlin, 1992)

[32] S. Brandis, DESY-report 94-70, extended version to appear in Phys. Rev. **E**

[33] A. Majda and J. Ralston, Duke Math. J. **46**, 725 (1979)

[34] R.B. Melrose, Comm. Part. Diff. Eq. **13**, 1431 (1988)

[35] M. Zworski, preprint John Hopkins University, Baltimore (1993)

[36] G. Vodev, Commun. Math. Phys. **146**, 205 (1992)

[37] W. John, B. Milek, H. Schanz and P. Seba, Phys. Rev. Lett. **67**, 1949 (1991)

[38] J. Eckmann and C.-A. Pillet, preprint UGVA-DPT 1994/10-860, Université de Genève

[39] C.E. Porter, *Statistical theory of spectra: Fluctuations*, (Academic, New York, 1965)

[40] W.H. Miller, Adv. Chem. Phys. **30**, 77 (1975)

[41] R. Bluemel and U. Smilansky, Phys. Rev. Lett **64**, 241 (1990)

[42] M.V. Berry, Ann. Phys. **131**, 163 (1981)

[43] G. Troll and U. Smilansky, Physica **D 34**, 60 (1989)

[44] P. Gaspard and S.A. Rice, J. Chem. Phys **90**, 2225 (1989); **90**, 2242 (1989); **90**, 2255 (1989)

[45] B. Eckhardt and C. Jung, J. Phys. **A19**, L829 (1986)

[46] B. Eckhardt, J. Phys. **A20**, 5971 (1987)

[47] G. Beneke, Diploma thesis, Universität Hamburg (1993)

[48] P. Cvitanovic and B. Eckhardt, Phys. Rev. Lett. **63**, 823 (1989)

[49] J.M. Robbins, Nonlinearity **4**, 343 (1991).

[50] J.-P. Eckmann and D. Ruelle, Rev. of Mod. Phys. **57**, 617 (1985).

[51] R. Abramowitz and J.E. Marsden, *Foundations of Classical Mechanics*, (Reading, Benjamin, 1978).

[52] S. Gallot, D. Hulin, and J. Lafontaine, *Riemannian Geometry*, Universitext (Springer, Berlin, 1990)

[53] L.D. Landau and E.M. Lifschitz, *Theoretische Mechanik*, (Akademie-Verlag, Berlin, 1976)

[54] M. Sieber and F. Steiner, Physica **D44**, 248 (1990).

[55] D. Ruelle, J. Stat. Phys. **44**, 281 (1986); *Thermodynamic Formalism*, (Addison-Wesley, Reading,MA 1978); P. Walters, *An Introduction to Ergodic Theory*, (Springer,Berlin,1981); see also articles in Y. G. Sinai, *Dynamical Systems II*, (Springer, Berlin, 1989)

[56] For a recent review see E. Ott and T.Tel in CHAOS **3**, 417 (1993), special issue on scattering theory.

[57] W. Parry and M. Pollicott, Ann. Math. **118**, 573 (1983)

[58] A. Knauf, private communication

[59] M. Sieber, Ph.D. thesis (DESY-Report 91-030, 1991)

[60] R. Aurich, J. Bolte, C. Matthies, M. Sieber and F. Steiner, Physica **D63**, 71 (1993)

[61] P. Gaspard and D. Alonso Ramirez, Phys. Rev. **A45**, 8383 (1992)

[62] J. Bolte, private communication

[63] R. Newton, *Scattering Theory of waves and particles*, (Springer, New York, 1982)

[64] M. Abramowitz and I. Stegun, *Handbook of Mathematical Functions*, (Dover Pub. Inc., New York, 1965)

[65] A.M. Ozorio de Almeida, Acta Cryst.**A31**, 435 (1975); 442 (1975)

[66] W. John and P. Ziesche, phys. stat. sol. (b) **47**, 555 (1971); K83 (1971)

[67] P. Ziesche and G. Lehmann (eds.), *Eletektronentheorie der Metalle*, (Springer, Berlin, 1983)

[68] J. Korringa, Physica **13**, 392 (1947); W. Kohn and N. Rostocker, Phys. Rev. **94**, 1111 (1954)

[69] see, e.g., S. Lang, *Linear Algebra*, (Addison-Wesley, Reading, 1966)

[70] R.F. Dashen, B. Hasslacher and A. Neveu, Phys. Rev. **D10**, 4114 (1974)

[71] W. Thirring, *Quantum Mechanics of Atoms and Molecules*, (Springer, Berlin, 1981)

[72] A. Böhm, *Quantum Mechanics*, (Springer, New York, 1979)

[73] A. Einstein, Verh. Dtsch. Phys. Ges. **19**, 82 (1917)

[74] M.C. Gutzwiller, in Proc. 1989 Les Houches School on Chaos and Quantum Physics, eds M.-J. Giannoni, A. Voros and J. Zinn-Justin, (Elsevier, Amsterdam, 1991)

[75] S.C. Creagh, J.M. Robbins and R.G. Littlejohn, Phys. Rev. **A42**, 1907 (1990)

[76] A. Bäcker, Diploma thesis, Universität Hamburg (1994); A. Bäcker, F. Steiner and P. Stifter, DESY-report 94-213 (1994)

[77] M. Sieber, U. Smilansky, S.C. Creagh and R.G. Littlejohn, J. Phys. **A26**, 6217 (1993); D. Alonso and P. Gaspard, J. Phys **A27**, 1599 (1994)

[78] T. Hesse, Diploma thesis Universität Hamburg (1994); R. Aurich, T. Hesse and F. Steiner, DESY-report 94-214 (1994)

[79] H. Ninnemann, Ph.D. thesis Universität Hamburg (1995) (DESY-report 94-241, 1994)

[80] M.V. Berry and K.E. Mount, Rep. Progr. Phys. **35**, 315 (1972)

[81] L.S. Schulman, *Techniques and Applications of path integration*, (Wiley, New York, 1981)

[82] R. Balian and C. Bloch, Ann. Phys. **85**, 514 (1974)

[83] H. Bohr, Erg. Math. I, 1 (1932)

[84] A.S. Besicovitch, *Almost Periodic Functions*, (Dover Pub., Cambridge, 1954)

[85] Y. Sinai, Russian Math. Surveys **48**, 1 (1993)

[86] T. Ericson, Phys. Rev. Lett. **5**, 430 (1960); Ann. Phys. **23**, 390 (1963)

[87] T. Ericson and T. Mayer-Kuckuk, Ann. Rev. Nucl. Sci. **16**, 13 (1966)

[88] C.M. Marcus, R.M. Westervelt, P.F. Hopkins and A.C. Gossard, Surface Science **305**, 480 (1994)

[89] A.M. Chang, H.U. Baranger, L.N. Pfeiffer and K.W. West, Phys. Rev. Lett. **73**, 2111 (1994)

[90] D. Weiss, K. Richter, A. Menschig, R. Bergmann, H. Schweizer, K. von Klitzing and G. Weimann, Phys. Rev. Lett. **70**, 4118 (1993)

[91] R.A. Jalabert, H.U. Baranger and A.D. Stone, Phys. Rev. Lett. **65**, 2442 (1990)

[92] B.D. Simons, P.A. Lee and B.L. Altshuler, Phys. Rev. Lett. **72**, 64 (1994)

[93] R. Blümel and U. Smilansky, Phys. Rev. Lett. **60**, 477 (1988)

[94] J. Main and G. Wunner, Phys. Rev. Lett. **69**, 586 (1992)

[95] D.M. Wardlaw and W. Jaworski, J. Phys. **A22**, 3561 (1989)

[96] A. Sushin and D.M. Wardlaw, J. Phys. **A25**, 1503 (1992)

[97] B. Jessen and H. Tornehave, Acta Math. **77**, 137 (1945)

[98] M.C. Gutzwiller, talk given on the 56th annual DPG-Tagung in Berlin (1995)

[99] G. Beneke and S. Brandis, in preparation

[100] M.C. Gutzwiller, Physica **D7**, 341 (1983)

[101] B. Eckhardt, CHAOS **3**, 613 (1993)

[102] A. Wintner, Am. J. Math **55**, 309 (1933)

[103] P.M. Bleher, Z. Cheng, F.J. Dyson and J.L. Lebowitz, Commun. Math. Phys. **154**, 433 (1993)